Influence of prior experience on spatial orientation and self-motion perception

Sophie Willemsen

DONDERS SERIES

RADBOUD UNIVERSITY PRESS

Radboud Dissertation Series

Influence of prior experience on spatial orientation and self-motion perception

Sophie Willemsen

The research presented in this thesis was carried out at the Radboud University, Donders Institute for Brain, Cognition and Behaviour, and was made possible by an internal grant from the Donders Centre for Cognition.

Influence of prior experience on spatial orientation and self-motion perception
Sophie Willemsen

Radboud Dissertation Series
ISSN: 2950-2772 (Online); 2950-2780 (Print)

Published by RADBOUD UNIVERSITY PRESS
Postbus 9100, 6500 HA Nijmegen, The Netherlands
www.radbouduniversitypress.nl

Design: Proefschrift AIO | Guus Gijben
Cover: Proefschrift AIO | Guntra Laivacuma
Printing: DPN Rikken/Pumbo

ISBN: 9789465151717
DOI: 10.54195/9789465151717
Free download at: https://doi.org/10.54195/9789465151717

RADBOUD
UNIVERSITY
PRESS

Influence of prior experience on spatial orientation and self-motion perception

Proefschrift ter verkrijging van de graad van doctor

aan de Radboud Universiteit Nijmegen

op gezag van de rector magnificus prof. dr. J.M. Sanders,

volgens besluit van het college voor promoties

in het openbaar te verdedigen op

maandag 12 januari 2026

om 14.30 uur precies

door

Cornelia Martine Johanna (Sophie) Willemsen

geboren op 23 mei 1997

te Tiel

Promotor:

Prof. dr. W.P. Medendorp

Copromotoren:

Dr. R.J. van Beers

Dr. M.G.M. Koppen

Dr. L. Oostwoud Wijdenes

Manuscriptcommissie:

Prof. dr. F.P. de Lange

Prof. dr. ing. S. Glasauer (Brandenburgische Technische Universität Cottbus-Senftenberg, Duitsland)

Dr. ir. D. Narain (Erasmus MC)

Table of Contents

Chapter 1

General introduction

Imagine you have just relocated and you wake up during the night in your new bedroom. You decide to get a glass of water from the kitchen. To do so, you first have to navigate to reach the door of your bedroom in complete darkness. In your mind, you have a rough idea about the distance from your bed to the door, but you are not very certain about this estimate. As you carefully start walking, the motor system generates movement which is sensed by multiple sensory systems. For example, the otoliths in your inner ear relay information about your linear motion. Furthermore, you are using your hands to feel around, gathering more information about where you are and how close you are to the door. Suddenly, your hands touch the bedroom door, revealing it to be much closer than anticipated based on the layout of your old bedroom. The memory of your old room has interfered with estimating the distance to the new door. This example illustrates the central question of this thesis: how does our memory of past experiences influence our spatial perception?

Spatial perception refers to the ability to perceive our own orientation and position in space as well as the orientation and position of objects around us, which enables us to successfully interpret and navigate our surroundings. In this thesis, I investigate how spatial perception, specifically the perception of our orientation (**Chapter 2**) and self-motion (**Chapters 3** and **4**) in space, is affected by the memory of past experiences. In the remainder of this chapter, I first discuss the functioning of the sensory systems involved in spatial perception. Second, I describe how different types of sensory information might be integrated with memorized prior knowledge to form a percept. Finally, spatial perception experiments are described, as well as systematic trial-to-trial errors in the behavior of participants that are often observed in these experiments.

1.1 Sensory signals in spatial perception

We experience the world through our sensors. Each sensory system contains specialized receptors that convert properties of the environment into neural activity. Sensory information in the form of action potentials then travels through afferent neurons in peripheral nerves to the central nervous system. The combined firing pattern of groups of sensory neurons encodes different features of the sensory input, such as stimulus intensity or duration. To determine our orientation and position in space, the brain appears to utilize and combine information from multiple sensory systems (Angelaki & Cullen, 2008; Clemens et al., 2011). The sensory signals involved in spatial perception are primarily provided by the visual, vestibular, somatosensory and motor systems.

The visual system plays an important role in spatial perception as it allows us to perceive different features of objects in the environment. This includes the orientation of static objects, such as buildings or trees, which can provide information about the direction of gravity and help us form an internal self-orientation estimate (Li & Matin, 2005). Static monocular and binocular cues also transmit information about where objects are positioned in space relative to ourselves (Brenner & Smeets, 2018). When we move through the environment, the apparent motion of objects across our retinae, referred to as optic flow (Gibson, 1950), generates dynamic information about our orientation and position in space. In darkness or in the case of an impaired visual system, these visual signals are completely absent or less available, forcing us to rely on other senses to form an orientation or position estimate. In this thesis, I investigate how humans perceive their orientation or self-motion when visual signals are unavailable.

1.1.1 Vestibular receptors

Together with the auditory cochlea, the peripheral vestibular system is located inside the labyrinth of the inner ear. This labyrinth lies within the head's temporal bone and contains ducts (the semicircular canals) and chambers (the ampullae, utricle and saccule) filled with endolymph (see Figure 1.1A).

Semicircular canals

The three semicircular canals measure angular velocity of the head in space brought about by angular movements (i.e., rotations). The canals are roughly arranged in three orthogonal planes: the lateral canal is positioned in the head's

yaw axis, the posterior canal in the head's roll axis and the anterior canal in the pitch axis, tilted approximately 30° upward from the head's horizontal plane (Blanks et al., 1975). At the base of each canal lies a chamber (ampulla), which contains hair cells. The hair cell endings (cilia) are embedded in a gelatinous membrane (cupula), through which the endolymph cannot pass. When the head is rotated relative to the body, or in the case of a full-body rotation, the canal rotates but the endolymph lags behind due to the fluid's inertia. This lag causes the endolymph to press against the elastic cupula within the ampulla, which in turn bends the embedded cilia. The flow of the endolymph is proportional to the head's angular acceleration, whereas the cupula deflection is roughly proportional to the head's angular velocity (Obrist, 2011). The afferent neurons have a spontaneous firing rate, which increases or decreases depending on how the cilia are deflected. The cilia consist of one long kinocilium and shorter stereocilia. Bending the stereocilia towards the kinocilium opens mechanically-gated ion channels at the tips of the stereocilia, allowing the influx of potassium, which depolarizes the hair cell's membrane. This depolarization opens voltage-gated calcium channels at the base of the hair cell. The subsequent influx of calcium results in the increased release of neurotransmitters that bind to receptors of the afferent neurons, causing increased neural firing. Bending the stereocilia away from the kinocilium causes the mechanically-gated channels to close, which hyperpolarizes the hair cell, resulting in a decrease in neurotransmitter release and afferent firing. The canals in one ear form pairs with the canals in the other ear, with their cilia oriented in opposite directions. The same head rotation therefore causes the corresponding hair cells to produce excitatory signals in one ear and inhibitory signals in the other ear, from which the direction of the head movement can be deduced (Purves et al., 2001; Kolb & Whishaw, 2014; Niehof, 2020; Kirby et al., 2024).

Otolith organs

In addition to the semicircular canals, the vestibular system contains the utricle and the saccule, referred to as the otolith organs. The otolith organs measure both static head orientation (i.e., head tilt relative to gravity) and dynamic head displacements (i.e., linear acceleration of the head). The utricle is oriented along the head's horizontal plane and the saccule along the head's vertical plane. Both otolith organs consist of macula tissue made up from hair cells and support cells (see Figure 1.1A, inset). The cilia of the hair cells extend into the otolithic membrane, a gelatinous layer on top of the macula. The top surface of the otolithic membrane is embedded with calcium carbonate crystals (otoconia), adding weight to the membrane. When the head is roll-tilted rightward relative to gravity, the otolithic membrane and therefore the cilia are displaced relative to the macula

with gravitational acceleration *-a* (see Figure 1.1B). This results in depolarization of some hair cells and hyperpolarization of others, encoding the orientation of the head. However, when the head is upright and laterally translated leftward with linear acceleration *a*, the cilia are similarly displaced due to the membrane's inertia, thus resulting in the same neural signal (see Figure 1.1C; Purves et al., 2001; Kolb & Whishaw, 2014; Niehof, 2020; Kirby et al., 2024). In real-world conditions, both forces act upon the head. To disambiguate between these forces, it is thought that the brain relies on signals from the semicircular canals and visual system (Laurens & Angelaki, 2011). In the more controlled spatial perception experiments presented in this thesis, participants are either roll-tilted or laterally translated with the head fixed upright, such that the otoliths either encode head tilt or linear acceleration.

Vestibular afferents can be categorized as regular or irregular in terms of their resting discharge variability (Cullen, 2019). In macaque monkeys, it has been found that regular otolith afferents transmit more information about static head tilt relative to gravity than irregular otolith afferents, whereas irregular afferents provide more information about translational motion than regular afferents (Jamali et al., 2019).

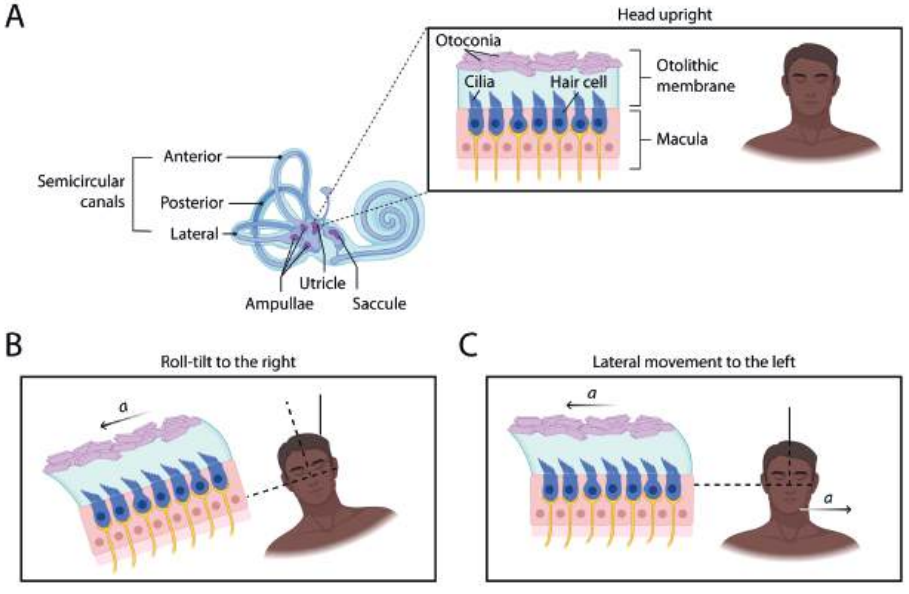

Figure 1.1. *A*: Anatomy of the vestibular system, illustrating the semicircular canals and the two otolith organs, the utricle and the saccule. *Inset*: A simplified schematic of the utricle when the head is upright. The macula tissue consists of hair cells surrounded by support cells. The cilia of the hair

cells are encapsulated in the otolithic membrane, a gelatinous layer on top of the macula. Embedded in the top surface of this membrane are calcium carbonate crystals, the otoconia. *B*: When the head is roll-tilted rightward relative to gravity, the otolithic membrane is shifted relative to the macula with gravitational acceleration *-a* in the axis of the macula, displacing the cilia of the hair cells. *C*: The cilia are displaced in the same manner, and thus the same neural signal is generated, when the head is upright and laterally translated leftward with linear acceleration *a*, causing the otolithic membrane to move with inertial acceleration *-a*. Figure adapted from images published under the CC BY 4.0 license (Kirby et al., 2024).

1.1.2 Somatosensory receptors

Nerve endings in the muscles, tendons and joints, referred to as proprioceptors, provide information about the orientation and displacement of the body in space. Movement stretches the muscle spindles and Golgi tendon organs, which are sensory receptors that detect muscle stretch and tension, respectively. Mechanoreceptors in musculoskeletal joints are thought to function as 'limit detectors', providing information about extreme joint positions to prevent injury (Tuthill & Azim, 2018). The somatosensory system also contains receptors for pain (nociceptors) and temperature (thermoreceptors), as well as mechanoreceptors (corpuscles) that measure pressure, touch, and vibration (Purves et al., 2001; Kolb & Whishaw, 2014). These receptors are found in the skin as well as in the body's interior. Studies on postural perception have suggested that the trunk contains somatic 'graviceptors', pointing to pressure receptors around the kidneys and in the cardiovascular system. When the body is tilted, the kidney slightly shifts within its surrounding capsule and blood shifts within the cardiovascular system, stimulating pressure receptors which in turn signal information about the body's orientation in space (Mittelstaedt, 1997, 1998; Vaitl et al., 1997, 2002).

1.1.3 Sensorineural processing

Brainstem and cerebellum

The signals from the semicircular canals and otolith organs are transmitted by afferent neurons in the vestibulocochlear nerve (cranial nerve VIII) to the vestibular nuclei in the brainstem (Khan & Chang, 2013). Proprioceptive information travels to the dorsal column nuclei in the brainstem, via the spinal cord (Delhaye et al., 2018). From the brainstem, both types of sensory information are relayed via the thalamus to the cortex as well as to the cerebellum.

Within the cerebellum, the fastigial nucleus (rFN) is suggested to be involved in reference frame transformations (Cullen, 2019, 2023). Because of the vestibular

labyrinth's location, which is fixed to the head, vestibular information is encoded in a head-centered reference frame. However, to keep our balance (e.g., through vestibulo-spinal reflexes), this information has to be transformed into a body-centered reference frame, which involves the integration of vestibular signals and neck proprioceptive signals. Experiments in rhesus monkeys indicate that this integration takes place in the rFN (Brooks & Cullen, 2009). Similarly, the vestibular cerebellum in monkeys is suggested to be involved in the transformation from a head-centered into a head-in-space reference frame by integrating otolith and canal information (Laurens et al., 2013).

There is also evidence that the rFN plays a role in distinguishing between sensory signals that are the result of our own movements (reafferent signals) and sensory signals that are generated by externally imposed passive motion (exafferent signals; Brooks et al., 2015). The cerebellum is believed to encode a forward model that computes the expected reafferent signal brought about by our motor command (von Holst & Mittelstaedt, 1950; Mittelstaedt, 1997). If the expected reafferent signal matches the actual sensory signal (i.e., if there is no sensory prediction error), the sensory signal is considered a result of our own movement and the cerebellum sends a reafference cancellation signal to the vestibular nuclei in the brainstem, suppressing the sensory signal (Brooks et al., 2015; Cullen, 2019, 2023). In the situation where there *is* a sensory prediction error, the sensory signal must have been (partially) generated by external motion and the neurons in the vestibular nuclei are not suppressed.

Thalamus and cortex

Neural signals from the vestibular, dorsal column, and deep cerebellar nuclei are relayed to the ventral posterior lateral nucleus (VPL) in the thalamus (Lopez & Blanke, 2011; Cullen, 2019). The thalamus in turn projects to cortical areas such as the temporo-parietal junction (TPJ), the anterior parietal cortex (APC), and the posterior parietal cortex (PPC) (Hitier et al., 2014; Ventre-Dominey, 2014; Orban et al., 2021), which are thought to be homologues of the parieto-insular vestibular cortex (PIVC), area 2v, area 3a, and the ventral intraparietal area (VIP) in monkeys (Lopez & Blanke, 2011; Cullen, 2019; see Figure 1.2). Both human and animal studies suggest that these cortical areas are involved in the processing of vestibular, visual, and somatosensory signals, and multisensory integration of these signals (see Section 1.2).

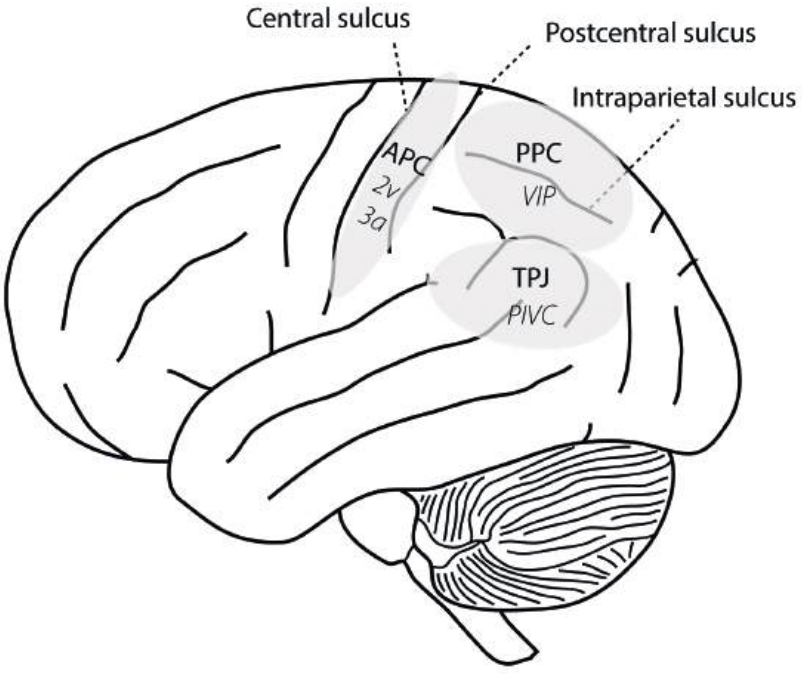

Figure 1.2. (Part of the) cortical projections of sensory afferents relevant for spatial perception. The ventral posterior lateral nucleus (VPL) in the thalamus projects to the temporo-parietal junction (TPJ), the anterior parietal cortex (APC), and the posterior parietal cortex (PPC). These cortical areas may be homologous to multisensory areas found in monkeys, shown in italics (*PIVC*: parieto-insular vestibular cortex, *VIP*: ventral intraparietal area). Figure adapted from image published under the CC BY-SA 3.0 license (NEUROtiker, 2007).

1.2 Integration of sensory and prior information

As discussed in the previous section, multiple sensory systems can provide information about the same stimulus. For example, when crossing the street, our visual and vestibular systems generate self-motion cues, which in turn provide information about the remaining distance to the opposite sidewalk. The brain might use the sensory signals in isolation to estimate the distance. However, each individual sensory signal is a noisy representation of the true distance. A statistically optimal approach would be to weigh the sensory signals relative to their precision and to also incorporate any prior information that we have about the distance (Landy et al., 1995; Jacobs, 1999; Ernst & Banks, 2002; Clemens, 2015).

This idea is referred to as Bayesian inference and will be discussed in more detail below.

1.2.1 Accuracy and precision

Before introducing Bayesian inference models, it is useful to discuss two distinct concepts that can be used to describe a distribution of data points: accuracy (with bias as its opposite) and precision (with variability as its opposite). These concepts are illustrated in Figure 1.3, which shows different distributions of shots on a target.

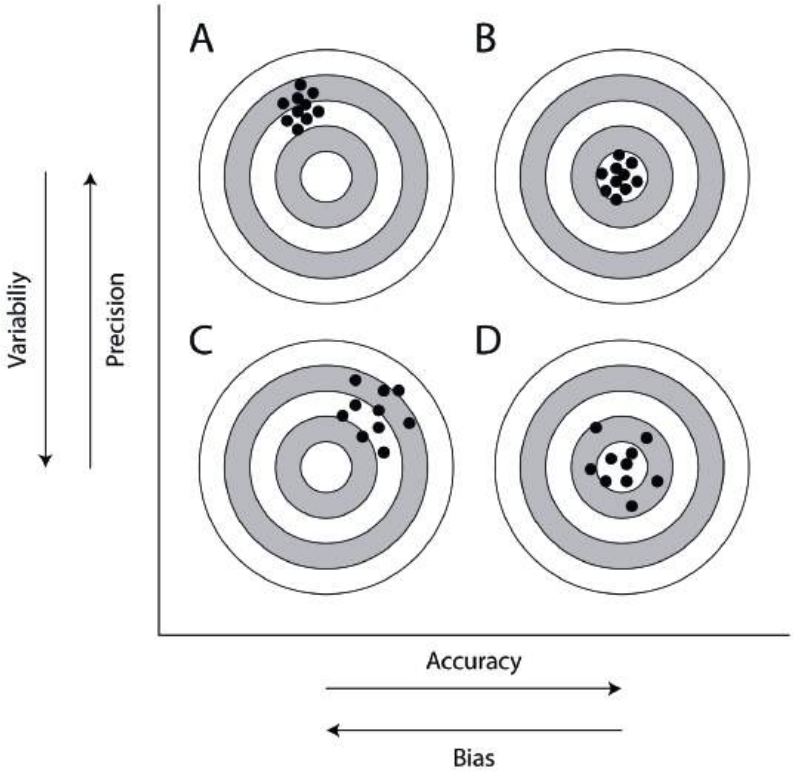

Figure 1.3. Targets with example shots (black points), illustrating different aspects of a distribution of data points. *A*: Shots that are close to each other, i.e., relatively precise/with a low variability, but systematically biased to the upper left. *B*: Shots that are on average close to the bullseye, i.e., relatively accurate/unbiased, with a similar precision as in *A*. *C*: Shots that are more variable than in *A*, with a similarly sized bias toward the upper right. *D*: Shots with a similar accuracy, but a higher variability than in *B*. Figure adapted from Sutter (2023).

Accuracy is high when shots are on average close to the bullseye, i.e., when there is no systematic deviation (bias). In Figure 1.3, this is true for panels *B* and *D*, while panels *A* and *C* show biases with similar magnitudes in two different directions. Precision is high when shots have only a small spread, as is the case in panels *A* and *B*; panels *C* and *D* show more variability.

1.2.2 Bayesian inference

Imagine observing an unknown stimulus, x (e.g., the head tilted at an unknown roll angle), resulting in a sensory measurement of this quantity, z, provided by one of our sensory systems. We typically assume that the measurements of this sensory system are on average unbiased but contaminated by independent Gaussian noise, $N(0, \sigma^2)$. The probability distribution of the measurement z given stimulus value x is then:

$$P\left(z \mid x\right) = N\left(x, \sigma^2\right). \tag{1.1}$$

Equation 1.1 is also referred to as the measurement distribution. From the brain's perspective, the sensory measurement is known, but the true stimulus has to be inferred. In other words, we want to compute the likelihood of the stimulus given the measurement, $\mathcal{L}\left(x|z\right)$, for all possible stimuli x. We assume that the measurement distribution is used as the likelihood function, but instead of interpreting it as a probability distribution across measurements, it is now interpreted as a function of the stimulus (Girshick et al., 2011). Generally, we might receive measurements from N sensory systems, $z_1, \ldots, z_N$, possibly with N different variances, $\sigma^2_{z_1}, \ldots, \sigma^2_{z_N}$. On the condition that the sensory measurements are independent, we can compute the likelihood of each stimulus x as:

$$\mathcal{L}\left(x \mid z_1, \ldots, z_N\right) = P\left(z_1, \ldots, z_N \mid x\right) = \prod_{n=1}^{N} P\left(z_n \mid x\right). \tag{1.2}$$

Using Bayes' rule (Bayes, 1763), it is now possible to compute the probability distribution of the stimulus given the measurements:

$$P\left(x \mid z_1, \ldots, z_N\right) = \frac{P\left(z_1, \ldots, z_N \mid x\right) P\left(x\right)}{P(z_1, \ldots, z_N)}. \tag{1.3}$$

In this equation, $P\left(x\right)$ is the prior distribution of the stimulus. This distribution expresses for every possible head roll-tilt angle how probable it is for that

orientation to occur, before observing any sensory measurements. The denominator, independent of stimulus x, is referred to as the marginal likelihood and normalizes the integration of the prior and likelihood, resulting in the posterior distribution, $P\left(x \mid z_1, \ldots, z_N\right)$. If the prior distribution and all sensory likelihoods are Gaussian, then the posterior distribution will also be Gaussian. In this situation, the prior and likelihoods can be regarded as similar signals, each transmitting an estimate of the stimulus, which are then combined into the posterior distribution (Ernst & Banks, 2002; Körding & Wolpert, 2004; Clemens, 2015).

How should we select a single estimate of the unknown stimulus x from the posterior distribution? We generally select the stimulus with the largest posterior probability, referred to as the maximum a posteriori (MAP) estimate:

$$\widehat{x} = \mathrm{argmax}_x P\left(z_1, \ldots, z_N \mid x\right) P\left(x\right). \tag{1.4}$$

It can be shown that the solution for $\widehat{x}$ is a weighted sum of the peak of the prior and the peaks of the sensory likelihoods (Landy et al., 1995; Jacobs, 1999; Ernst & Banks, 2002; Bays & Wolpert, 2007; Clemens et al., 2011):

$$\widehat{x} = w_{\text{prior}} \cdot \mu_{\text{prior}} + w_{z_1} \cdot z_1 + \cdots + w_{z_N} \cdot z_N, \tag{1.5}$$

with each weight equal to the signal's normalized precision, defined as the inverse of its variance ($1/\sigma^2$):

$$w_{\text{prior}} = \frac{1/\sigma^2_{\text{prior}}}{1/\sigma^2_{\text{prior}} + 1/\sigma^2_{z_1} + \cdots + 1/\sigma^2_{z_N}}, \tag{1.6}$$

$$w_{z_n} = \frac{1/\sigma^2_{z_n}}{1/\sigma^2_{\text{prior}} + 1/\sigma^2_{z_1} + \cdots + 1/\sigma^2_{z_N}}. \tag{1.7}$$

From this follows that signals with a higher precision have a larger influence on the posterior estimate. Since the weights add up to 1, each weight can be interpreted as the relative contribution of its corresponding signal to the overall estimate.

The variance of the posterior distribution can be interpreted as a measure of the brain's uncertainty in the posterior estimate:

$$\sigma^2_{\widehat{x}} = \frac{1}{1/\sigma^2_{\text{prior}} + 1/\sigma^2_{z_1} + \cdots + 1/\sigma^2_{z_N}}. \tag{1.8}$$

From Equation 1.8 follows that the posterior provides a more precise estimate than we would obtain from the individual signals. The same solution arises when minimizing the posterior variance (Ghahramani et al., 1997; Cooke, 2019). In other words, the estimate is statistically optimal in terms of acquiring the minimum possible variance given the individual signals (Ernst & Banks, 2002). This is illustrated in Figure 1.4, which shows the posterior distribution for different variances of the prior and likelihood. In all panels, the posterior variance is lower than the variances of the prior and likelihood. However, optimal integration in terms of a lower-variance posterior also results in a bias toward the prior distribution (see Figure 1.4A). This is sometimes referred to as an accuracy-precision trade-off[1]: an upright head-orientation prior will reduce perceptual uncertainty at the expense of a bias toward the upright head orientation, which becomes more pronounced at larger tilt angles (de Vrijer et al., 2009). In Section 1.3.1, this bias is discussed in more detail.

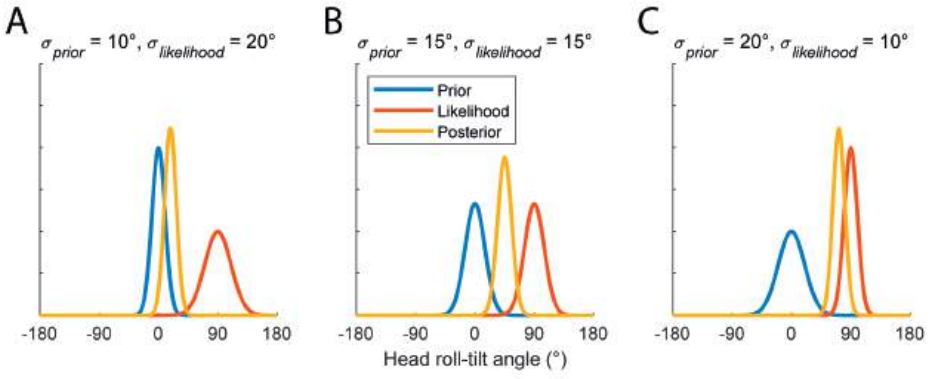

Figure 1.4. Bayesian integration of prior and sensory signals representing information about an unknown head roll-tilt angle. In all panels, the prior distribution (blue) is centered on 0°, which can be interpreted as the most probable head orientation before observing any sensory measurements. The sensory likelihood (red) is centered on 90°. The posterior distribution (yellow) is the result of integrating the prior and likelihood, and the peak of this distribution depends on the individual signals' respective precisions. *A*: The posterior is shifted towards the more precise, i.e., lower-variance, prior. *B*: The prior and likelihood have equal variances, and the posterior peak is the average of the individual peaks. *C*: The posterior is shifted towards the more precise likelihood. In all panels, the posterior distribution has a lower variance than the individual signals.

1. Note that on average the posterior mean, which coincides with the posterior mode (Equation 1.4) and median when the distributions are Gaussian, is an optimal estimate as it minimizes the expected squared error. In other words, where on a single trial (or in this case in a specific part of the tilt range) the estimate may be off, the estimate is still the overall best possible estimate given the sensory uncertainty and the prior.

If all stimuli are equally likely to occur, a flat prior can be used in the integration. In this case, the MAP estimate in Equation 1.4 reduces to the maximum likelihood estimate (MLE):

$$\widehat{x} = \text{argmax}_x P\left(z_1, \ldots, z_N \mid x\right). \tag{1.9}$$

Parameter estimation

To compute the posterior distribution, we need to know the variances of the individual signals, $\sigma^2_{\text{prior}}, \sigma^2_{z_1}, \ldots, \sigma^2_{z_N}$. As our best guess for the value of these model parameters, we generally use the maximum likelihood estimate of these parameters given the data:

$$\hat{\theta} = \text{argmax}_\theta P\left(d_1, \ldots, d_T \mid \theta\right), \tag{1.10}$$

where $\theta = \left\{\sigma^2_{\text{prior}}, \sigma^2_{z_1}, \ldots, \sigma^2_{z_N}\right\}$ and $d_1, \ldots, d_T$ are the data from T different trials. For some problems, Equation 1.10 has a closed-form solution. However, generally, no closed-form solution exists, leaving us to numerically approximate the solution. Instead of maximizing the likelihood, most optimization algorithms equivalently minimize the negative log-likelihood for numerical stability:

$$\hat{\theta} = \text{argmin}_\theta \left[-\ln\left(P\left(d_1, \ldots, d_T \mid \theta\right)\right)\right]. \tag{1.11}$$

To find the numerical solution, we first define the likelihood function. This function compares the model prediction, generated with specific parameter values, θ, to the data and outputs a value indicating how likely it is that the data was generated by this set of parameter values. The negative log-likelihood function is then minimized by an optimization algorithm that evaluates the function for θ. Initially, the values for θ might be a random guess. By comparing the output of the likelihood function for different θ values, the optimization algorithm further refines the estimate for θ until it converges onto a 'good enough' guess, defined by a criterion that is specified before running the optimization algorithm (Taboga, 2021).

The likelihood value of one converged model, $\hat{\mathcal{L}}$, can be compared to the likelihood of a different model version. However, if the models have different numbers of model parameters, $K = |\theta|$, the comparison should take this difference into account. Two measures that are often used for model comparison are the Akaike information criterion (AIC; Akaike, 1974) and the Bayesian information criterion (BIC; Schwarz, 1978):

$$\mathrm{AIC} = -2\ln(\hat{\mathcal{L}}) + 2K, \tag{1.12}$$

$$\mathrm{BIC} = -2\ln(\hat{\mathcal{L}}) + K\ln\left(T\right), \tag{1.13}$$

where T is the number of explained data points. To increase the model likelihood, one could add more parameters to the model, but this could lead to a model that overfits the data and therefore does not generalize well to unseen data. The AIC and BIC scores include a penalty term for the number of model parameters, where the BIC score penalizes model complexity more than the AIC score (Bishop, 2006). When comparing the AIC or BIC scores of multiple models, a lower score indicates a more preferred model.

1.2.3 Sequential Bayesian inference

In Section 1.2.2, I described a general Bayesian inference model that computes the posterior distribution of an unknown stimulus on a given trial (or more generally, time point) based on that trial's sensory measurement. Assuming independent trials, on the next trial a new posterior distribution is computed based on the measurement of that trial, independent of the estimate on the previous trial. Instead, assuming dependence between consecutive trials, sequential Bayesian inference models iteratively update over time by computing the posterior on a given trial based on that trial's measurement and the previous trial's estimate.

In this context, the unknown stimulus on trial t, x_t, that we try to estimate, can be regarded as the model's unobserved state that might change over time. The sensory measurement, z_t, is an observation of this hidden state. How the measurement relates to the state and how the state evolves over time is captured by the measurement and state transition equations, respectively. As an example, we will define these equations as follows:

$$z_t = x_t + \eta, \tag{1.14}$$

$$x_t = x_{t-1} + \varepsilon, \tag{1.15}$$

where η and ε refer to the measurement and process noise, respectively. Here, the sensory measurement is assumed to be a noisy readout of the state, and the state is assumed to depend only on the previous state, with random variation introduced by process noise.

As before, we can compute the posterior distribution of the stimulus on trial t by applying Bayes' rule:

$$P\left(x_t \mid z_{1:t}\right) = \frac{P\left(z_t \mid x_t\right) P\left(x_t \mid z_{1:t-1}\right)}{P\left(z_t \mid z_{1:t-1}\right)}. \tag{1.16}$$

Contrary to the static Bayesian inference model outlined in Section 1.2.2, a sequence of sensory measurements up to and including the current trial, $z_{1:t}$, is now available. Here, $P\left(z_t \mid x_t\right)$ can be interpreted as the likelihood of the measurement, which is a Gaussian distribution defined by the measurement equation (see Equation 1.14). $P\left(x_t \mid z_{1:t-1}\right)$ can be seen as the prior for the current state, before observing measurement z_t, and is referred to as the predictive distribution (Ho & Lee, 1964; Cooke, 2019).

If we assume the measurement and state transition models to be linear, and the measurement and process noise to be normally distributed, say $\eta \sim N(0, r)$ and $\varepsilon \sim N(0, s)$, the derivations of the posterior mean and variance are mathematically equivalent to the so-called Kalman filter equations (Kalman, 1960). The Kalman filter model consists of two steps. The first step is the prediction step in which the predictive distribution $P\left(x_t \mid z_{1:t-1}\right)$ is computed. In our example, $P\left(x_t \mid z_{1:t-1}\right)$ is Gaussian with the following mean $\widehat{x}_{t|t-1}$ and variance $P_{t|t-1}$:

$$\widehat{x}_{t|t-1} = \widehat{x}_{t-1|t-1}, \tag{1.17}$$

$$P_{t|t-1} = P_{t-1|t-1} + s. \tag{1.18}$$

Here, the prediction of the state for the current trial, $\widehat{x}_{t|t-1}$, is equal to the posterior state estimate from the previous trial, $\widehat{x}_{t-1|t-1}$, and the variance of the predictive distribution, $P_{t|t-1}$, is equal to the posterior variance from the previous trial, $P_{t-1|t-1}$, increased with process noise variance s.

The prediction step is followed by the update step, in which the posterior distribution is computed by refining the prediction of the state, $\widehat{x}_{t|t-1}$, by taking into account the new measurement, z_t. The posterior distribution is again Gaussian with mean $\widehat{x}_{t|t}$ and variance $P_{t|t}$:

$$K_t = \frac{P_{t|t-1}}{P_{t|t-1} + r}, \tag{1.19}$$

$$\widehat{x}_{t|t} = \widehat{x}_{t|t-1} + K_t \left(z_t - \widehat{x}_{t|t-1}\right), \tag{1.20}$$

$$P_{t|t} = \left(1 - K_t\right) P_{t|t-1}. \tag{1.21}$$

In Equation 1.19, K_t is referred to as the Kalman gain, which is essentially a ratio between the process noise and measurement noise that determines how much the prediction of the state is shifted towards the measurement (see Equation 1.20). By observing a new measurement, the variance of the predictive distribution is reduced (see Equation 1.21). The posterior state estimate and variance, $\widehat{x}_{t|t}$ and $P_{t|t}$, become $\widehat{x}_{t-1|t-1}$ and $P_{t-1|t-1}$ on the next trial.

In a behavioral experiment, during which stimuli are typically randomly presented, the participant may (implicitly) assume that the stimuli come from a *static* prior distribution, i.e., a distribution of probable stimuli that does not change across trials. However, in more naturalistic scenarios, stimuli often do not succeed one another randomly. For example, when estimating tomorrow's stock value, rather than assuming that the values are randomly sampled from a fixed distribution, a more useful, *iterative* assumption would be that tomorrow's value is equal to today's value with a small, random variation. A third, intermediate assumption would be to assume that the stimulus comes from a stimulus distribution of which the mean can change across time. Whereas the static Bayesian inference model only allows the incorporation of a static prior distribution, the sequential model enables us to also test the iterative assumptions. To do so, the Kalman filter model is extended to estimate two states, the stimulus x_t and the mean of the estimated stimulus distribution m_t, referred to as the *two-state* model (Glasauer & Shi, 2022):

$$z_t = x_t + \eta \,\text{with}\, \eta \sim N(0, r), \tag{1.22}$$

$$x_t = m_{t-1} + \varepsilon_x \,\text{with}\, \varepsilon_x \sim N(0, v), \tag{1.23}$$

$$m_t = m_{t-1} + \varepsilon_m \,\text{with}\, \varepsilon_m \sim N(0, q). \tag{1.24}$$

In this model, variance *v* determines the width of the estimated stimulus distribution and variance *q* determines how much the mean of this distribution changes across trials. This model encompasses the static and iterative assumptions. The *static* variant is obtained by fixing q at 0, such that the mean of the stimulus distribution does not change across trials. By fixing v at 0, the estimated stimulus is always equal to the estimated stimulus distribution mean, resulting in a model where the estimated stimulus distribution is iteratively updated on each trial (the *iterative* variant). In **Chapter 3**, I estimate the variance parameters r, v and/or q from data gathered in a path integration experiment, in order to evaluate whether different assumptions about the stimulus distribution can explain the observed biases in this experiment (see Section 1.3.2).

1.3 Studying spatial perception

A variety of experimental paradigms have been developed to study human spatial orientation and self-motion perception. In **Chapter 2**, I study whether, instead of using a Gaussian-distributed prior, spatial orientation estimates from two laboratory-based psychophysical tasks can be better explained by a prior distribution that matches the natural statistics of head orientations measured outside the laboratory. In **Chapters 3** and **4**, I study how estimates of travelled distance in a laboratory-based path integration task are affected by the distribution and the presentation order of the experimental stimuli. These experimental paradigms as well as typical perceptual biases that are often found in these experiments are explained below in more detail.

1.3.1 Spatial orientation perception

In **Chapter 2**, I reanalyze previously gathered data (Clemens et al., 2011) from two psychophysical tasks that measure how humans perceive body orientation and visual vertical orientation in space: the subjective body tilt (SBT) and subjective visual vertical (SVV) task, respectively (see Box 1). Clemens et al. (2011) found that in the SBT task, participants accurately estimated their body orientation in space across the measured tilt range. On the contrary, at large tilt angles in the SVV task, the line orientation estimates were biased away from vertical toward the body midline. This bias is referred to as the Aubert effect (Aubert, 1861). The findings from both tasks were well explained by a Bayesian inference model (see Section 1.2.2). This model provided an explanation for the Aubert effect by including a Gaussian prior distribution of head orientation that was centered on upright. In other words, the most probable head orientation before observing any sensory measurements is the upright orientation, reflecting the observation that our head is usually in an upright position during everyday behavior and that large head roll-tilts are less common. The idea that orientation perception is influenced by the statistics of natural stimuli has been substantiated by studies in the visual domain. Examples of such visual scene statistics are light that usually comes from above (Adams et al., 2004), and the predominance of horizontal and vertical orientations (Girshick et al., 2011).

Box 1. Psychophysical tasks

Psychophysical tasks measure the relationship between a physical stimulus (e.g., the orientation of the body or the orientation of a visual line) and the participant's perception of this stimulus. A readout of this relationship is obtained by systematically varying the stimulus value around a reference value. On each trial, the participant indicates whether the stimulus orientation is clockwise (CW) or counterclockwise (CCW) relative to the reference orientation. The responses are used to estimate the parameters of a psychometric function. A psychometric function that is often used is the cumulative Gaussian function including a lapse parameter (Clemens et al., 2011):

$$P(x) = \lambda + (1 - 2\lambda) \frac{1}{\sigma\sqrt{2\pi}} \int_{-\infty}^{x} e^{-(y-\mu)^2/2\sigma^2} \mathrm{d}y. \qquad (1.25)$$

The mean of the curve μ reflects the point of subjective equality (PSE) where the participant perceives the stimulus orientation to be equal to the reference orientation. A difference between μ and the reference orientation indicates a systematic perceptual bias. The variance of the curve σ^2 can be interpreted as a measure of perceptual uncertainty and is inversely related to the precision (see Section 1.2.1). The lapse parameter λ is included to account for participant errors that are not related to the stimulus. To obtain psychometric measures of spatial orientation perception, Clemens et al. (2011) roll-tilted the participant using a vestibular chair (see Figure 1.5A). Participants performed two psychophysical tasks in complete darkness: the subjective body tilt (SBT) task (see Figure 1.5B), which provides a measure of perceived body orientation in space, and the subjective visual vertical (SVV) task (see Figure 1.5C), which provides a measure of perceived earth-vertical orientation.

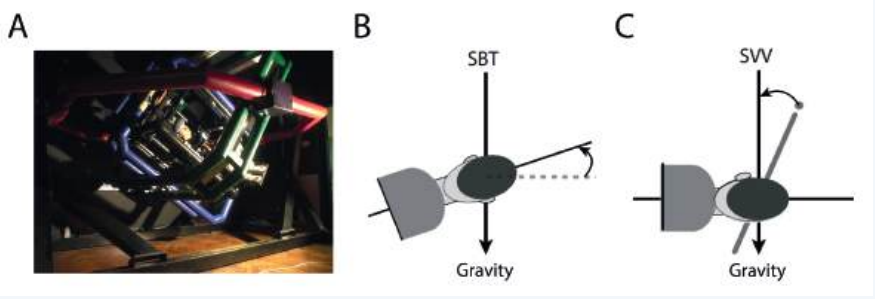

Figure 1.5. *A*: Vestibular chair setup consisting of a computer-controlled chair that rotates the participant in the roll axis. *B*: SBT task. On each trial, the participant is roll-tilted at a given stimulus orientation and asked to indicate whether they perceive their orientation to be CW or CCW relative to the reference orientation (dashed line). *C*: SVV task. On each trial, the participant is roll-tilted at a given stimulus orientation and asked to indicate whether they perceive the visual line orientation to be CW or CCW relative to gravity. Panel *B* and *C* are adapted from Alberts et al. (2015).

To what extent does the assumed Gaussian prior distribution in the Bayesian inference model of Clemens et al. (2011) match the distribution of head orientations measured outside the laboratory? To answer this question, I analyze previously gathered (but unpublished) data (Pomante, 2019) from five out-of-lab tasks (see Box 2). The probability density function that best describes the natural out-of-lab head orientations is subsequently incorporated as a prior distribution of head orientation in the Clemens et al. (2011) model to evaluate to what extent natural head statistics influence orientation perception.

Box 2. Out-of-lab tasks

To measure natural motion statistics, we can make use of inertial measurement units (IMUs). Each IMU contains an accelerometer, a gyroscope, and a magnetometer. Using a Kalman filter model, the different sensor measurements are combined to provide a measurement of the device's orientation with respect to a fixed reference frame (Xsens, 2018). By attaching the IMUs to body segments, we can obtain a readout of the segment's orientation across time. Participants wore 11 IMUs placed on the upper body (see Figure 1.6A) and performed 5 out-of-lab tasks in and around the university: walking, running, sitting, standing, and going up and down the stairs. Figure 1.6B shows example traces of head orientations in the roll axis for one of the participants in the out-of-lab experiment. Pooling the data of all tasks results in a distribution of natural head orientations (see Figure 1.6C). Using maximum likelihood estimation, I identified the probability density function (PDF) that best describes the head orientation data.

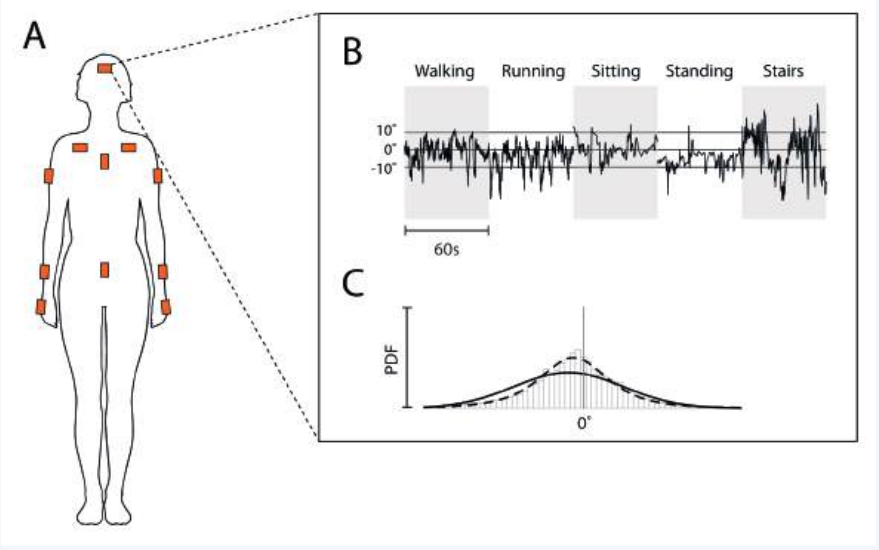

Figure 1.6. *A*: Placement of the IMUs on the upper body. Figure adapted from image published under the CC BY 4.0 license (Servier, 2016). *B*: Example 60-s traces of the measured head roll-tilt data in the five tasks for one participant. *C*: The best-fitting Gaussian (solid line) and *t*-location-scale (dashed line) PDFs plotted on top of all head roll-tilt data, pooled across tasks, for the same participant as in panel *B*.

1.3.2 Self-motion perception

When we move along a path in space, we continuously keep track of our position by integration of successive self-motion signals. This process is referred to as path integration (Darwin, 1873; Mittelstaedt & Mittelstaedt, 1980; Etienne & Jeffery, 2004). Path integration is often studied using distance reproduction tasks: on each trial, the participant is presented with a stimulus distance which they subsequently try to reproduce. The reproduction task can be virtual, providing the participant with only visual signals (Petzschner & Glasauer, 2011). Reproducing physical distances, e.g., by walking (Lappe & Frenz, 2009) or driving a vehicle (Israël et al., 1997), additionally generates vestibular, somatosensory, and reafferent sensory signals. In **Chapters 3** and **4**, I study how the distribution and presentation order of experimental stimuli affect vestibular self-motion perception using a physical path integration task (see Box 3).

Box 3. Path integration task

To study self-motion perception, we test participants in a path integration task that makes use of a vestibular sled (see Figure 1.7). The vestibular sled setup consists of a chair on top of a linear motion platform that can produce lateral translations. A steering wheel is mounted on a table in front of the chair. The sled can be passively moved by the experimenter or actively controlled by the participant through rotation of the steering wheel. The angle of the steering wheel relative to the upright steering wheel position encodes the linear velocity of the sled. This means that the further CW/CCW the steering wheel is rotated from its neutral position, the faster the sled moves to the right/left. The sled can be stopped by rotating the steering wheel back to the upright neutral position. During a trial of the path integration task, the sled first passively moves the participant a pre-defined stimulus distance. Subsequently, the participant is tasked with actively reproducing this distance. By comparing the measured reproduced distances to the stimulus distances, the participant's reproduction behavior can be quantified.

The task is performed in complete darkness and the participant wears headphones that play white noise to mask the sound that is generated by the sled. The head is fixated upright using ear cups such that the vestibular signals encode lateral head movement. During the passive stimulus movement, the participant receives no reafferent sensory signals, ensuring that the sensory signals that are available during the stimulus movement are limited to inertial (vestibular and somatosensory) signals. Somatosensory signals (e.g., generated by the pressure of the chair against the body) seem to play a minor role in self-motion perception compared to vestibular signals (Walsh, 1961; Harris et al., 2002). Given that the stimulus movement mostly activates the vestibular system, this task is therefore referred to in this thesis as a vestibular path integration task.

Figure 1.7. The vestibular sled setup, consisting of a chair on top of a linear motion platform. Image reproduced (with permission) from van Helvert (2025).

Central tendency and serial dependence

It has often been observed that reproductions are not veridical but biased by previously experienced stimuli. Two biases that are prevalent across reproduction tasks are referred to as the central tendency effect and the serial dependence effect. Central tendency describes the observation that reproductions are generally biased toward the center value of the experimental stimulus distribution, characterized by overestimations of short stimuli and underestimations of long stimuli (Hollingworth, 1910). This effect has been observed in a wide range of perceptual tasks, including the perception of distances (Loomis et al., 1993; Philbeck & Loomis, 1997; Israël et al., 1997; Grasso et al., 1999; Riecke et al., 2002; Bergmann et al., 2011; Petzschner & Glasauer, 2011; Petzschner et al., 2012; Prsa et al., 2015), heading (Warren & Saunders, 1995; Sun et al., 2020), durations (Jazayeri & Shadlen, 2010; Cicchini et al., 2012; Murai & Yotsumoto, 2016; Roach et

al., 2017), line lengths (Duffy et al., 2010; Ashourian & Loewenstein, 2011), and colors (Olkkonen & Allred, 2014; Olkkonen et al., 2014).

Serial dependence refers to the finding that the reproduction on the current trial is affected by the stimulus on the previous trial (Holland & Lockhead, 1968; Cross, 1973). Attractive serial dependence reflects reproductions that are biased toward the previous stimulus (Fischer & Whitney, 2014; Liberman et al., 2014; Motala et al., 2020; Manassi & Whitney, 2022, 2024; Guan & Goettker, 2024), whereas repulsive serial dependence indicates reproductions that are biased away from the previous stimulus (Fritsche et al., 2017; Sun et al., 2020). Both the central tendency and serial dependence biases reflect an effect of stimulus history but on different timescales: central tendency can be seen as the long-term effect of the measured stimuli across the experiment, whereas serial dependence captures the short-term effect of the previous stimulus (Saarela et al., 2023).

In **Chapter 3**, I study whether central tendency and serial dependence effects are present in vestibular path integration behavior. Furthermore, I examine whether the experimental stimulus distribution from which the stimulus distances are sampled, as well as the presentation order of the stimulus distances, affect these biases in vestibular path integration. Stimulus distances are sampled from two probability distributions, covering a range of short and long distances, and presented in two experimental conditions with different presentation orders. In the blocked condition, the short and long distances are presented in two separate blocks, whereas in the mixed condition, the same short and long distances are randomly interleaved. The effects of stimulus distribution (short/long) and presentation order (mixed/blocked) on the central tendency and serial dependence biases are then evaluated. Finally, I test to what extent the biases can be explained by sequential Bayesian inference models with different assumptions about the experimental stimulus distribution (see Section 1.2.3; Glasauer & Shi, 2022).

In **Chapter 4**, I examine a different aspect of the stimulus presentation order: the amount of autocorrelation in the stimulus sequence. Autocorrelation measures the similarity between values in a sequence. More specifically, it quantifies the correlation of a sequence with a lagged version of itself, where the lag-1 autocorrelation indicates how similar each value in the sequence is to the immediately preceding value. When stimuli are randomly sampled from the stimulus distribution (as in **Chapter 3**), the autocorrelation is (close to) 0. However, a value in a time series (e.g., today's stock value or temperature) is often similar to the previous value, resulting in an autocorrelated sequence. We can create a stimulus sequence with a high autocorrelation by simulating a random walk, where

the next stimulus is equal to the current stimulus plus a small normally-distributed random shift.

Studies on duration reproduction indicate that the autocorrelation of the stimulus sequence could cause a central tendency bias (Glasauer & Shi, 2021). The central tendency effect was present in reproduced durations when stimulus durations were presented in a randomized order (i.e., with no autocorrelation), whereas the effect was diminished when the same stimuli were presented in a random-walk order (i.e., with a high autocorrelation). The autocorrelation of the stimuli also seems to affect the serial dependence bias in duration reproductions: in the randomized order, the reproductions showed attractive serial dependence while in the random-walk order, the reproductions reflected repulsive serial dependence (Glasauer & Shi, 2022). In **Chapter 4**, I explore whether the amount of autocorrelation in the stimulus sequence could similarly affect the biases in vestibular path integration. To do so, stimulus distances are presented in a no- and high-autocorrelation condition, and the biases in the measured reproduced distances are compared across conditions. Central tendency and serial dependence are computed using a multiple linear regression model that controls for a potential indirect effect of the serial dependence bias on the central tendency bias (and vice versa) through the autocorrelated stimulus sequence (see Box 4).

Box 4. Central tendency and serial dependence computation

Central tendency is quantified as the slope of the linear least-squares regression of the reproduction error on the current trial, e_t, on the stimulus distance on the current trial, s_t. Here, the reproduction error refers to the difference between the reproduced and stimulus distance. A central tendency effect is indicated by a negative slope: shorter distances result in a more positive reproduction error than longer distances. Serial dependence is expressed as the slope of the linear regression of the current reproduction error, e_t, on the stimulus distance on the previous trial, s_{t-1}. The two biases are presented in a graph in Figure 1.8A. This figure illustrates the situation in which there is autocorrelation in the stimulus sequence, i.e., the value for s_t depends on the value of s_{t-1}. When computing the central tendency effect (i.e., the direct effect of s_t on e_t), we see that there may also be an indirect effect of s_t on e_t via s_{t-1}. Here, s_{t-1} is a common cause of both s_t and e_t, and to isolate the direct effect of s_t on e_t, the values for s_{t-1} should be

adjusted for in the central tendency regression. Similarly, when computing the serial dependence effect (i.e., the direct effect of s_{t-1} on e_t), there is an indirect effect through s_t. Here, s_{t-1}, s_t, and e_t form a causal chain, and to isolate the direct effect of s_{t-1} on e_t we should again control for the intermediate variable in the serial dependence computation. By adjusting for s_t, we can test whether s_{t-1} and e_t are conditionally independent.

This idea is formalized by the graphical *d*-separation criterion for directed acyclic graphs (DAGs; Pearl, 2009). The criterion states that if two variables X and Y form a causal chain (see Figure 1.8B) or have a common cause (see Figure 1.8C), the variables are conditionally independent if we condition on intermediate variable M. If two variables have a common effect (see Figure 1.8D), they are conditionally independent, *unless* we condition on M.

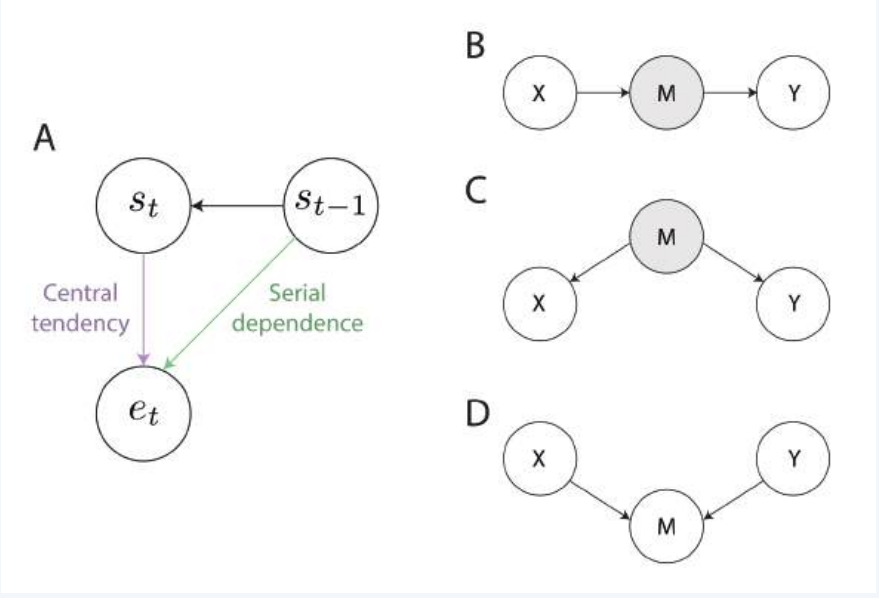

Figure 1.8. *A*: Graph illustrating the relationship between the central tendency and serial dependence effects when there is autocorrelation in the stimulus sequence. Nodes s_t, s_{t-1}, and e_t represent the stimulus distance on the current trial, the stimulus distance on the previous trial, and the reproduction error on the current trial, respectively. *B, C*: Causal chain and common cause structures, respectively. Conditioning (in gray) on variable M renders variables X and Y conditionally independent. *D*: Common effect structure, in which X and Y are conditionally independent unless M is conditioned on.

1.4 Thesis outline

In this thesis, I investigate the effect of prior information about previously experienced stimuli on spatial perception. I focus on two aspects of spatial perception: spatial orientation (**Chapter 2**) and self-motion perception (**Chapters 3** and **4**).

In **Chapter 2**, I examine to what extent different Bayesian prior distributions of head orientation can explain spatial orientation behavior. More specifically, I study whether spatial orientation estimates measured in two psychophysical tasks are better explained by a prior distribution that matches head orientations measured outside the laboratory, than by the previously assumed Gaussian prior distribution.

In **Chapter 3**, I examine whether central tendency and serial dependence biases are present in vestibular path integration behavior, and to what extent sequential Bayesian inference models can explain these biases. Additionally, I study how different experimental stimulus distributions (covering a range of short/long distances) and stimulus presentation orders (mixed/blocked) affect the central tendency and serial dependence biases.

In **Chapter 4**, I examine whether central tendency and serial dependence biases in vestibular path integration can be explained by different amounts of autocorrelation in the stimulus sequence. More specifically, stimulus distances are presented in a randomized order (with no autocorrelation) and in a random-walk order (with a high amount of autocorrelation), and the measured biases are compared across conditions.

In **Chapter 5**, I summarize and discuss the main findings of this thesis. Additionally, I identify limitations and propose ideas for future research.

Chapter 2

Natural statistics of head roll: Implications for Bayesian inference in spatial orientation

This chapter has been adapted from:

Willemsen, S. C. M. J., Oostwoud Wijdenes, L., van Beers, R. J., Koppen, M., & Medendorp, W. P. (2022). Natural statistics of head roll: Implications for Bayesian inference in spatial orientation. *Journal of Neurophysiology*, *128*(6), 1409-1420, with corrections incorporated from the published corrigendum.

2.1 Abstract

We previously proposed a Bayesian model of multisensory integration in spatial orientation (Clemens et al., 2011). Using a Gaussian prior, centered on an upright head orientation, this model could explain various perceptual observations in roll-tilted participants, such as the subjective visual vertical, the subjective body tilt (Clemens et al., 2011), the rod-and-frame effect (Alberts et al., 2016), as well as their clinical (Alberts et al., 2015) and age-related deficits (Alberts et al., 2019). Because it is generally assumed that the prior reflects an accumulated history of previous head orientations, and recent work on natural head motion suggests non-Gaussian statistics, we examined how the model would perform with a non-Gaussian prior. In the present study, we first experimentally generalized the previous observations in showing that also the natural statistics of head orientation are characterized by long tails, best quantified as a *t*-location-scale distribution. Next, we compared the performance of the Bayesian model and various model variants using such a *t*-distributed prior to the original model with the Gaussian prior on their accounts of previously published data of the subjective visual vertical and subjective body tilt tasks. All of these variants performed substantially worse than the original model, suggesting a special value of the Gaussian prior. We provide computational and neurophysiological reasons for the implementation of such a prior, in terms of its associated precision-accuracy trade-off in vertical perception across the tilt range.

2.2 Introduction

Sensory systems are thought to be optimized for processing naturalistic stimuli (Attneave, 1954; Simoncelli & Olshausen, 2001; Carriot et al., 2014; Mitchell et al., 2018). Given the uncertainty in the moment-to-moment sensory information, the statistical regularities within the sensory environment, which can be inferred from an accumulated history of the system's previous sensory states, add informational value to creating perception. For example, it has been shown that the "light-comes-from-above" experience is used to interpret complex and ambiguous visual input (Adams et al., 2004) and that the predominance of horizontal and vertical orientations in natural scenes is used in visual orientation perception (Girshick et al., 2011).

Bayesian theory provides a formal framework to describe sensory processing under uncertainty. According to this theory, next to the available sensory evidence also a default assumption about the state, expressed in the form of a prior distribution, is taken into account. Bayes' rule is the statistically optimal way to combine this prior with noisy sensory information. In laboratory-based paradigms, the prior often accounts for otherwise unexplainable biases (Mamassian & Goutcher, 2001; de Vrijer et al., 2008). Although the prior distribution can be of any type (Stocker & Simoncelli, 2006; Girshick et al., 2011), it is often assumed to be a Gaussian distribution for reasons of computational convenience (Bishop, 2006; Parise et al., 2014).

Earlier work from our laboratory has proposed a Bayesian model of multisensory integration for spatial orientation (Clemens et al., 2011). In this model, we assumed that, to process vestibular and other sensory information, the brain uses a Gaussian prior centered on upright. Based on this prior, the model could explain the well-known Aubert effect, the underestimation of head tilt, when the head is roll-oriented using a vestibular chair (Aubert, 1861; Udo De Haes, 1970; Mittelstaedt, 1983; van Beuzekom & van Gisbergen, 2000). In subsequent studies, we showed that this model could also explain age-related sensory reweighting in spatial orientation (Alberts et al., 2019), certain behavioral observations in patients (Alberts et al., 2015), and visual contextual effects on spatial orientation (Alberts et al., 2016). The model could also explain vertical perception in monkeys and proprioceptive reweighting following complete vestibular loss (Angelaki & Laurens, 2020). However, whether the Gaussian prior in this model reflects the statistics of head orientation during natural activities is unclear.

There are studies that suggest that natural motion statistics are typically described by non-Gaussian distributions (Schwabe & Blanke, 2008; Carriot et al., 2014; Hausamann et al., 2019). For example, Carriot et al. (2014) recorded the head's angular velocity and linear acceleration while participants performed everyday movements such as walking, running, or riding a bus. Measured probability distributions of the head's angular velocity and linear acceleration were not Gaussian but had long tails as quantified by large positive excess kurtosis values. Hausamann et al. (2019) measured head and trunk movements for long durations (>10 h) without explicit instructions and reported skewed acceleration distributions.

Building further on this work, in the present study, we test the hypothesis that the Aubert effect in spatial orientation is explained by a prior that corresponds to the statistics of head orientation during natural activities. Adding to and generalizing the existing literature about the statistics of natural head motion, we first recorded head orientation in human participants while they performed everyday movements and calculated probability density distributions of head orientation in space. The kurtosis values obtained generally indicated clearly non-Gaussian distributions. Next, the original Gaussian model by Clemens et al. (2011) with a closed-form solution was converted into a numerical model to enable computations with non-Gaussian priors. This numerical model was fit to the previously obtained psychometric data on spatial orientation to test whether alternative real-world priors account for laboratory-derived Aubert effects. As all data are interpreted within the general structure of the model by Clemens et al. (2011), we begin with a short modeling background.

2.2.1 Modeling background

Clemens et al. (2011) proposed a Bayesian model of the transformation and integration of various sensory signals (from body, head, and neck) into two spatial orientation estimates: the subjective body tilt (SBT) and subjective visual vertical (SVV) (see Figure 2.1). The sensory signals considered are body orientation in space from tactile receptors in the skin, head orientation in space as being provided by the otoliths, and head orientation relative to the body by neck proprioception. These sensory signals are represented by Gaussian distributions. The neck signal provides a transformation between body orientation and head orientation, thus creating indirect sources of information for both estimates. Final optimal estimates involve the integration of direct and indirect information as well as prior information.

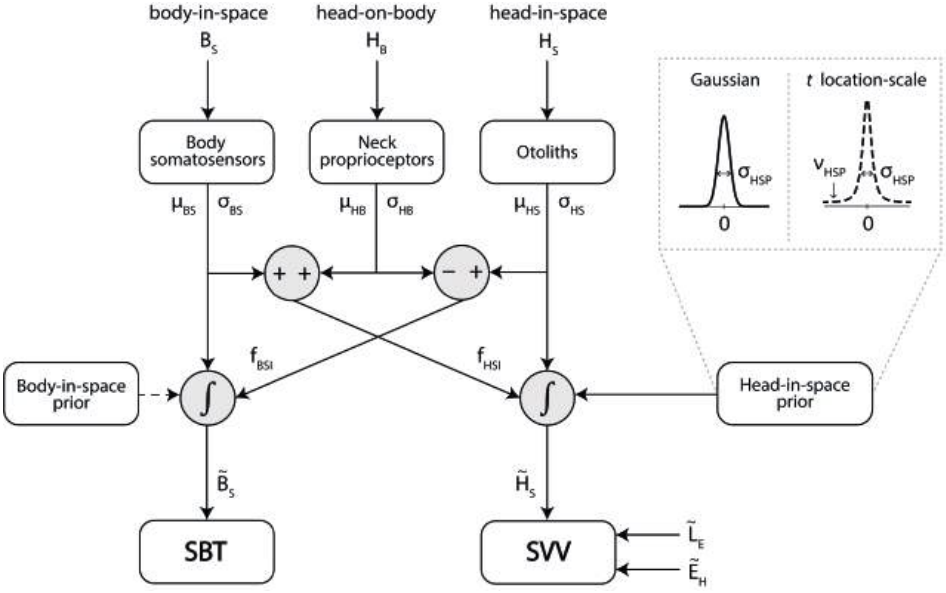

Figure 2.1. Schematic representation of the sensory integration model by Clemens et al. (2011). Body somatosensors, neck proprioceptors, and otoliths measure the orientation of the body in space (B_S), the head on the body (H_B), and the head in space (H_S), respectively. The neck signal enables a reference frame transformation of the body-tilt signal into a head-in-space signal (f_{HSI}) and a transformation of the head-tilt signal into a body-in-space signal (f_{BSI}). To compute the optimal estimate of body orientation ($\tilde{B}_S$), the body-tilt signal is combined with the transformed head-tilt signal, assuming a uniform body-in-space prior. The optimal estimate of head-in-space orientation ($\tilde{H}_S$) is determined by integration of the otolith signal, the transformed body-in-space signal and a head-in-space prior. The original model by Clemens et al. (2011) represents the head-in-space prior as a Gaussian distribution with a mean fixed at 0 and standard deviation σ_{HSP}. In the current study, we consider a *t*-location-scale distribution with a location parameter fixed at 0, scale parameter σ_{HSP}, and shape parameter ν_{HSP} as head-in-space prior. To acquire an estimate of the line-in-space orientation, $\tilde{H}_S$ is combined with estimates of the eye-in-head ($\tilde{E}_H$) and line-on-eye ($\tilde{L}_E$) orientation. SBT, subjective body tilt; SVV, subjective visual vertical.

Clemens et al. (2011) took all three sensory distributions to be unbiased Gaussians, i.e., with a mean equal to the actual tilt angle. The standard deviations of the body sensor and neck sensor constitute two free parameters σ_{BS} and σ_{HB}, respectively, whereas the standard deviation of the otolith signal is assumed to increase linearly with absolute tilt angle (de Vrijer et al., 2008, 2009), requiring another two free parameters a_{HS} and b_{HS}, with $\sigma_{\mathrm{HS}} = a_{\mathrm{HS}} \cdot |\mathrm{tilt}| + b_{\mathrm{HS}}$.

Because the SBT data were virtually unbiased across the tilt range, an uninformative, flat body-in-space prior was used, but Clemens et al. (2011) included a head-in-space prior centered on zero to account for the systematic

underestimation at large tilt angles as observed in the SVV data – the Aubert effect. This prior distribution was also assumed to be Gaussian, with standard deviation σ_{HSP} as another free parameter.

As the SVV pertains to the perceived orientation of a visual line, the final head-in-space estimate is to be supplemented with an eye-in-head estimate (E_H), involving the amplitude of the uncompensated ocular counterroll (A_{OCR}) as a free parameter, and a retinal line orientation estimate (L_E), assumed to be accurate. Both E_H and L_E have small noise levels (<1°), which were ignored. In addition to the six parameters mentioned, the model has a seventh parameter λ to account for lapses with an upper bound of 0.06.

In the current study, we focused on the assumption that prior knowledge about head orientation is represented as a Gaussian distribution, and we wanted to test whether the Clemens et al. (2011) model can better explain the data using a prior distribution corresponding more closely to the statistics of head orientation in everyday life. Based on previous results (Schwabe & Blanke, 2008; Carriot et al., 2014; Hausamann et al., 2019) as well as newly recorded data (see Methods and Results), we considered the *t*-location-scale distribution as an alternative distribution for the head-in-space prior. The *t*-location-scale distribution is symmetric and unimodal (bell-shaped), like the Gaussian, but it has heavier tails. It has one more parameter than the Gaussian distribution, which influences the shape of the distribution. The *t*-location-scale probability density function is given by

$$p\left(x \mid \mu, \sigma, \nu\right) = \frac{\Gamma\left(\frac{\nu+1}{2}\right)}{\Gamma\left(\frac{\nu}{2}\right)\sqrt{\pi\nu}\sigma}\left(1 + \frac{1}{\nu}\left(\frac{x-\mu}{\sigma}\right)^2\right)^{-\frac{\nu+1}{2}}, \quad (2.1)$$

where $\Gamma(\cdot)$ is the gamma function, μ the location parameter, σ the scale parameter, and ν the shape parameter ($\nu > 0$). Smaller values of ν yield heavier tails; as ν increases towards infinity, the *t*-location-scale distribution approaches the Gaussian distribution. A direct consequence of this adaptation to the Clemens et al. (2011) model is that closed-form expressions for the posterior distribution in terms of the likelihood and prior distributions no longer exist. All computations were therefore done numerically.

2.3 Methods

2.3.1 Data sets

Two data sets were used to test the model predictions. The first data set, collected previously, is extensively described in Clemens et al. (2011). This data collection tabulates psychometric data of seven participants (6 males, 1 female), aged 23–65 yr, each performing the SBT and SVV task at different tilt angles, passively imposed by a vestibular chair. Each participant performed 20 experimental sessions of 45 min each, yielding over 15 h of recording time. In short, in the SBT task, participants were first rotated to a randomly chosen tilt angle and then asked to indicate whether their body orientation was clockwise (CW) or counterclockwise (CCW) from an instructed reference orientation [i.e., either upright (0°), 45° or 90° right side down, or 45° or 90° left side down]. Responses were collected using the method of constant stimuli, yielding 140 data points for each instructed reference orientation. The SVV was tested at nine roll-tilt angles, ranging from -120° to 120° at 30° intervals. At each tilt angle, a luminous line was briefly flashed, and the participant indicated whether its orientation in space was CW or CCW from the perceived direction of gravity. The line orientation was selected randomly from a set of 11 line orientations. Each set was tested 12 times, thus yielding a total of 132 data points for each tilt angle. The original model by Clemens et al. (2011), which assumed a Gaussian head-in-space prior, provided a very good account of these data.

The second data set was collected anew as a supplement to the existing literature about the statistics of natural head motion (Carriot et al., 2014; Hausamann et al., 2019; MacNeilage, 2020). Six participants (3 males, 3 females) aged 23–28 yr, free of any known neurological or movement disorders, gave written informed consent to track their unconstrained naturalistic motion using inertial measurement units (Xsens MTw Awinda), placed on the pelvis, shoulders, sternum, upper arms, forearms, hands, and head. The system was calibrated while the participant was standing in a relaxed, upright position, with their feet parallel to each other and their arms flat against their body, while looking straight ahead with a natural head position. Analogous to Carriot et al. (2014), participants performed five different naturalistic tasks in and around our university, each one to three times, for 2 min each: walking, running, going up and down the stairs, sitting, and standing. This study was approved by the ethics committee of the Faculty of Social Sciences of Radboud University Nijmegen, the Netherlands. To bring this data set to bear on the Clemens et al. (2011) model, we analyzed the roll-tilt angles of the head in space, in degrees. The preprocessing of the raw head orientation data (which was

measured in quaternion form) consisted of transforming the raw data to Euler roll-tilt angles in degrees. Head orientation distributions are described in terms of four statistical moments: mean, standard deviation, skewness, and kurtosis. To determine which probability distribution best captured the natural head statistics, theoretical distributions were fitted to the head orientation data using Matlab's built-in maximum likelihood estimation function. We considered the following probability distributions: the Gaussian, logistic, *t*-location-scale (McDonald & Newey, 1988), extreme value (Gumbel, 1985), and generalized extreme value distributions (Jenkinson, 1955). The resulting fits were ranked using the Akaike information criterion (AIC).

2.3.2 Modeling

Model implementation

The model was implemented in Matlab (R2019a, RRID: SCR_001622) and numerically simulated under different assumptions of the prior distribution. Incorporating a non-Gaussian prior into the model caused the closed-form expressions in the original model to no longer exist. Therefore, the probability distributions in the new model implementation were numerically approximated in a circular plane with a resolution of 0.1°. A smaller step size did not impact the model predictions but increased the duration of the fitting procedure considerably.

The model was evaluated 500 times for each tilt angle tested in the SBT and SVV tasks. On each of these 500 replications, the mean of each sensory signal (μ_{BS}, μ_{HB}, and μ_{HS}) was randomly drawn from a circular normal distribution, using the actual tilt angle on that trial (B_S, H_B, or H_S) as mean and the standard deviation of the sensory signal (σ_{BS}, σ_{HB}, or σ_{HS}) as standard deviation. The distributions of the indirect signals (f_{BSI} and f_{HSI}) were computed following the expressions in Clemens et al. (2011) (Equations 2, 4, 6, and 8) as circular normal distributions with means $\mu_{\mathrm{HS}} - \mu_{\mathrm{HB}}$ and $\mu_{\mathrm{BS}} + \mu_{\mathrm{HB}}$ and standard deviations $\sqrt{\sigma_{\mathrm{HS}}^2 + \sigma_{\mathrm{HB}}^2}$ and $\sqrt{\sigma_{\mathrm{BS}}^2 + \sigma_{\mathrm{HB}}^2}$, respectively. The body-in-space posterior distribution consists of an integration of the directly and indirectly measured body-in-space information. Similarly, the head-in-space posterior distribution was computed by integrating the (direct and indirect) sensory information and the prior distribution. Taking the mode of the posterior distributions then resulted in the final, optimal estimates (denoted by $\tilde{B}_S$ and $\tilde{H}_S$ in Figure 2.1). Note that with the prior in the form of a *t*-location-scale distribution, the resulting posterior is no longer symmetric. Finally, we averaged the modes across the 500 model simulations to determine $\mu(\tilde{B}_S)$ and $\mu(\tilde{H}_S)$ for each tilt angle tested in the two tasks. Similarly, the variance of the

modes represents $\sigma^2(\tilde{B}_S)$ and $\sigma^2(\tilde{H}_S)$. We verified our numerical implementation by fitting the model with a Gaussian prior and found similar model likelihoods and fitted parameter values via the original estimation procedure used in Clemens et al. (2011), validating the new implementation.

Model variants and their evaluation

The numerical model version allows to test the model architecture under various assumptions. Models were fitted to the data set from Clemens et al. (2011) by minimizing the negative log-likelihood function using the Matlab function *fmincon* [see Clemens et al. (2011) for a detailed description of the fitting procedure]. We tested various variants of the model with a Gaussian prior (GP models) or a *t*-location-scale prior (TP models), which are summarized in Figure 2.4. We computed AIC scores to evaluate their performance by accounting for different numbers of free parameters. A lower AIC score indicates a better description of the data by a model variant.

Model variant 1: m1-GP. This GP model is the numerical version of the original model by Clemens et al. (2011) (from here on denoted as the m1-GP model). The original model contains seven free parameters: a_{HS}, b_{HS}, σ_{BS}, σ_{HB}, A_{OCR}, λ, and σ_{HSP} as the standard deviation of the Gaussian prior. Per participant, this model was fitted 100 times. For half of the fitting runs, random values within fixed bounds (a_{HS}: [0, 0.5]°/°, b_{HS}, σ_{BS}, σ_{HB}, σ_{HSP}: [1e-05, 50]°, A_{OCR}: [0, 30]°, λ: [0, 0.06]) were used as start values for the free parameters to maximize the possibility of convergence to the global minimum. The remaining runs were started with the fitted values from the Clemens et al. (2011) study. Note, allowing a free parameter for the mean of the prior led to a fitted value close to 0. Therefore, this parameter was fixed at 0 during fitting.

Model variant 2: m2-TP. This TP model fitted the Clemens et al. (2011) data set with the same free parameters but under the assumption of a *t*-location-scale prior (from here on denoted as the m2-TP model), which turned out to be the best description of the naturalistic head orientations in our data (see Figure 2.2B), corroborating previous literature (Carriot et al., 2014). The shape parameter of the *t*-location-scale-prior distribution (ν_{HSP}) was fixed at the average parameter value of the best-fitting distribution on the naturalistic head orientation data (see Supplemental Table 2.S2 in the Supplemental material). The fitting procedure was as for model 1. In further analyses, we also fitted this model using the shape parameter fixed at either 6, 10, 25, 50, 100, or 300 (resembling a Gaussian distribution), each fitted 50 times.

Model variant 3: m3-GP, m3-TP. In models 1 and 2, the standard deviation of the otolith noise depends linearly on the absolute head tilt. Instead, in model variant 3, we fitted a TP model without an imposed relationship between otolith noise and tilt angle, i.e., we allowed the standard deviation of the otolith noise to be a free parameter for each absolute tilt angle (from here on denoted as the m3-TP model). We used the fitted intercept and slope values of the Clemens et al. (2011) study to compute a standard deviation for each tilt angle. These values were then used as the initial values for the free parameters in the fitting procedure, after which the parameters could take on any value within [1e-05, 50]°. We also repeated the fitting procedure with random start values for the free parameters. For comparison, this assumption was also tested for a Gaussian prior (the m3-GP model). Each version was fitted 100 times.

Model variant 4. This model variant involved a Gaussian-mixture distribution as head-in-space prior. A mixture of two Gaussians with the same mean but different SDs yields a distribution with heavier tails (to approximate the measured prior). We tested a prior distribution characterized by three parameters: the standard deviations of the two Gaussians, $\sigma_{\mathrm{HSP}-1}$ and $\sigma_{\mathrm{HSP}-2}$, and their mixing coefficient *c*, defined between 0 and 1, which weighs the two distributions. The means of both Gaussians were fixed at 0. The fitted values from Clemens et al. (2011) were used as start values for the fitting procedure, where the fitted value for the standard deviation of the prior, σ_{HSP}, served as start value for $\sigma_{\mathrm{HSP}-1}$. The start value for $\sigma_{\mathrm{HSP}-2}$ was 50° and the initial value of the mixing coefficient was valued either 0.25, 0.5, 0.75, or 1. The model was fitted 50 times for each of the different start values for the mixing coefficient.

Model variant 5: m5-GP, m5-TP. In the original model, the sensory measurements at a particular tilt angle are assumed to be unbiased on average but contaminated with independent Gaussian noise. This is referred to as a measurement distribution, i.e., the distribution of sensory tilt signals that is produced when the head is tilted at a specific angle. However, the brain must perform the inverse approach to find out which tilt angle has been responsible for the sensory signal that it receives. Hence, it must compute the sensory likelihoods. If the measurement distribution of a sensory signal is Gaussian with a constant standard deviation, irrespective of tilt, the likelihoods will be Gaussian as well. For the otoliths, however, the standard deviation of the noise was assumed to be increasing with tilt angle, which formally results in a skewed otolith likelihood [see Girshick et al. (2011) for a more detailed explanation]. This nonlinear transformation was neglected in the original model – we assumed a symmetric otolith likelihood – but was put to test in variant 5. This model variant contained

the same free parameters as m1-GP and m2-TP and was again fitted 100 times per prior form (from here on denoted as the m5-GP and m5-TP models).

2.4 Results

We investigated the role of the prior's form in a Bayesian model of spatial orientation, as assessed by the subjective visual vertical and subjective body tilt tasks at tilt angles between -120° to 120° using non-naturalistic stimuli in a laboratory-based environment. Data from these tasks were previously collected and extensively described and modeled using a Gaussian head-tilt prior in Clemens et al. (2011). However, more recent work on head motion statistics reported that probability distributions of angular velocity and linear acceleration averaged across natural activities were not Gaussian, showing large positive excess kurtosis values (Carriot et al., 2014). We first examined whether this observation can be generalized to head tilt distributions by measuring the head orientation statistics of human participants during typical everyday activities, and subsequently tested whether the model fit of the Clemens et al. (2011) data can be improved by canceling the restriction to a Gaussian prior and allowing prior distributions more akin to these naturalistic head orientation distributions.

2.4.1 Natural head orientation statistics

Figure 2.2A shows head orientation as a function of time for the various activities (i.e., walking, running, going up and down the stairs, sitting, and standing), separately for each participant. We found that the recorded head orientations varied across the activities. For example, over consecutive samples, the changes in head tilt were smaller during sitting and standing than during the other activities. Furthermore, we found that probability distributions of head orientation pooled across activities were not Gaussian (Figure 2.2B) as quantified by large (between 5 and 142) kurtosis values across participants (Figure 2.2B, insets). This indicates that head tilt distributions have longer tails and a higher peak than would be expected from normally distributed data. Across participants the ranges of the first three statistical moments of the head orientation data were $M = -2.9^\circ - 1.0^\circ$, $SD = 6.3^\circ - 10.3^\circ$ and $S = -2.1 - 3.2$, indicating that the head tilt distribution centers on upright and shows no systematic skewness.

We next tested for each participant which of several probability distributions – the Gaussian, logistic, *t*-location-scale, extreme value, and generalized extreme value

distributions – best accounted for the measured head orientation statistics. We found that, pooled across activities, a *t*-location-scale distribution provided the best fit for five of the six participants, outperforming the Gaussian distribution in all cases (compare solid and dashed lines in Figure 2.2B). The relatively skewed data of participant 2 are described best by the extreme value distribution, followed by the *t*-location-scale distribution. We refer to Supplemental Table 2.S1 in the Supplemental material for a comparison of the AIC scores of all fitted distributions. The parameters of the fitted *t*-location-scale distribution are consistent across participants (see Supplemental Table 2.S2); the location parameter is close to 0 (range: -1.9° to 1.1°), indicating that participants held their head on average upright, the scale parameter ranged between 3.9° and 6.8°, and the shape parameter was small (range: 2.2 – 4.3), corresponding to a characterization in terms of long tails. The results are consistent with previously reported distributions of head velocity and acceleration (Carriot et al., 2014; Hausamann et al., 2019).

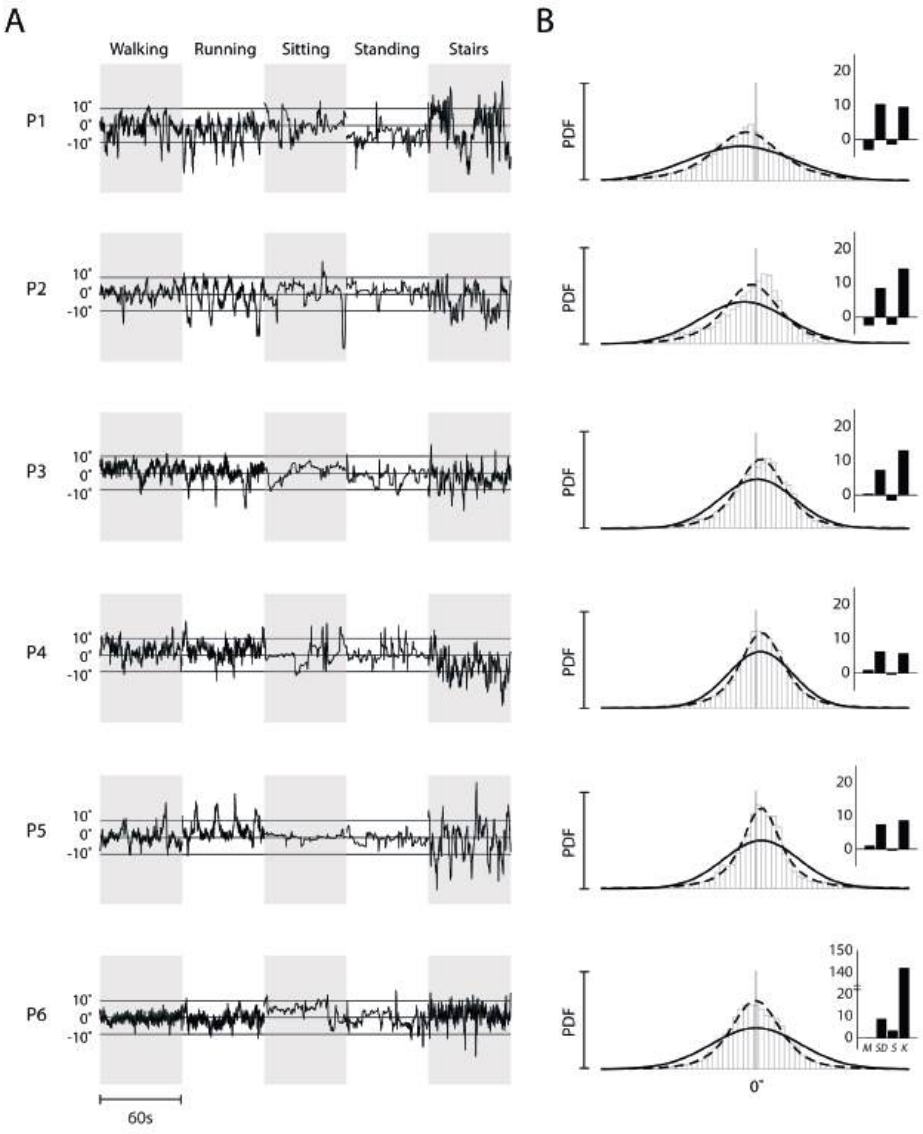

Figure 2.2. *A*: Representative 60-s traces of the measured head orientations during the different activities, for each participant. *B*: Fitted normal (solid line) and *t*-location-scale (dashed line) probability density distributions (PDFs), plotted on top of all head roll-tilt data, pooled across activities for each participant in the naturalistic motion tracking experiment. Insets show the four statistical moments (mean M, standard deviation SD, skewness S and kurtosis K) of the pooled data.

2.4.2 Bayesian modeling of spatial orientation

Model variants 1 and 2

We subsequently tested the assumption that these natural statistics of head orientation are used as a prior in spatial orientation and can account for the observations in the SVV and SBT tasks reported by Clemens et al. (2011). Within the structure of their Bayesian model of spatial orientation (Figure 2.1), we compared the predicted performance in the SBT and SVV tasks under the assumption of a Gaussian-head-tilt prior (m1-GP) and a *t*-location-scale prior [m2-TP, shape parameter fixed at 3.4, which was the average best-fitting shape parameter value on the naturalistic head orientation data (see Supplemental Table 2.S2)].

Figure 2.3 shows these predictions as the average (±SD) of the individual best fits superimposed on the mean data across participants. The prediction of the m1-GP model replicates well the closed-form model fit. In contrast, the m2-TP model provides a poor fit, both with regard to the observed bias in the SVV (the Aubert effect) and, more prominently, its variance. Also, the variance of the SBT seems not well accounted for by this TP model.

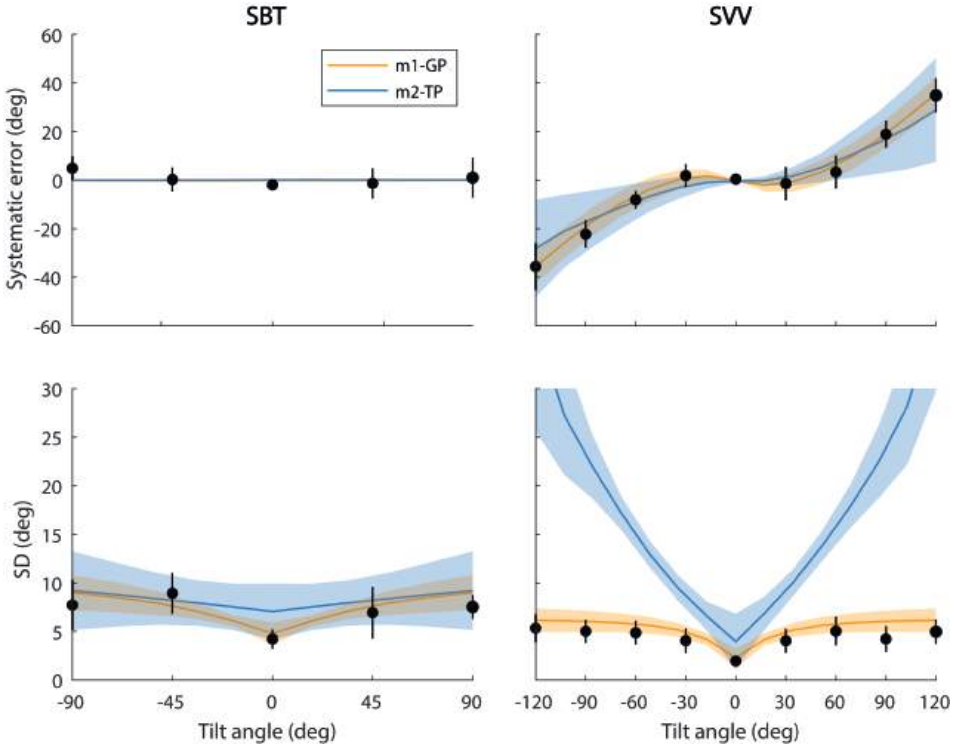

Figure 2.3. Predictions of the m1-GP (orange) and m2-TP models ($\nu = 3.4$, blue) of the SBT (left column) and SVV (right column), generated with the best-fitting parameter values per participant and then averaged across participants, plotted on top of the mean parameters from the psychometric fits (•). Shaded areas and error bars show one standard deviation above and below the participant mean. SBT, subjective body tilt; SVV, subjective visual vertical.

To compare the quality of various model variants, we computed their AIC scores, averaged across participants. The baseline in this comparison is the mean AIC score of the m1-GP model, set to zero at the left in Figure 2.4. As shown, the m2-TP model ($\nu = 3.4$) performs substantially worse than the m1-GP model.

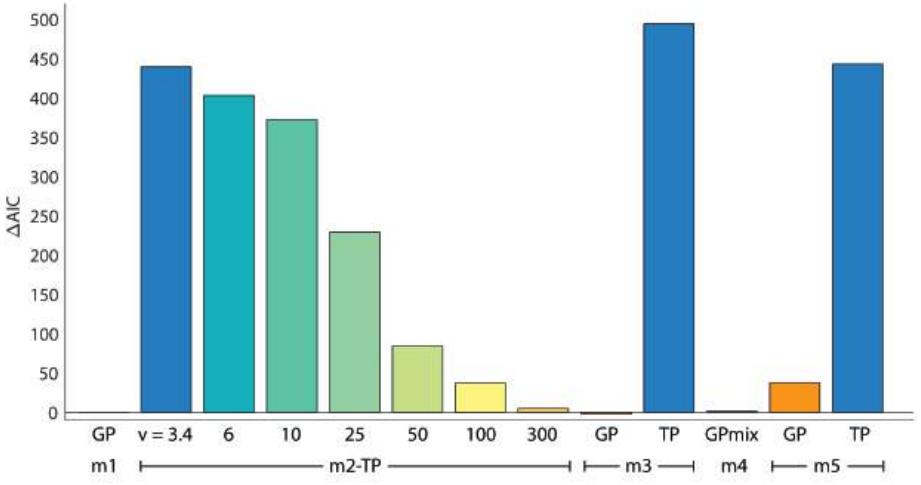

Figure 2.4. Comparison of the mean best Akaike information criterion (AIC) scores over participants of the different model variants, relative to the mean AIC score (439.2) of the Gaussian-prior model (m1-GP). A lower value indicates a better fit to the data. The different model variants are explained above (see Methods, Modeling, Model variants and their evaluation).

Table 2.1 illustrates the best-fit parameter values for each participant for the m1-GP and m2-TP ($\nu = 3.4$) models as well as the fit parameters reported in Clemens et al. (2011) based on the original closed-form implementation. Comparing the m1-GP model with the closed-form implementation reveals similar fitted parameter values, confirming the numerical implementation of the Clemens et al. (2011) model. The best-fitting m2-TP model yields large interparticipant variability for most of the parameters, suggesting that this TP variant does not capture the data very well.

Table 2.1. Best-fitting parameter values for the original implementation of the model as presented in Clemens et al. (2011) (O), the numerical model with a Gaussian prior (m1-GP) and the numerical model with the t-location-scale prior (m2-TP, $\nu = 3.4$). The mean parameter values and their respective standard deviations are computed by averaging across participants. The fit parameters had the following lower and upper bounds: a_{HS}: [0, 0.5]°/°, $b_{HS}, \sigma_{BS}, \sigma_{HB}, \sigma_{HSP}$: [1e-50, 50]°, A_{OCR}: [0, 30]°, λ: [0, 0.06] (fitted lapse rates not presented).

Parameter	a_{HS} **(°/°)**			b_{HS} **(°)**			σ_{BS} **(°)**		
Model version	**O**	**m1-GP**	**m2-TP**	**O**	**m1-GP**	**m2-TP**	**O**	**m1-GP**	**m2-TP**
Participant									
1	0.23	0.23	0.23	1.2	1.4	5.5	12.3	12.4	8.2
2	0.12	0.12	0.24	1.2	1.2	0.8	8.4	8.3	9.8
3	0.20	0.21	0.32	1.1	1.1	0.5	6.7	6.4	3.1
4	0.07	0.07	0.30	3.9	3.9	30.7	12.6	12.6	9.9
5	0.11	0.11	0.49	3.3	3.4	22.7	15.0	15.1	9.9
6	0.23	0.23	0.18	3.0	3.2	3.1	8.0	8.2	6.1
7	0.20	0.20	0.18	3.2	3.4	2.5	12.7	12.6	40.8
Mean ± SD	0.16 ± 0.06	0.17 ± 0.06	0.28 ± 0.11	2.4 ± 1.2	2.5 ± 1.2	9.4 ± 12.2	10.8 ± 3.1	10.8 ± 3.2	12.5 ± 12.7

Parameter	σ_{HB} **(°)**			A_{OCR} **(°)**			σ_{HSP} **(°)**		
Model version	**O**	**m1-GP**	**m2-TP**	**O**	**m1-GP**	**m2-TP**	**O**	**m1-GP**	**m2-TP**
Participant									
1	3.3	3.3	47.5	27.0	26.9	7.0	11.6	11.5	38.8
2	6.4	6.7	49.9	17.0	17.1	11.5	9.4	9.7	18.0
3	9.3	10.4	30.4	17.5	17.6	10.0	14.4	15.3	30.4
4	7.1	7.1	38.3	0.0	0.0	30.0	11.2	11.2	15.5
5	3.6	3.6	38.9	1.0	1.0	29.7	18.7	18.8	17.6
6	1.8	2.0	35.9	18.8	18.8	2.4	9.5	9.6	35.5
7	3.0	3.0	1.5	20.8	20.7	1.8	12.8	12.9	21.2
Mean ± SD	4.9 ± 2.7	5.2 ± 3.0	34.6 ± 16.1	14.6 ± 10.2	14.6 ± 10.1	13.2 ± 11.9	12.5 ± 3.2	12.7 ± 3.3	25.3 ± 9.5

Within the context of the m2-TP model, the decay rate of the prior distribution is captured by the shape parameter. The larger the value of this parameter, the closer

the distribution approximates a Gaussian distribution. Figure 2.5 illustrates the predictions of the m2-TP model with the shape parameter fixed at 6, 10, 25, 50, 100, and 300 and averaged across participants, superimposed on the prediction of the m1-GP model. The model fit clearly improves with a larger shape parameter, which is confirmed by the corresponding ΔAIC scores in Figure 2.4, suggesting that the model better operates as the *t*-location-scale prior approximates a Gaussian. This is in stark contrast with the shape parameter values of 2.2 – 4.3 that we observed in the natural head orientations.

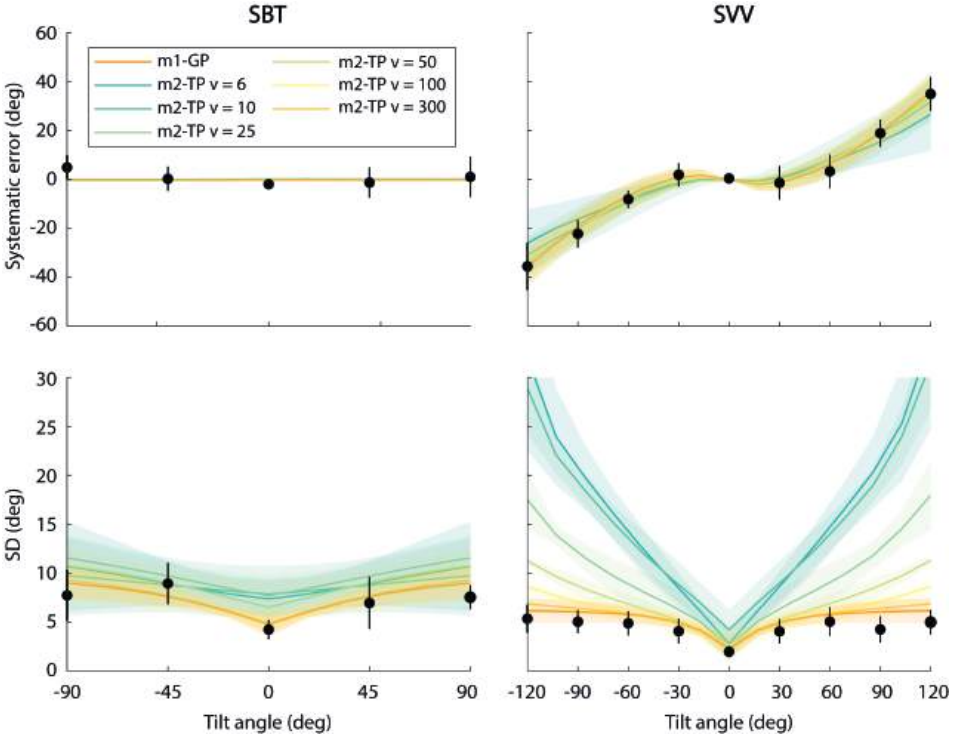

Figure 2.5. Predictions of the m2-TP model with different shape parameters (ν = 6, 10, 25, 50, 100, or 300) and the m1-GP model, plotted on top of the mean parameters from the psychometric fits (•). Data are in the same format as in Figure 2.3.

Model variant 3

We next examined if releasing other model constraints can redeem the TP model. One constraint of the original model is that the standard deviation of the otolith noise depends linearly on the (absolute) tilt angle. In model variant 3, we lifted this constraint and fitted the GP and TP models with the standard deviation of the otolith noise as a free parameter for each absolute tilt angle. With this additional

flexibility, the m3-GP model still performed very well, but the m3-TP model did not improve, showing a higher ΔAIC score than without this flexibility (see Figure 2.4).

Figure 2.6 shows for both models the best-fitting values of otolith noise SD as a function of tilt angle, averaged across participants. For both models, there seems to be a linear relationship with absolute tilt angle, validating this constraint within the original model.

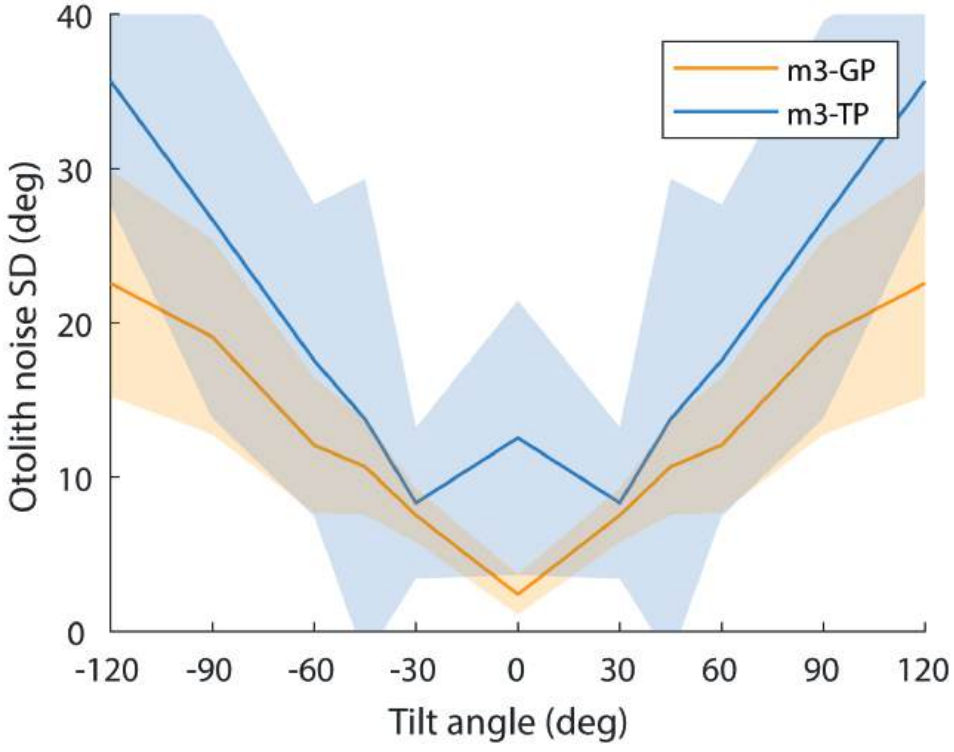

Figure 2.6. Best-fitting otolith noise values of the Gaussian-prior (orange) and *t*-location-scale-prior (blue) models as a function of tilt angle, averaged across participants. Shaded areas show one standard deviation above and below the participant mean.

Model variant 4

In model variant 4, we tested if a head-tilt prior that consists of a mixture of two Gaussians, which compared with a *t*-location-scale distribution, can result in an alternative prior distribution with longer tails than a single Gaussian, fitted the data of Clemens et al. (2011). The AIC score of the best-fitting Gaussian-mixture-prior model is comparable to the m1-GP model AIC score [but slightly higher, caused by the extra free parameters of the Gaussian-mixture prior (see Figure 2.4)]. However,

we found the mixing coefficients to be exactly 1, reducing the Gaussian-mixture distribution in fact to the single Gaussian distribution of the m1-GP model. Thus, the m1-GP model holds as the most parsimonious explanation of the data.

Model variant 5

Finally, we fitted a model variant that contains a skewed distribution for the otolith likelihood instead of the symmetric, Gaussian otolith likelihood in the original model. Again, the GP version of this model outperformed the same model with a *t*-location-scale prior. Furthermore, the m5-GP model performed worse than the original model in terms of AIC score (see Figure 2.4) and the m5-TP variant did not lead to an improved fit, showing a similar ΔAIC score as the m2-TP ($\nu = 3.4$) model.

2.5 Discussion

The starting point of the present study is the Bayesian model of spatial orientation that we first proposed in 2011 based on recordings in a non-naturalistic laboratory-based environment (Clemens et al., 2011). Specifically, a Gaussian-prior probability distribution of head roll was imposed to explain biases in the subjective vertical – known as the Aubert effect (see Figure 2.1). This prior probability distribution was regarded as a Bayesian observer's assumption that the head is usually nearly upright (Eggert, 1998; de Vrijer et al., 2008). Under the assumption that human observers are performing Bayesian inference for spatial orientation, we asked the question whether this form of the prior probability distribution is consistent with the natural statistics of head orientation, generated by human participants during everyday activities.

The answer is no. We found that the natural statistics of head orientation were poorly represented by Gaussian probability distributions but were characterized by long tails, as quantified by large kurtosis values. This observation extends observations by Carriot et al. (2014) on head velocity and acceleration distributions. Their kurtosis values (>10) are similar to the range we found (between 5 and 14, with the exception of the much larger kurtosis value of participant 6). In both studies, these statistics are based on the combined distribution of all activities tested, even though the range of head orientations varied across the activities. Also, separate analyses of the activities within subjects revealed distributions with excess kurtosis in nearly all cases (see Supplemental Table 2.S3), suggesting that the kurtosis does not originate from sampling from

different Gaussian distributions. This does not seem a divergent finding, as Schwabe & Blanke (2008) also reported deviations of normality of measured head pitch of human participants when they were standing, walking around, or moving as if they were playing tennis. Similar observations were made in visual and auditory modalities (Ruderman & Bialek, 1994; Attias & Schreiner, 1996; Geisler, 2008; Pavão et al., 2020). Also in songbirds, the distribution of the sung pitches is observed to have long, non-Gaussian tails (Zhou et al., 2018).

To model the naturalistic head orientation data, we fitted several probability distributions – the Gaussian, logistic, *t*-location-scale, extreme value, and generalized extreme value distributions – to the head orientation data of each participant. A Gaussian distribution was never the best-fitting function but was always outperformed by a *t*-location-scale distribution. The *t*-location-scale distribution approaches the Gaussian distribution as the shape parameter tends to infinity, whereas smaller values of the shape parameter yield heavier tails. The latter is what we observed. The best-fitting shape parameter ranged between 2.2 and 4.3 across our participants.

We further performed a Bayesian modeling analysis using the *t*-location-scale distribution of head roll as the prior. To this end, the original closed-form Bayesian model by Clemens et al. (2011) was turned into a numerical version. Although the numerical model could equally well account for response bias and variance in the subjective visual vertical and subjective body tilt tasks under the assumption of a Gaussian prior as the original model (see Figure 2.3), it failed dramatically with a *t*-location-scale prior (see ΔAIC scores in Figure 2.4). Indeed, the larger we allowed the shape parameter of the *t*-location-scale prior to be, i.e., the better it approximated a Gaussian, the better the model accounted for SVV and SBT performance. Adding more flexibility to the model by releasing constraints on the otolith likelihood did not improve the model with the *t*-location-scale prior form. Fitting the model with a Gaussian-mixture prior (an alternative prior distribution allowing long tails) returned a single Gaussian distribution as the best account. Also extending the model by including the nonlinear transformation between the otolith measurement distribution and likelihood failed to improve the *t*-location-scale prior fit (see Figure 2.4).

Given that natural statistics of head orientation are best characterized by a non-Gaussian distribution, why is SVV and SBT performance so much better accounted for by a Bayesian observer assuming a Gaussian head-in-space prior? We can only speculate about the answers to this question. First, the statistics of natural head motion may simply not be incorporated as a prior in such perceptual computations.

Carriot et al. (2014) have shown that the statistics of signals experienced during active movements differed from those experienced during passive movement. For instance, their participants experienced greater translational accelerations and angular velocities during active motion than passive motion. Typically, during active exploitation, the system relies heavily on sensory feedback to control our body to remain within limits of stability and to prevent falling. A *t*-distribution prior could define a "zone of stability" – a movement-relevant prior distribution to control the deliberate exploration of plausible motor commands that keeps the body within the borders of postural stability [cf. Zhou et al. (2018)].

A more theoretical explanation arises if one realizes that observing new evidence not always reduces uncertainty under Bayes' rule. In other words, a posterior distribution does not necessarily have a lower variance than the prior or likelihood distributions it is based upon. It can be shown that this holds in the case when the prior and likelihoods are Gaussian, but not in all other cases (Petty, 2018). Figure 2.7 illustrates this point. The posterior that follows from a Gaussian likelihood and *t*-location-scale prior can have a larger variance than either prior or likelihood, consistent with the predictions in Figure 2.3, where the SD of the SVV posterior is much larger with a *t*-location-scale prior than with a Gaussian prior. This increase in width (or decrease in precision) occurs when the distance between the prior and likelihood means becomes large enough. Hence, a *t*-location-scale prior can lead to a negative information gain (Petty, 2018), which is a situation that the brain may want to prevent. Instead, the posterior yields a smaller variance if it follows from a Gaussian prior. Gaussian priors will reduce the variance of the posterior across all Gaussian sensory likelihoods, thus creating a positive information gain (irrespective of the distance between the prior and likelihood distribution). New sensory evidence will thus decrease the system's uncertainty about the state it has adopted. In functional terms, for vertical perception, a Gaussian prior therefore amounts to a particular precision-accuracy trade-off across the tilt range; it suppresses uncertainty at the expense of a systematic bias at larger tilt angles (de Vrijer et al., 2008). This cannot generally be achieved with a *t*-location-scale prior in the context of the structure of the model by Clemens et al. (2011). We do not argue that no other model structures can be conceived that deal with this notion, but such conceptual analysis goes beyond the present investigation.

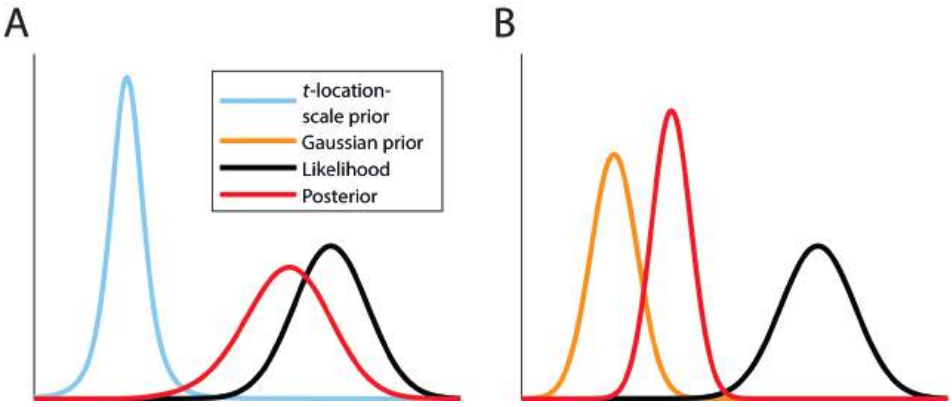

Figure 2.7. *A*: Integrating a *t*-location-scale prior (blue), which resembles the natural statistics of head orientations, with a Gaussian likelihood distribution (black) can lead to a posterior distribution (red) with a larger variance than the variances of the individual signals in the integration. *B*: Instead, the integration of a Gaussian prior (orange) and Gaussian likelihood (black) always results in a Gaussian posterior (red) with a lower variance than the variances of the individual signals.

The subsequent question then is, how can the brain develop a Gaussian head-in-space prior, while the natural head motion statistics are best approximated by a *t*-location-scale distribution? As in any biological system, neural variability plays a role in vestibular processing and determines the neural code at central levels (Sadeghi et al., 2007). Therefore, the signals at the level of the vestibular afferents will be noisier than the signals measured by the inertial measurement units, which will be close to the actual physical orientations. In other words, vestibular processing of head orientation signals is corrupted by additive (or multiplicative) noise (Mallery et al., 2010). Based on the central limit theorem, this could, over an extended exposure to natural stimuli and daily life tasks, convert the heavy-tailed distribution of measured head orientations into a more Gaussian distribution at the central level. If so, our results suggest that the brain stores this information and uses it as a prior in sensory processing for vertical perception.

At the neural level, vestibular afferents transmit data to the brain in trains of action potentials, and the brain needs to decode this information in terms of the head orientation, as well as other kinematic variables of head motion. It has been suggested that regular afferents transmit more information about changes in static head orientations than irregular afferents (Sadeghi et al., 2007; Jamali et al., 2019). The likelihood distribution of the head's kinematic state at the time of a spike of a given neuron differs from the prior distribution of states (Paulin & Hoffman, 2019). Because a single spike transmits only a small amount of information, the observer's uncertainty about the head's kinematic state will be reduced (i.e., the variance of

the posterior distribution will be smaller) if the prior distribution of states has a Gaussian form. More generally, it has been suggested that Bayesian computations with prior probabilities can rely on population vector decoding of neural populations with nonuniform preferred directions (Girshick et al., 2011; Cuturi & MacNeilage, 2013).

As a final note, the considerations above assume the notion of a stable real-world prior, derived from the statistics of movements during natural activities over a long time. Stable priors have also been suggested for processing in other sensory modalities, e.g., predominance of horizontal and vertical orientations in natural scenes for visual orientation perception (Attneave, 1954; Simoncelli & Olshausen, 2001; Vinje & Gallant, 2002; Girshick et al., 2011). However, priors could also be more flexible, or context-dependent, and adapt over a short time scale, as for example has been shown in perceptual (Roach et al., 2017), motor (Körding & Wolpert, 2004), or language-learning experiments (Griffiths & Kalish, 2005). It remains to be tested how participants can develop a context- or task-dependent prior based on the orientations experienced during the experiment. The optimal strategy, in this case, is called dynamic or sequential Bayesian inference, which assumes conditionally independent measurements and Markovian dynamics. Under a recursive structure, it minimizes uncertainty in task outcome or state by using the posterior distribution given all previous measurements as the prior distribution for inferring the posterior on the next trial (Doucet et al., 2001; Verstynen & Sabes, 2011; Petzschner et al., 2015; Zhou et al., 2018). More specifically, a prior belief is computed by prediction, requiring a kinematic forward model, and then the posterior is updated by combining the likelihood with the prior (Laurens & Droulez, 2007; Ellis & Mast, 2017). It would be an interesting avenue for future work to embed the spatial orientation model of Clemens et al. (2011) in this framework to find out which specific kinematic model could explain the dynamic SVV and SBT.

2.6 Supplemental material

Table 2.S1. Best-fitting distributions on the head roll-tilt data pooled across activities, per participant, and their respective AIC scores, relative to best fitting distribution.

Participant	Fitted probability distribution	AIC
1	*t*-location-scale	0
	logistic	5338.41
	extreme value	18082.09
	normal	24217.90
	generalized extreme value	44213.82
2	extreme value	0
	t-location-scale	11050.19
	logistic	15751.84
	generalized extreme value	32034.44
	normal	33534.12
3	*t*-location-scale	0
	logistic	5968.01
	normal	29410.35
	extreme value	32701.38
	generalized extreme value	51737.02
4	*t*-location-scale	0
	logistic	2560.41
	normal	13790.25
	generalized extreme value	29936.73
	extreme value	44681.60
5	*t*-location-scale	0
	logistic	11048.67
	normal	31269.14
	generalized extreme value	47624.77
	extreme value	66517.03
6	*t*-location-scale	0
	logistic	12507.65
	normal	92083.58
	generalized extreme value	250067.32
	extreme value	373372.50

Table 2.S2. Location, scale and (in the case of the *t*-location-scale distribution) shape parameter values of the *t*-location-scale and normal distributions that were fitted on the data pooled across activities for each participant. The bottom row shows the mean location, scale and shape parameters of the distributions, averaged across participants. The mean value of the shape parameter is used in the model fitting (see Methods, Modeling, Model variants and their evaluation, Model variant 2).

Participant	Probability distributions	Location parameter (°)	Scale parameter (°)	Shape parameter
1	*t*-location-scale normal	-1.91 -2.86	6.77 10.32	3.28
2	*t*-location-scale normal	-0.79 -2.27	5.57 8.48	3.33
3	*t*-location-scale normal	0.95 0.25	4.81 7.23	3.55
4	*t*-location-scale normal	1.11 0.86	4.39 6.29	3.52
5	*t*-location-scale normal	1.05 1.04	3.93 7.37	2.23
6	*t*-location-scale normal	-0.11 0.00	4.91 8.69	4.28
Mean	*t*-location-scale normal	0.05 -0.50	5.06 8.06	3.36

Table 2.S3. Kurtosis values of the data of each activity of each participant.

Participant	Walking	Running	Standing	Sitting	Stairs
1	7.24	11.27	7.23	2.83	6.68
2	8.95	3.99	12.89	26.80	2.46
3	13.70	9.26	23.85	7.11	5.36
4	5.31	4.37	4.48	5.20	3.79
5	15.86	4.17	14.07	57.37	3.51
6	5.59	4.16	83.99	3.56	5.50

Chapter 3

Central tendency and serial dependence in vestibular path integration

This chapter has been adapted from:

Willemsen, S. C. M. J., Oostwoud Wijdenes, L., van Beers, R. J., Koppen, M., & Medendorp, W. P. (2024). Central tendency and serial dependence in vestibular path integration. *Journal of Neurophysiology*, *132*(5), 1481-1493.

3.1 Abstract

Path integration, the process of updating one's position using successive self-motion signals, has previously been studied with visual distance reproduction tasks in which optic flow patterns provide information about traveled distance. These studies have reported that reproduced distances show two types of systematic biases: central tendency and serial dependence. In the present study, we investigated whether these biases are also present in vestibular path integration. Participants were seated on a linear motion platform and performed a distance reproduction task in total darkness. The platform first passively moved the participant a predefined stimulus distance, which they then actively reproduced by steering the platform back the same distance. Stimulus distances were sampled from short- and long-distance probability distributions and presented either in a randomized order or in separate blocks to study the effect of presentation context. Similar to the effects observed in visual path integration, we found that reproduced distances showed an overall positive central tendency effect as well as a positive, attractive serial dependence effect. Furthermore, reproduction behavior was affected by presentation context. These results were mostly consistent with predictions of a Bayesian Kalman filter model, originally proposed for visual path integration.

3.2 Introduction

How do we keep track of our position when navigating our surroundings? An important aspect of human spatial navigation is path integration, which is the process of continuously updating one's position using successive self-motion signals (Mittelstaedt & Mittelstaedt, 1980; Etienne & Jeffery, 2004). These self-motion signals can come from various senses, such as the visual and vestibular systems (ter Horst et al., 2015), and can also be derived from motor signals (Laurens & Angelaki, 2017; van Helvert et al., 2022; Cullen, 2023).

To investigate the mechanisms underlying path integration, studies often make use of distance reproduction tasks (Israël et al., 1997; Lappe & Frenz, 2009; Petzschner & Glasauer, 2011). Typically, in such tasks, a participant is virtually or physically moved an unspecified distance and then asked to reproduce that same distance. Generally, participants show systematic biases in their reproductions. Some studies show an overall overestimation (Redlick et al., 2001; Lappe & Frenz, 2009), whereas others report an underestimation of the reproduced distance (Frenz & Lappe, 2005; Lappe et al., 2011). There is also work that reports that shorter distances are overestimated while longer distances are underestimated (Loomis et al., 1993; Israël et al., 1997; Philbeck & Loomis, 1997; Grasso et al., 1999; Riecke et al., 2002; Bergmann et al., 2011; Petzschner & Glasauer, 2011; Prsa et al., 2015).

The underestimation of traveled distance has been modeled by assuming that the integration of self-motion information is leaky (Mittelstaedt & Glasauer, 1991; Lappe et al., 2007). This model can also predict an overestimation if instead of the already traveled distance, the remaining distance to a target position must be judged (Lappe et al., 2007). However, these types of models cannot explain the observation that reproduced distances are also affected by the history of experienced distances (Petzschner & Glasauer, 2011). Indeed, several studies have shown that path integration is biased by the distribution of distances a participant encounters during an experiment as well as the sequence in which these distances are presented (Sun et al., 2020; Glasauer & Shi, 2022). The former is referred to as the central tendency bias (Hollingworth, 1910) and the latter as serial dependence (Holland & Lockhead, 1968; Cross, 1973), both well-known observations across perceptual domains (Saarela et al., 2023). What is the origin of these biases in path integration?

Recent studies suggest that the observed biases do not reflect a distorted integration process but rather arise from probabilistic computations that perform near-optimal Bayesian inference on noisy but unbiased self-motion velocity signals

(Jürgens & Becker, 2006; Petzschner & Glasauer, 2011; Petzschner et al., 2012; Prsa et al., 2015; Lakshminarasimhan et al., 2018). In more detail, because sensory information and motor commands, as well as the neural processing itself, are endowed with intrinsic random noise, the self-motion cues should not be treated as point estimates but rather be approached as probability distributions. For path integration, the Bayesian framework states that the observer estimates the most probable distance (the posterior) by integrating noisy sensory signals (the likelihood) with prior expectations (as derived from past experiences), following Bayes' rule.

In support, Lakshminarasimhan et al. (2018) found that the bias in visual path integration was better explained by a Bayesian prior favoring slower speeds than by leaky integration of unbiased self-motion velocity. Glasauer & Shi (2022) showed that a static Bayesian prior, i.e., a distribution with a fixed variance and a fixed mean, could account for central tendency biases in visual path integration but could not explain the serial dependence effects showing that responses were attracted toward the previously presented distance. To account for both types of biases, they proposed instead a Bayesian model that assumes that stimuli are drawn from a distribution with a fixed variance but whose mean changes from trial to trial (Glasauer & Shi, 2022). Can this model also explain the biases in vestibular (or more generally, idiothetic) path integration?

In the present study, we first investigated whether the central tendency and serial dependence effects are also observed in vestibular path integration. If path integration relies on a single multimodal representation of estimated distance irrespective of the type of sensory input, then we expect to find similar central tendency and attractive serial dependence biases as observed in visual path integration (Glasauer & Shi, 2022). However, it is also possible that the reproduced distances show no or even repulsive serial dependence, biasing perception away from the previously presented distance to increase overall sensitivity to different distances instead of keeping the continuity of vestibular path integration (Sun et al., 2020). To obtain more insight into the origin of the biases, we studied whether these biases are affected by the presentation context in which the stimulus distances are experienced. To do this, we sampled distances from two probability distributions covering a range of "short" and "long" distances and created two different contexts by changing the order in which the stimuli were presented. Second, we tested whether the reproduced distances and observed biases, and their potential dependence on presentation context, could be explained by the model proposed by Glasauer & Shi (2022) for visual path integration.

3.3 Methods

3.3.1 Participants

Thirty-one participants took part in the experiment. All participants were naive as to the purpose of the study and had normal or corrected-to-normal vision as well as no hearing issues or history of motion sickness. The experiment took ~90 min, and participants received course credits or €15 as reimbursement. One participant was excluded because of problems with sound masking during the task, so that data of 30 participants (11 men and 19 women, aged 18 – 31 yr) are reported. The study was approved by the ethics committee of the Faculty of Social Sciences of Radboud University Nijmegen, and all participants gave written informed consent.

3.3.2 Setup

We implemented a distance reproduction task using a vestibular sled, consisting of a chair mounted on top of a linear motion platform, that moved along the participant's interaural axis on an ~95-cm-long track (see Figure 3.1). A linear motor (TB15N; Tecnotion, Almelo, The Netherlands) and servo drive (Kollmorgen S700; Danaher, Washington, DC) were used to power and control the platform. Participants wore a five-point seat belt, and their head was fixated with ear cups. The chair contained emergency buttons that could be pressed at any time during the experiment to stop the motion of the platform. The platform could move passively, i.e., outside of the participant's control, or actively, by the participant rotating a steering wheel (G27 Racing Wheel; Logitech, Lausanne, Switzerland) that was mounted on a table at chest level in front of them. The steering wheel had a range of rotation from -450° to +450° with a resolution of 0.0549° and encoded the linear velocity of the sled (1 cm/s per degree). The mapping between the steering wheel angle and sled velocity was kept constant throughout the experiment. The task took place in total darkness and did not contain visual stimuli. We used an OLED screen (55EA8809-ZC; LG, Seoul, South Korea) placed in front of the sled to present instruction messages that explained the task before data collection started. The participant wore in-ear headphones with active noise canceling (QuietComfort 20; Bose, Framingham, MA) that played a white noise sound to mask noise produced by the motion platform, alternated by single-tone beeps indicating the different stages of each trial. The experiment code was written in Python (v.3.6.9; Python Software Foundation).

3.3.3 Reproduction task

Participants performed a vestibular distance reproduction task (see Figure 3.1). Every trial started with a *stimulus* movement, where the chair was passively moved by a predefined distance. The participant's task was then to actively reproduce the distance by steering the sled in the opposite direction: the *reproduction* movement. In essence, the participant always had to move the chair back to the location from which the stimulus movement started. The direction of the stimulus movement was the same across the trials of one participant. Half of the participants were randomly assigned to leftward stimulus movements and the other half to rightward stimulus movements.

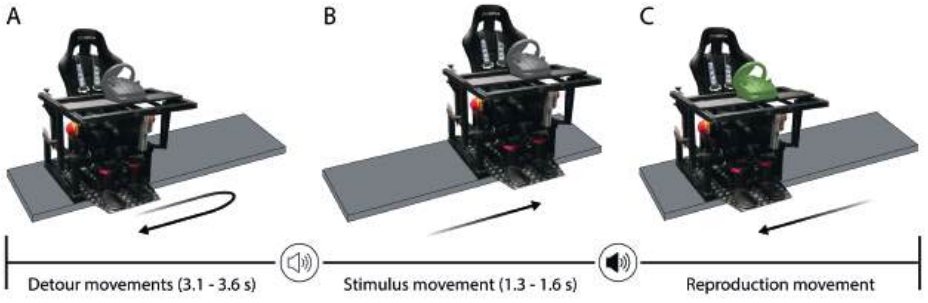

Figure 3.1. Distance reproduction task in a vestibular sled. Participants were seated in a chair mounted on top of a linear motion platform. At the start of each trial, participants were moved to a new start position via two detour movements (*A*). Then, a low-tone beep cued that the participant would be moved over the stimulus distance (*B*). Finally, a high-tone beep instructed the participant to use the steering wheel to move the sled over the same distance in the opposite direction: the reproduced distance (*C*).

Before the stimulus movement, the chair was passively moved via two random detour movements to one of two start locations, to ensure enough space on the track for the upcoming stimulus movement. Detours were used to prevent participants from receiving feedback about their previously reproduced distance. The first detour moved the chair to a random location within ±30 cm from the middle of the track with a random duration between 1.8 s and 2.3 s. The second detour movement subsequently brought the chair to the start location in 1.3 s. This start location was on the left side of the track for rightward stimulus movements and on the right side of the track for leftward stimulus movements.

Subsequently, a low-tone beep was played to alert the participant to the upcoming stimulus movement. This movement had a random duration between 1.3 s and 1.6 s. The lower bound was determined such that none of the stimulus movements

had a peak acceleration exceeding 1 G and a peak absolute velocity exceeding 100 cm/s. The upper bound resulted in the shortest stimulus movement having a peak acceleration of ~38 cm/s^2 and a peak absolute velocity of ~20 cm/s, such that the vestibular thresholds for perceiving the direction of linear lateral movements were well exceeded (Kingma, 2005). All passive movements, i.e., the detours and stimulus movement, followed a minimum-jerk profile.

After the stimulus movement finished and a random waiting time between 0.5 s and 1 s had passed, a high-tone beep cued the participant to make the reproduction movement by steering the sled in the opposite direction for the same distance as the stimulus movement. If the participant moved the steering wheel too soon (i.e., before the beep), the trial was aborted. Participants could steer the sled up to a maximum absolute velocity of 100 cm/s and could stop the movement by rotating the steering wheel back to the upright position. The chair stopped moving when the absolute velocity became lower than 2 cm/s, after which the trial ended. To cover the case that the participant intends to stop the sled movement but fails to rotate the wheel completely upright, the movement also ended when the absolute velocity fell below 6 cm/s while the steering wheel angle was constant for 100 ms or the steering changed direction (mean ± SD: 87 ± 78 trials). Participants were instructed to make one smooth movement, i.e., it was not possible to steer back or resume steering after the chair had come to a stop. Participants were free to choose the duration of their reproduction and did not receive feedback about their reproduction performance (except in the training block, see below).

3.3.4 Paradigm

We sampled the stimulus distances from two probability distributions covering a range of short and long distances (see Figure 3.2A). Because magnitudes seem to be internally represented on a logarithmic scale (Dehaene, 2003; Jürgens & Becker, 2006; Stocker & Simoncelli, 2006; Durgin et al., 2009; Petzschner & Glasauer, 2011), we sampled the stimulus distances from log-normal distributions. Log-transforming these distances yielded equal-variance normal distributions (see Figure 3.2A, inset). Before log-transforming, we divide the distances by a reference distance (1 cm) so all log-transformed distances are dimensionless. Stimulus distances on linear scale varied overall between 17 cm and 60 cm. The medians of the short and long stimulus distributions were 24.6 cm and 45 cm, respectively, where the distance between the medians of the distributions was determined such that there was a negligible probability of 0.0001 for a random draw from the long distribution to be shorter than a random draw from the short distribution. The variances of the short and long log-normal distributions were 8.2 cm^2 and 27.4 cm^2, respectively.

Per participant, we randomly sampled 65 distances from each distribution and used these to generate two presentation contexts (see Figure 3.2B). In the "blocked" context the short and long distances were presented in separate blocks and therefore separated in time, whereas in the "mixed" context the same short and long distances were randomly interleaved. Participants experienced both contexts during one experimental session of 260 test trials, where the order of the contexts (including the order of the short and long blocks in the blocked context) was counterbalanced across participants. There was no instruction about the existence of the two types of distances and contexts. After every 52 trials (i.e., ~10 min), there was a short break (~2 min) during which the lights were turned on to prevent dark adaptation.

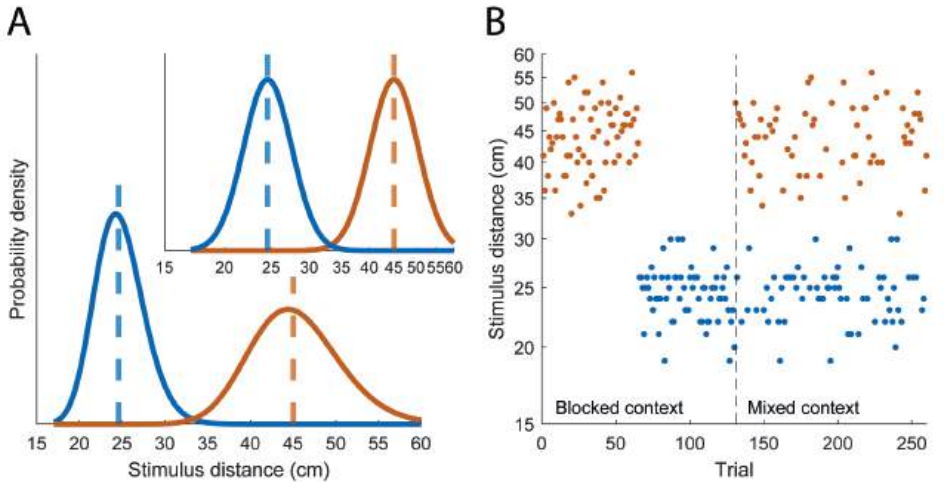

Figure 3.2. *A*: Distributions of stimulus distances. Distances were sampled from two log-normal probability distributions on linear scale covering a "short" (blue) and a "long" (orange) range of distances. Dashed lines indicate the median distance. *Inset*: The same probability distributions on logarithmic scale. *B*: Example presentation order of stimulus distances. In the blocked context, short and long distances were presented in blocks; in the mixed context, the same distances were randomly interleaved.

The experimental session started with 20 training trials to familiarize the participant with the task. The stimulus distances in the training trials were drawn from a uniform distribution on linear scale, covering all possible distances (17 to 60 cm). The training trials took place in the dark and followed the same paradigm as the test trials. Contrary to the test trials, the training trials ended with visual feedback on the reproduction error: after the reproduction movement ended, the signed reproduction error in centimeters was presented on the screen. The training trials were not analyzed.

3.3.5 Data analysis

Data from the test trials were processed offline in MATLAB (v.R2019a; MathWorks). The recorded sled position profiles showed that in some trials the movement speed plateaued at a low but nonzero value before the movement was terminated. We therefore corrected the movement end to the first time point with sled speed < 8 cm/s (instead of the online threshold of 6 cm/s) when the steering wheel angle remained constant for at least 100 ms or the steering direction changed. This resulted in an average of 20 corrected trials per participant (mean ± SD: 20 ± 18 trials). The reproduced distance was taken as the distance between the end and start point of the reproduction movement in centimeters. The reproduction error was defined as the difference between the reproduced and stimulus distance in centimeters, where negative and positive values represent an undershoot and overshoot, respectively. Trials in which the reproduction movement started too soon, with reproduction movements in the wrong direction, or with reproduced distances of < 1 cm were excluded (mean ± SD: 4 ± 4 trials). Because there was no effect of movement direction on the mean unsigned reproduction error across trials (Wilcoxon rank-sum test: p = 0.300, r = 0.19), we regarded all participants as one group.

Central tendency was defined as 1 minus the slope of the linear least-squares regression of the reproduced distance on the stimulus distance on logarithmic scale. In other words, a slope closer to 0 corresponds to a higher central tendency value and reproduced distances that tend more toward the mean of the stimulus distribution. We computed the central tendency of the short and long distances separately within each presentation context. We tested whether there was an effect of distance type (short/long) and context (mixed/blocked) on the central tendency values with a repeated-measures ANOVA. Because we found no significant effects (see Results), we averaged the central tendency values for every participant. A one-sample t-test was used to analyze whether central tendencies differed from 0. Partial eta-squared (η_p^2) (Cohen, 1973) and Cohen's d (Cohen, 1988) are reported for the ANOVA and t-test, respectively.

To study whether the perception of the short and long stimulus distances was affected by the context in which they were presented, we used the same linear regressions to extrapolate how participants would have reproduced the median distance of the entire distance range (on logarithmic scale, which corresponds to a distance of 31.9 cm on linear scale). We tested the effect of distance type and context on these estimated reproductions with a repeated-measures ANOVA, followed by simple effect tests of the interaction effect levels with Bonferroni correction. Partial eta-squared (η_p^2) is reported for the ANOVA.

We calculated serial dependence, defined as the slope of the linear least-squares regression of the reproduction error on trial *n* on the stimulus distance on trial *n* - 1 on logarithmic scale (Glasauer & Shi, 2022). The reproduction error was computed by subtracting the reproduced distance on logarithmic scale from the stimulus distance on logarithmic scale. We computed the serial dependence of the short and long distances separately within each presentation context. Because not all of the difference scores were normally distributed, we performed Wilcoxon signed-rank tests to analyze whether there were differences in serial dependence values between distance types and contexts. As in the central tendency analysis, we found no significant differences (see Results) and averaged the serial dependence values for every participant. A one-sample *t*-test was performed to test whether serial dependencies differed from 0. Effect size *r* (Rosenthal et al., 1994) and Cohen's *d* are reported for the Wilcoxon test and *t*-test, respectively.

3.3.6 Modeling

The two-state model and special cases

We implemented a Bayesian model, similar to the "two-state" model developed by Glasauer & Shi (2022) for visual path integration, to evaluate whether it could also explain the central tendency and serial dependence biases in vestibular path integration. The model first transforms the sensory input d_i to logarithmic scale with $z_i = \ln(d_i)$, to which the following three generative assumptions are applied:

$$z_i = x_i + \eta \text{ with } \eta \sim N(0, r), \tag{3.1}$$

$$x_i = m_{i-1} + \varepsilon_x \text{ with } \varepsilon_x \sim N(0, v), \tag{3.2}$$

$$m_i = m_{i-1} + \varepsilon_m \text{ with } \varepsilon_m \sim N(0, q). \tag{3.3}$$

The model thus assumes *1*) that the sensory measurement on trial i, z_i, is drawn from a normal distribution centered on the log-transformed stimulus distance x_i with a fixed variance *r* (Equation 3.1); *2*) that the stimulus distance x_i is drawn from a normal distribution with mean m_{i-1} and fixed variance v (Equation 3.2); and *3*) that the mean of this distribution m_i varies over trials following a random walk with a fixed variance q (Equation 3.3). The stimulus distance x_i and the mean of the stimulus distribution m_i are the two states of the two-state model, which are estimated on every trial by a time-discrete Kalman filter. Here, the Kalman filter estimates of the two states on trial i, $\widehat{x}_i$ and $\widehat{m}_i$, are based on the sensory measurement z_i and the estimated mean of the stimulus distribution on the previous trial $\widehat{m}_{i-1}$, which are weighted by the Kalman gain (see Appendix for the

equations). The final estimated reproduced distance on trial i on logarithmic scale is computed as $\widehat{y}_i = \widehat{x}_i + \Delta x$, where Δx is a shift term that accounts for global under- or overestimation. In total, the model has four free parameters that are fitted to the reproduction data: the variances r, v, and q and the shift term Δx.

Identical to Glasauer & Shi (2022), we considered two special cases of the two-state model based on the assumed stimulus distribution. The "static" variant is obtained by fixing variance q at 0, corresponding to a stimulus distribution with a fixed mean. This results in distance estimates that are independent across trials and thus show no serial dependence. In the other special case, the "iterative" variant, variance v is set to 0, causing the stimulus distribution to depend on the distance estimate in the previous trial and the estimates to show maximal serial dependence. Both variants, with only three free parameters, were fitted to the present data.

Sensitivity of the two-state model to different stimulus distributions

The v and q parameters of the two-state model capture assumptions about the stimulus distribution. To explore to what extent the observed differences in reproduction behavior between presentation contexts can be explained by different assumptions, we adapted the two-state model by introducing separate v and q parameters for the mixed, short, and long blocks. The resulting model has eight free parameters (r, v_{mixed}, v_{short}, v_{long}, q_{mixed}, q_{short}, q_{long}, Δx).

We also tested whether the context-dependent differences in the reproduction data are better explained by a block-dependent shift parameter Δx rather than block-dependent variances. We therefore adapted the two-state model by allowing different shift parameters in the three blocks, while keeping the other parameters constant across blocks, resulting in a model with six free parameters (r, v, q, Δx_{mixed}, Δx_{short}, Δx_{long}). Both adapted versions of the two-state model contain only one measurement variance parameter r because we assumed that the measurement noise would not change over the course of the experiment.

Model fitting and comparison

We determined the log-likelihood of the data given the model parameters across all trials. On every trial, we computed the probability density of the participant's reproduced distance, given the model's distribution of possible reproduced distances (equations are included in the Appendix). The free parameters of the models were fitted to the data of each participant individually with the MATLAB

function *fmincon*, which minimized the total negative log-likelihood summed over trials. Lower bounds were set to 0 for the variance parameters r, v, and q. Start values were set to 1 for the variance parameters and to 0 for the Δx parameter(s) to initialize the GlobalSearch algorithm [MATLAB function *GlobalSearch* (Ugray et al., 2007)], which iteratively executed the *fmincon* function with different start values.

For comparison, we computed the Bayesian information criterion (BIC) score of each model variant. The BIC is based on the log-likelihood, while taking into account the number of free parameters of the model. A lower BIC score indicates a better description of the data. We computed the BIC scores of the model variants relative to the two-state model for every participant separately, which are graphically presented in violin plots showing the median, interquartile range (IQR), and 1.5x IQR of the relative BIC scores across participants. Median values and IQRs of the fitted parameters across participants are reported because of outliers in the fitted values. To visualize the model predictions, stimulus distances as well as actual and predicted reproduced distances were binned into 10 bins per distance type and per context, separately for each participant. Of these variables, we subsequently computed the means and standard errors across participants per bin.

3.4 Results

We studied vestibular path integration by measuring participants' performance in a distance reproduction task in the dark and analyzing central tendency and serial dependence biases in the reproduced distances. The stimulus distances were sampled from either a short-distance or a long-distance probability distribution, and different presentation contexts were created by varying the order in which these distances were presented. In the mixed context the short and long distances were randomly interleaved, whereas in the blocked context the same short and long distances were presented in separate blocks.

3.4.1 Central tendency bias

Figure 3.3, A and B, show the raw reproduction data of a representative participant, measured in the mixed and blocked contexts respectively, plotted as a function of the stimulus distance. The regression lines indicate the central tendency. All slopes are smaller than 1, which corresponds to a positive central tendency. A repeated-measures ANOVA on the central tendency values of all

participants indicates that there were no significant differences between distance types (short / long, $p = 0.105$, $\eta_p^2 = 0.09$) or contexts (mixed/blocked, $p = 0.245$, $\eta_p^2 = 0.05$) as well as no interaction effect ($p = 0.091$, $\eta_p^2 = 0.10$). We therefore averaged the central tendency values for every participant and performed a one-sample *t*-test to study whether the resulting central tendency values differed from 0. On average, we found a positive central tendency effect of 0.39 ($\mathrm{SD} = 0.21$, $p < 0.0001$, Cohen's $d = 1.86$), which corresponds to a regression line with a slope of 0.61.

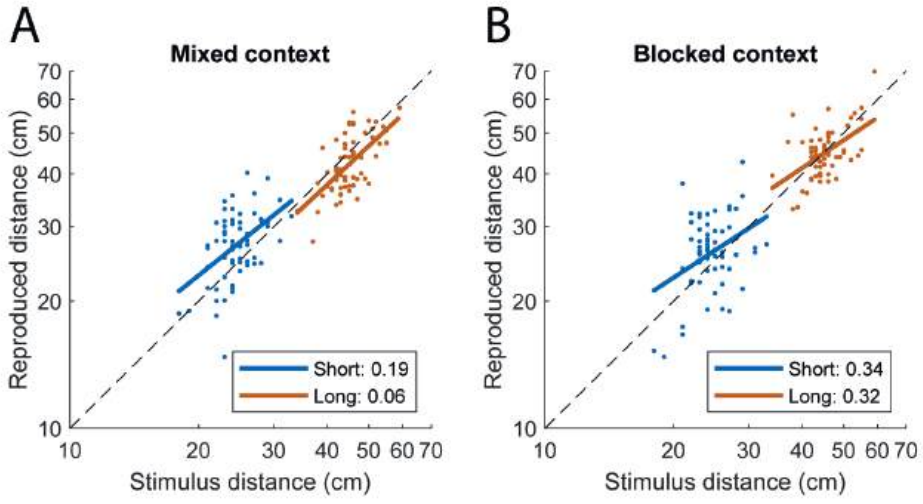

Figure 3.3. Reproduced distance as a function of stimulus distance in the mixed (*A*) and blocked (*B*) contexts of a representative participant. Regression lines show the central tendency bias. Within each presentation context, separate regressions were performed on the short (blue) and long (orange) distances. Central tendency values (1 - slope of the regression line) are reported in the key.

We performed an additional analysis to study how the short and long stimulus distances were perceived depending on the context in which they were presented. Based on the same linear regressions, we estimated how the median distance of the entire stimulus distance range would have been reproduced in the two presentation contexts (see Figure 3.4, A and B). A repeated-measures ANOVA with factors distance type and presentation context on these estimates yielded a main effect of distance type, indicating larger estimated reproductions of the median stimulus distance based on the long-distance regression lines than on the short-distance regression lines ($p = 0.032$, $\eta_p^2 = 0.15$). In other words, the median stimulus distance would have been reproduced longer if it had been part of the long as compared to the short stimulus distance range. There was no main effect of presentation context

($p = 0.563$, $\eta_p^2 = 0.01$), but, crucially, there was a significant interaction between distance type and presentation context ($p = 0.005$, $\eta_p^2 = 0.24$; see Figure 3.4C). Follow-up tests showed that the abovementioned effect of distance type was only present in the blocked context (mean reproduction based on short-distance regression line $= 26.5$ cm and long-distance regression line $= 29.8$ cm, $p = 0.004$), whereas the mixed context showed no difference (mean reproduction based on short-distance regression line $= 29.1$ cm and long-distance regression line $= 28.4$ cm, $p = 0.318$). This indicates that reproduction behavior depends on the context in which the stimuli were presented.

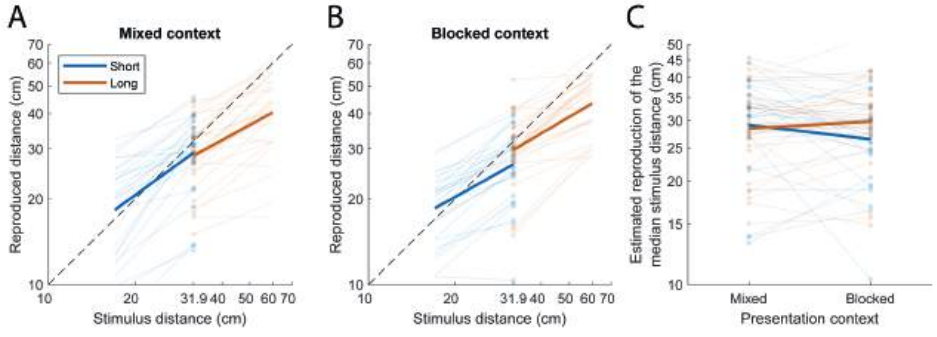

Figure 3.4. *A*, *B*: Regression lines based on the stimulus and reproduced distances for short (blue) and long (orange) distances in the mixed (*A*) and blocked (*B*) contexts for all participants (transparent lines) as well as the mean (bold lines) on logarithmic scale. The dots represent the estimated reproduced distance at the median of the entire distance range. *C*: Distance type-by-context interaction effect on the estimated reproductions of the median stimulus distance.

3.4.2 Serial dependence bias

As an illustration of serial dependence, Figure 3.5 shows the reproduction error on trial n plotted against the stimulus distance on trial $n - 1$ for the same participant as in Figure 3.3. The regression lines of the illustrated participant show a slight positive serial dependence, except for the short distances in the mixed context. We performed Wilcoxon signed-rank tests on the serial dependence values of all participants and found no significant main or interaction effects for distance type and context (all p values ≥ 0.185, all r values ≤ 0.24). After averaging the serial dependence values for every participant, a one-sample *t*-test revealed a positive serial dependence of 0.13 ($\mathrm{SD} = 0.15$, $p < 0.0001$, Cohen's $d = 0.87$). This suggests that the reproduced distance on trial *n* is attracted toward the stimulus distance on trial $n - 1$.

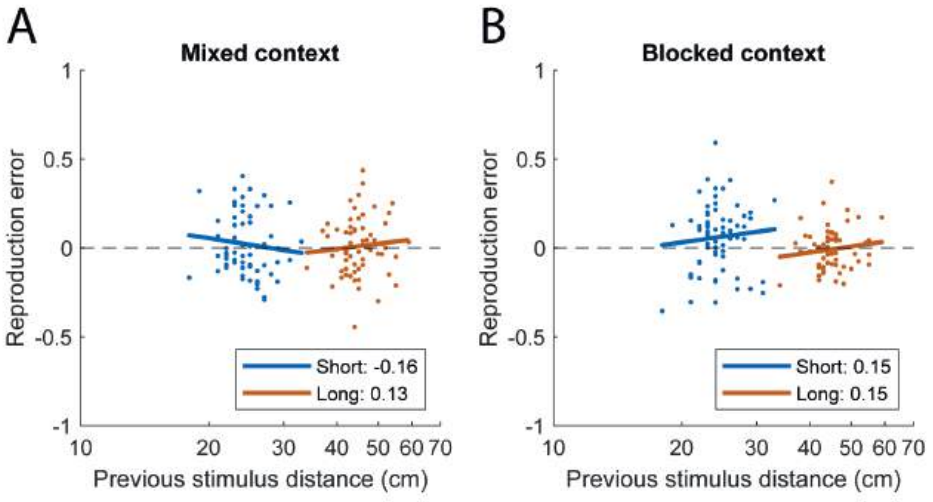

Figure 3.5. Reproduction error on the current trial as a function of stimulus distance on the previous trial in the mixed (*A*) and blocked (*B*) contexts of the same participant as in Figure 3.3. Reproduction errors were computed on logarithmic scale. Regression lines show the serial dependence bias and were computed for the short (blue) and long (orange) distances separately. Serial dependence values (slope of the regression line) are reported in the key.

3.4.3 Both the static and two-state models can explain vestibular path integration behavior

We fitted the static, iterative, and two-state model variants to all trials of a participant, examining a computational, i.e., Bayesian, explanation of these findings. The model variants differ in their assumptions about how the stimulus distances are generated. As explained in detail in the Methods, the static model variant assumes that the stimulus distances are independent draws from a static, trial-independent stimulus distribution. This predicts no serial dependence in the participant's reproductions. The iterative model variant instead assumes a stimulus distribution shifting from trial to trial, the distribution on a specific trial being centered on the stimulus distance of the previous trial. This clearly results in serial dependence in the model predictions. The two-state model variant represents the more general case, where the mean of the stimulus distribution on a specific trial is close but not identical to the stimulus distance on the previous trial, still inducing some level of serial dependence. In all model variants, the variance of the stimulus distribution is constant across trials. By fitting these different model variants to the data, we aimed to determine whether these assumptions about how the stimuli are generated can explain the observed perceptual biases in vestibular path integration behavior.

Figure 3.6 shows the mean binned data and model predictions of the three fitted model variants. In the mixed context, all model predictions are close to the reproduced distance data. In the blocked context, the static and two-state models also provide a relatively good explanation of the reproductions. However, the iterative model underestimates the participants' reproductions of the short distances and overestimates those of the long distances.

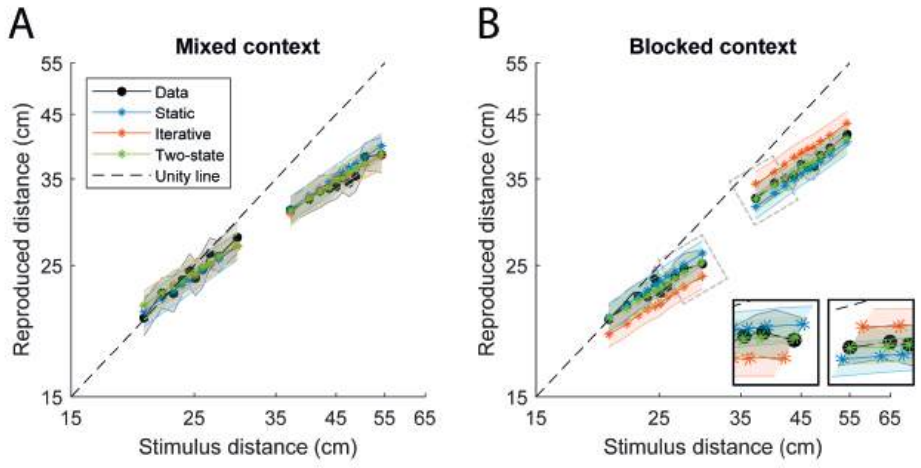

Figure 3.6. Binned reproduced distances (black) predicted by the static (blue), iterative (orange), and two-state (green) model variants as a function of stimulus distance on logarithmic scale for the mixed (*A*) and blocked (*B*) contexts. The stimulus distances and the according actual and predicted reproduced distances were binned for each participant individually. Symbols represent the mean per bin, and shaded areas show ±SE, both computed across participants. Unity lines (dashed) show where stimulus and (predicted) reproduced distances are equal.

Next, we computed the central tendency and serial dependence biases as predicted by the three model variants. As illustrated in Figure 3.7, the predictions of all model variants show relatively similar central tendency values as found in the data. The serial dependence on the other hand is less well predicted by the models. In general, the iterative model overestimates the serial dependence in the reproduction data except for the participants who show a high serial dependence (> 0.30). The static and two-state models tend to underestimate the serial dependence in the data, with the two-state model more often predicting values closer to those found in the actual reproductions than the static model. The figure also shows that the best models in terms of BIC score are also close to the unity line for the central tendency but that this is not the case for the serial dependence.

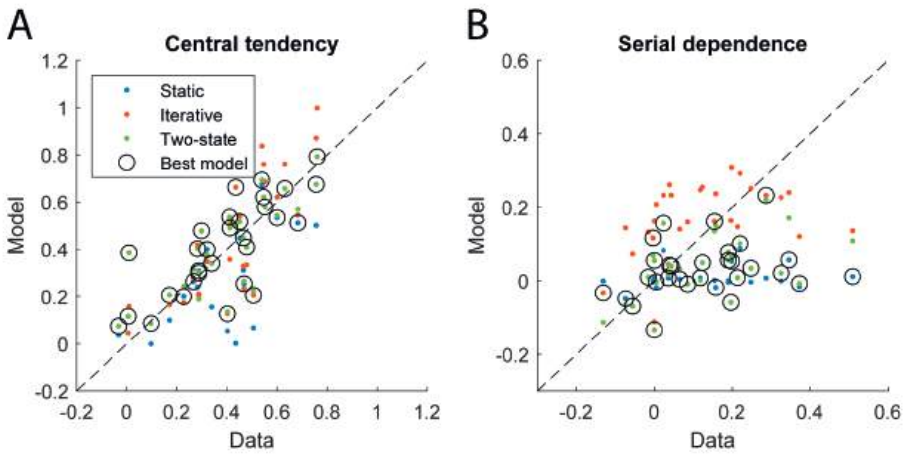

Figure 3.7. Central tendency (*A*) and serial dependence (*B*) values for the static (blue), iterative (orange), and two-state (green) model predictions as a function of their measured values. Within a color group, each point represents a participant. Black open circles indicate the models with the lowest Bayesian information criterion (BIC) score per participant, and dashed lines show where the biases in the data and model predictions are equal.

The differences in predicted serial dependence between models are reflected by the fitted model parameter values (see Table 3.1). The median value of the variance parameter q, which determines how much the mean of the assumed stimulus distribution varies over trials, is 0.14 for the iterative model, resulting in serial dependence in the model predictions. The same parameter has a value close to 0 for the two-state model for most participants, predicting virtually no serial dependence and essentially causing the two-state model to behave as the static model. The fitted models show similar measurement variances (r) and shift terms (Δx), whereas fitting the static model to the reproduction data resulted in larger values for the stimulus distribution variance (v) than in the case of the two-state model. Notably, the fitted parameters show large intersubject variability.

Table 3.1. Median (first – third quartiles) of the fitted parameter values across participants for the static, iterative and two-state model variants. The parameters r, v, and q refer respectively to the measurement variance, the variance of the assumed stimulus distribution and the variance with which the mean of this distribution varies. The Δx parameter is a shift term that represents global under- or overestimation of the reproduced distances.

	Median fitted parameter values (Q1 – Q3)			
Models	r	v	q	Δx
Static	0.17 (0.09 – 0.22)	0.26 (0.17 – 0.66)		-0.06 (-0.22 – 0.01)
Iterative	0.15 (0.09 – 0.31)		0.14 (0.06 – 0.38)	-0.06 (-0.21 – -0.01)
Two-state	0.17 (0.10 – 0.30)	0.17 (0.12 – 0.25)	0.001 (5.38 x 10^{-11} – 0.05)	-0.06 (-0.21 – 0.01)

As a final comparison, Figure 3.8 shows the BIC scores of the static and iterative models relative to the BIC scores of the two-state model, where a relative BIC score > 6 is interpreted as strong evidence in favor of the two-state model (Kass & Raftery, 1995). Despite substantial interindividual variability, the static and two-state models have similar median BIC scores. The static model has a median relative BIC score of -3.16, describing the data equally well with one less free parameter than the two-state model. The iterative model is outperformed by the two-state model, indicated by a median relative BIC score of 14.16.

To summarize, the reproduction behavior is best explained by the static and two-state models and less so by the iterative model (see Figure 3.8), especially in the blocked context (see Figure 3.6). All models are able to capture the central tendency effects in the data relatively well but perform worse in explaining the serial dependence (see Figure 3.7).

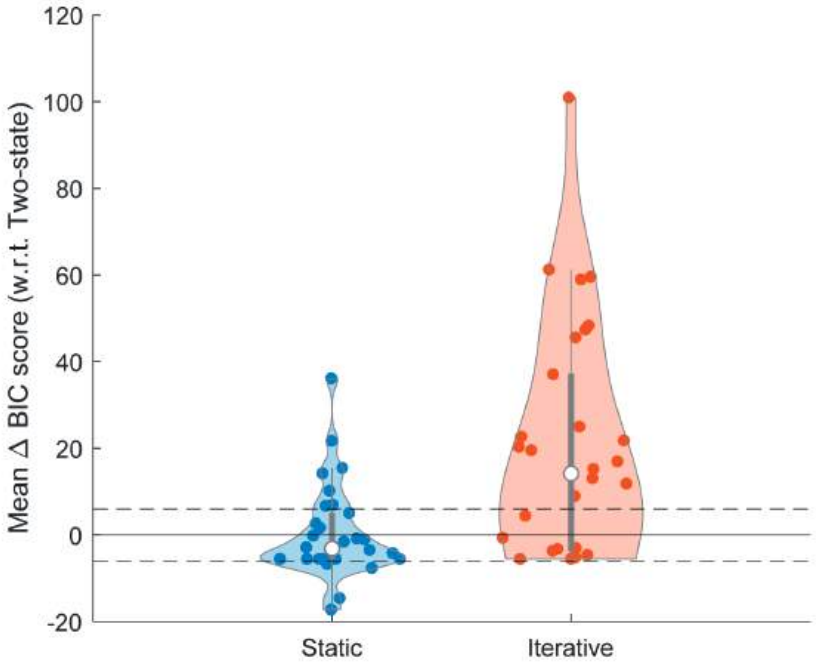

Figure 3.8. Model Bayesian information criterion (BIC) scores relative to the BIC scores of the two-state model. Colored data points represent individual participants. White data points show the median relative BIC scores and bold and thin gray lines the interquartile range (IQR) and 1.5x IQR across participants. Dashed lines represent a BIC score difference of -6 and 6, where relative BIC scores smaller than -6 or larger than 6 provide strong evidence against or in favor of the two-state model, respectively.

3.4.4 The shift parameter of the two-state model can capture context-dependent differences

Can the difference in reproduction behavior across contexts be explained by different assumptions about the experimental stimulus distributions in the different blocks? To examine this, we adapted the two-state model by including separate v (representing the variance of the assumed stimulus distribution) and q (representing the variance with which the mean of the assumed stimulus distribution changes across trials) parameters for the mixed, short, and long blocks (see Methods). The yellow symbols in Figure 3.9A show the resulting BIC scores relative to the BIC scores of the original two-state model with one v and one q parameter across all blocks. As in the previous BIC score comparison, there is considerable spread in the relative BIC scores. The adapted model had a median relative BIC score of 3.98, thus performing similarly as the original two-state model. In other words, allowing different assumptions about the underlying

stimulus distribution between the blocks at the cost of more free parameters does not result in a better description of the vestibular path integration data.

Next, we explored whether allowing separate shift parameters for each of the blocks ($\Delta x_{\mathrm{mixed}}$, $\Delta x_{\mathrm{short}}$, Δx_{long}) could explain the differences in the reproductions across contexts. The median relative BIC score of this model with respect to the original two-state model is -16.64 (see Figure 3.9A in purple), showing that the additional parameters do improve model performance over the original two-state model. This improvement is not directly apparent in the mean model predictions (see Figure 3.9, B and C) or the predicted perceptual biases (see Figure 3.9, D and E) but is visible on the level of the individual participant (see Figure 3.9, B and C, insets). The medians (Q1 – Q3) of the fitted $\Delta x_{\mathrm{mixed}}$, $\Delta x_{\mathrm{short}}$, and Δx_{long} parameter values across participants are -0.08 $(-0.21 - 0.05)$, -0.03 $(-0.37 - 0.05)$, and -0.12 $(-0.29 - 0.06)$, respectively. Taken together, these findings suggest that the differences in reproduction behavior across the contexts are explained by block-dependent global underestimations rather than by block-dependent assumptions about the experimental stimulus distributions.

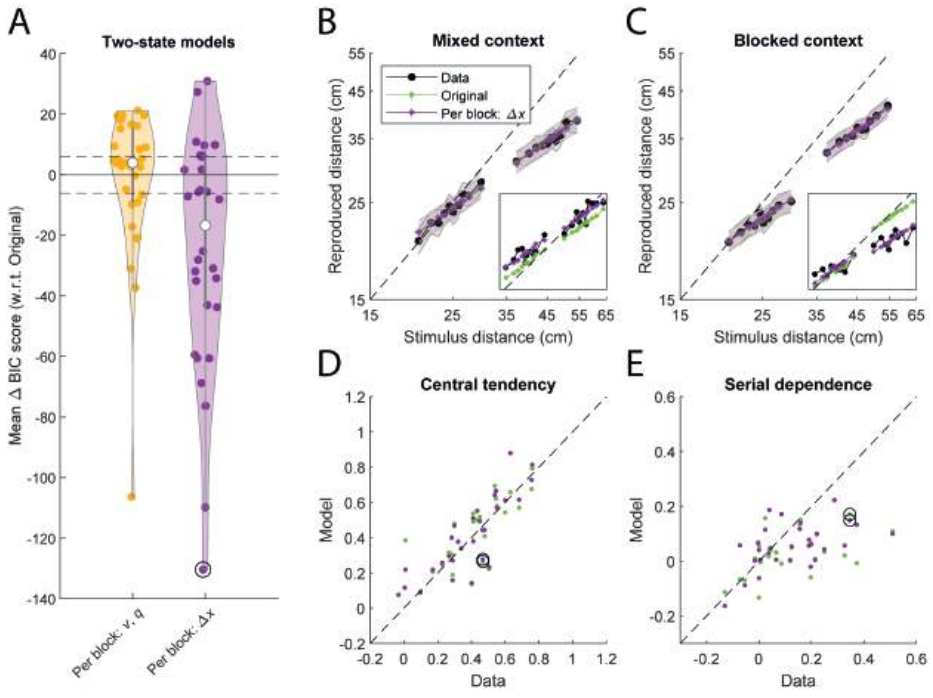

Figure 3.9. Comparison between original and block-dependent two-state models. *A*: Bayesian information criterion (BIC) scores of the adapted two-state models with either free *v* and *q* parameters (yellow) or a free Δx parameter for the mixed, short, and long blocks (purple), relative to the BIC scores of the original two-state model. *B*, *C*: Binned reproduced distances predicted by the original two-state model (green) and the adapted two-state model with a block-specific Δx parameter as a function of stimulus distance for the mixed (*B*) and blocked (*C*) contexts. *D*, *E*: Central tendency (*D*) and serial dependence (*E*) values for the same models as a function of their measured values. *A*, *B-C*, and *D-E* are in the same format as in Figure 3.8, Figure 3.6, and Figure 3.7, respectively. Black open circles in *A*, *D-E*, and insets in *B-C* show an individual participant for whom the adapted two-state model with block-dependent Δx parameters has the largest decrease in BIC score relative to the original two-state model.

3.5 Discussion

In this study, we measured human path integration behavior based on vestibular signals and investigated the extent to which distance reproductions show central tendency and serial dependence effects. Participants were seated in a vestibular sled and performed a distance reproduction task in the dark. The sled passively moved the participant with a predefined stimulus distance, which they actively reproduced by steering the sled back to the location from which the stimulus movement started. Stimulus distances were drawn from short- and long-distance

probability distributions and presented in either a randomized order (the mixed context) or in two separate blocks (the blocked context).

We found a positive central tendency effect that was not affected by distance type (whether the distance was sampled from the short- or long-distance probability distribution) or presentation context (mixed or blocked). The positive central tendency effect indicates that reproductions were drawn toward the mean of the underlying stimulus distribution. This effect has the same direction as the central tendency effects found in visual path integration (Riecke et al., 2002; Petzschner & Glasauer, 2011; Petzschner et al., 2012; Glasauer & Shi, 2022) and other nonvisual path integration (Loomis et al., 1993; Israël et al., 1997; Philbeck & Loomis, 1997; Grasso et al., 1999; Bergmann et al., 2011) studies. This suggests that this bias does not originate within a single sensory modality but might be better understood as the explicit learning of the statistical structure of multimodal motion information.

In addition to a central tendency bias, we found a positive serial dependence bias, again irrespective of distance type or presentation context. This indicates that the reproduced distance on a trial is attracted toward the stimulus distance on the previous trial. This is in line with positive serial dependence effects found in reproductions based on visual information (Glasauer & Shi, 2022). Functionally, positive serial dependence could help to maintain the continuity of the context and promote stable representations for path integration (Sun et al., 2020; Manassi & Whitney, 2024).

We implemented a Bayesian model, originally proposed by Glasauer & Shi (2022) to explain perceptual biases in visual path integration, to evaluate whether it could also explain vestibular path integration. The model contains three variants based on different assumptions about the stimulus distribution (the static, iterative, and two-state variants). On every trial, the model estimates the stimulus distance with a Kalman filter that weighs the sensory measurement on the trial with the mean of the stimulus distribution estimated on the previous trial.

We found that the static and two-state model variants provided comparable fits to the vestibular path integration data (see Figure 3.8). A similar finding was reported by Glasauer & Shi (2022), where the two-state model provided the best fit to duration reproduction data for 8 of 14 participants, whereas for the remaining participants the static model was sufficient. It is important to point out, however, that the model captured the central tendency effect relatively well (see Figure 3.7) but performed worse in explaining the serial dependence effect. Hence, although the model by Glasauer & Shi (2022) provided a joint explanation for the central

tendency and serial dependence effects in visual path integration, the present results do not validate this unification in vestibular path integration. Could this be taken to suggest that these biases in vestibular path integration occur because of separate mechanisms?

We prefer to be careful with this conclusion. There are a few differences that should be noted. First, the present data may be noisier, causing the model to not accurately capture all aspects of the reproduction data. Furthermore, the present task was not purely perceptual but also involved a motor component. Compared to a passive reproduction task, in which both the stimulus and reproduction movements are experienced passively and the reproduced distance is indicated by a button press, additional motor-based self-motion signals could contribute to distance estimates and perhaps trial-to-trial correlations (Medendorp, 2011; Carriot et al., 2013; Laurens & Angelaki, 2017; Brooks & Cullen, 2019; van Helvert et al., 2022). In support, it has been shown that reproducing perceived angular displacements actively reduces the variability compared to passive reproduction (Becker et al., 2002; Jürgens & Becker, 2006). The active steering movement in the present task therefore could have introduced nonperceptual effects (i.e., motor biases) in the reproductions. For example, larger distances might have been underestimated more because larger reproduction movements require more effort. In this study, we opted for a more naturalistic, active reproduction task, but in a future experiment it would be interesting to compare central tendency and serial dependence in active versus passive reproduction tasks of vestibular path integration.

We also studied the effect of different presentation orders on the reproduced distances by presenting the stimulus distances in a mixed and a blocked context (see Figure 3.2). As indicated by the central tendency analysis, the short- and long-distance regression lines have similar slopes in both presentation contexts. However, the estimated reproductions of the median stimulus distance differ in the blocked context, indicating that presentation context affects vestibular distance reproductions (see Figure 3.4). A similar interaction between distance type and presentation context was reported in Petzschner et al. (2012) for visual path integration, as well as in other magnitude estimation tasks [e.g., Roach et al. (2017) for duration reproduction]. Although the interaction effect is significant on the group level, the individual participants show a large spread in the estimated reproductions of the median stimulus distance (see Figure 3.4C). This variation seems mostly caused by interindividual differences in the size of the estimated reproductions, where some participants generally produce larger reproductions than others, irrespective of the context. Visual inspection of the individual

interaction plots shows that the estimated reproductions of the median stimulus distance are in the same direction as the mean effect for 17 participants, in a different direction for 6 participants, and suggests no interaction for 7 participants.

To investigate the origin of the mean interaction effect, we modified the two-state model by incorporating information about the block (mixed, short, or long) in which the stimulus distance was presented. We first ruled out as a cause of this interaction that participants have different assumptions about the stimulus distribution in the different presentation contexts. More specifically, allowing block-specific parameters for the assumed stimulus distribution (v and q) did not result in a better description of the reproduced distances (see Figure 3.9A). Rather, we found that the model variant with block-specific Δx parameters, allowing different global under- or overestimations across blocks, provided a better explanation than the original two-state model. We can only speculate about the functional meaning of this parameter. The global undershooting of reproductions might be caused by increasing uncertainty in the position estimate as more distance is covered (Lakshminarasimhan et al., 2018). Indeed, the observed pattern in the fitted Δx_{short}, Δx_{mixed}, and Δx_{long} parameter values decreasing with longer distances (-0.03, -0.08, and -0.12, respectively) is consistent with Δx varying linearly with distance, as internally represented on a logarithmic scale. Future studies are needed to examine this potential interpretation.

Furthermore, within this perspective, we emphasize that we studied different presentation contexts, and drew stimuli from a normal distribution rather than a uniform distribution, but we did not vary how we selected the stimuli in each specific block of trials. That is, for each trial we randomly selected the stimulus distance from the defined stimulus distribution (mixed, short, or long). Recently, Glasauer & Shi (2021) argued that the central tendency is the result of an unnatural experimental randomization protocol: randomly presenting stimulus distances with large trial-to-trial variability. In many natural circumstances, successive stimuli typically vary only in a small range, not randomly jumping from one magnitude to another. Using a duration production-reproduction task, Glasauer & Shi (2021) showed that the central tendency was greatly reduced if the sequence of the stimulus durations mimicked a random walk compared to that of a randomized sequence. It would therefore be interesting to test how the central tendency effect in vestibular path integration depends on the randomization protocol.

Recent neurophysiological work suggests that the posterior parietal cortex might be involved in producing the perceptual biases affecting path integration. Using a parametric working memory task in rats, Akrami et al. (2018) found that the

posterior parietal cortex plays a key role in modulating the central tendency bias. When the region was optogenetically inactivated, not only was this bias attenuated but there was also a suppression of serial dependence, suggesting that the two phenomena may be interrelated. In subsequent neural network modeling work, the same authors explain the two biases through a single mechanism (Boboeva et al., 2024). Sensory inputs relayed from the posterior parietal cortex can lead to serial dependence in working memory, from which central tendency naturally emerges.

In conclusion, our results show that distance reproductions based on vestibular signals exhibit positive central tendency and attractive serial dependence, as has been found in visual path integration, suggesting that the biases might arise on a multimodal processing level. Furthermore, reproduced distances were affected by the presentation context of the stimulus distances. The modeling approach suggested that different distance-dependent global underestimations could best account for this contextual effect.

3.6 Appendix

In this Appendix, we provide the equations of the two-state model proposed by Glasauer & Shi (2022) and the equations used in the maximum likelihood estimation. The static and iterative model variants are special cases of this model by fixing $q = 0$ or $v = 0$, respectively. (For the definition of parameters v and q, see Methods, *Modeling* and below.) Equations 3.1-3.3 in *Modeling* can be rewritten in matrix notation as follows:

$$z_i = HX_i + \eta$$

$$X_i = FX_{i-1} + \varepsilon$$

where $X_i = \begin{bmatrix} x_i \\ m_i \end{bmatrix}$, $\varepsilon = \begin{bmatrix} \varepsilon_x \\ \varepsilon_m \end{bmatrix}$, $F = \begin{bmatrix} 0 & 1 \\ 0 & 1 \end{bmatrix}$, and $H = \begin{bmatrix} 1 & 0 \end{bmatrix}$. The state estimate $\widehat{X}_i$ on trial i is determined using a time-discrete Kalman filter:

$$\widehat{X}_{i|i-1} = F\widehat{X}_{i-1}$$

$$P_{i|i-1} = FP_{i-1}F^T + Q$$

$$K_i = P_{i|i-1}H^T\left(HP_{i|i-1}H^T + r\right)^{-1}$$

$$\widehat{X}_i = \widehat{X}_{i|i-1} + K_i\left(z_i - H\widehat{X}_{i|i-1}\right)$$

$$P_i = \left(I - K_iH\right)P_{i|i-1}$$

with covariance matrix $Q = \begin{bmatrix} v & 0 \\ 0 & q \end{bmatrix}$ and measurement noise variance r. The steady state can be written as

$$\widehat{X}_i = F\widehat{X}_{i-1} + K_i\left(z_i - HF\widehat{X}_{i-1}\right).$$

Contrary to Glasauer & Shi (2022), we fitted the model's predictions to the data in logarithmic space using maximum likelihood estimation. Given that there is uncertainty in the measurement z_i on trial i, represented by measurement variance r, it is possible to compute a distribution of possible reproductions on trial i. We computed the expected value $E[\widehat{X}_i]$ and covariance matrix $\mathrm{cov}[\widehat{X}_i]$ of the

estimated stimulus distribution on trial i by rewriting the steady-state equation as follows:

$$\begin{aligned}\widehat{X}_i &= F\widehat{X}_{i-1} + K_i(z_i - HF\widehat{X}_{i-1}) \\ &= F\widehat{X}_{i-1} + K_i\left(HX_i + \eta\right) - K_iHF\widehat{X}_{i-1} \\ &= (F - K_iHF)\widehat{X}_{i-1} + K_iHX_i + K_i\eta\end{aligned}$$

$$\begin{aligned}E[\widehat{X}_i] &= \left(F - K_iHF\right)E[\widehat{X}_{i-1}] + K_iHE[X_i] + K_i \cdot 0 \\ &= \left(F - K_iHF\right)E[\widehat{X}_{i-1}] + K_ix_i\end{aligned}$$

$$\begin{aligned}\mathrm{cov}[\widehat{X}_i] &= \left(F - K_iHF\right)\mathrm{cov}[\widehat{X}_{i-1}]\left(F - K_iHF\right)^T \\ &\quad + K_iH\mathrm{cov}[X_i]H^TK_i^T + K_i\mathrm{cov}[\eta]K_i^T \\ &= \left(F - K_iHF\right)\mathrm{cov}[\widehat{X}_{i-1}]\left(F - K_iHF\right)^T \\ &\quad + K_i \cdot 0 \cdot K_i^T + K_i \cdot r \cdot K_i^T \\ &= \left(F - K_iHF\right)\mathrm{cov}[\widehat{X}_{i-1}]\left(F - K_iHF\right)^T \\ &\quad + K_i \cdot r \cdot K_i^T\end{aligned}$$

The first element of the resulting expected value vector and covariance matrix correspond to the mean $\widehat{x}_i$ and variance σ_i^2 of the estimated stimulus distribution. The model's prediction of the reproduction on trial i is then determined by adding the shift term Δx to the mean of this distribution: $\widehat{y}_i = \widehat{x}_i + \Delta x$. Finally, the negative log-likelihood on trial i (NLL_i) is computed based on the probability that the participant's reproduction on that trial, y_i, came from the (normal) estimated response distribution, i.e., the estimated stimulus distribution of which the mean is shifted by Δx:

$$\mathrm{NLL}_i = -\ln\left(\mathcal{N}\left(y_i \mid \widehat{y}_i, \sigma_i^2\right)\right).$$

Chapter 4

Does stimulus order affect central tendency and serial dependence in vestibular path integration?

This chapter has been adapted from:

Willemsen, S. C. M. J., Oostwoud Wijdenes, L., van Beers, R. J., Koppen, M., & Medendorp, W. P. (2025). Does stimulus order affect central tendency and serial dependence in vestibular path integration? *In revision*.

4.1 Abstract

The reproduction of a perceived stimulus, such as a distance or a duration, is often influenced by two biases. Central tendency indicates that reproductions are biased toward the mean of the stimulus distribution. Serial dependence reflects that the reproduction of the current stimulus is influenced by the previous stimulus. Although these biases are well-documented, their origins remain to be determined. Studies on duration reproduction suggest that autocorrelation within a stimulus sequence may play a role. In this study, we explored whether the level of autocorrelation in a stimulus sequence affects central tendency and serial dependence in vestibular path integration. Participants (n = 24) performed a vestibular distance reproduction task in total darkness by actively replicating a passively moved stimulus distance with a linear motion platform. We compared two conditions: a high-autocorrelation condition, where stimulus distances followed a random walk, and a no-autocorrelation condition, where the same distances were presented in a randomly shuffled order. We quantified both biases using two approaches: separate simple linear regressions and a joint multiple linear regression model that accounts for the autocorrelation in the stimulus sequence. Simple linear regressions revealed that central tendency was weaker and serial dependence reversed in the high-autocorrelation condition compared to the no-autocorrelation condition. However, these differences were no longer observed in the multiple linear regression analysis, indicating that these biases were independent of the specific stimulus sequence protocol. We conclude that these perceptual biases in vestibular path integration persist regardless of stimulus autocorrelation, suggesting that they reflect robust strategies of the brain to process vestibular information in self-motion perception.

4.2 Introduction

Two perceptual biases that are often observed in reproduction tasks are central tendency and serial dependence. Central tendency is the notion that the participant's reproductions tend to be biased toward the mean of the underlying stimulus distribution (Hollingworth, 1910). This bias typically leads to an overestimation of smaller stimuli and an underestimation of larger stimuli (Loomis et al., 1993; Israël et al., 1997; Philbeck & Loomis, 1997; Grasso et al., 1999; Riecke et al., 2002; Jazayeri & Shadlen, 2010; Bergmann et al., 2011; Petzschner & Glasauer, 2011; Cicchini et al., 2012; Prsa et al., 2015; Murai & Yotsumoto, 2016; Roach et al., 2017; Sun et al., 2020; Willemsen et al., 2024). Serial dependence reflects that reproductions depend on the stimulus presented on the preceding trial (Holland & Lockhead, 1968; Cross, 1973). Most studies have identified attractive serial dependence, where the reproduction on the current trial is biased towards the stimulus on the previous trial (Fischer & Whitney, 2014; Liberman et al., 2014; Motala et al., 2020; Manassi & Whitney, 2022, 2024; Guan & Goettker, 2024; Willemsen et al., 2024). However, other research has reported repulsive serial dependence, indicating that the reproduction of the current stimulus is biased away from the previous stimulus (Fritsche et al., 2017; Sun et al., 2020).

Central tendency and serial dependence have been found to affect the perception of various stimuli, such as time durations, heading directions, and distances. Veridical distance perception is essential for path integration, a process in which one uses self-motion signals to continuously estimate one's position relative to a starting point (Mittelstaedt & Mittelstaedt, 1980; Etienne & Jeffery, 2004). These signals can be derived from our sensory systems, including the visual and vestibular systems (ter Horst et al., 2015), as well as the motor system (Laurens & Angelaki, 2017; van Helvert et al., 2022; Cullen, 2023). In previous work on path integration, where participants had to mainly rely on the vestibular sense, we found central tendency and attractive serial dependence effects (Willemsen et al., 2024). However, what causes these perceptual biases in vestibular path integration is not yet understood.

Recently, Glasauer & Shi (2021, 2022) have shown that the extent to which central tendency and serial dependence effects are present in duration reproduction tasks is affected by the autocorrelation in the stimulus sequence. When durations were presented randomly shuffled, without autocorrelation, reproductions showed central tendency and attractive serial dependence. However, when the same

durations were presented in a random-walk sequence with high autocorrelation, central tendency nearly disappeared and serial dependence became repulsive.

The origin of the different results between protocols remains unclear. Are these differences caused by participants responding differently in each condition, or are they byproducts of the different levels of stimulus autocorrelation? To address this question, it is important to note that central tendency and serial dependence are statistical concepts, usually defined as linear least-squares regression slopes. As such, their values can vary significantly based on the specific regression model employed and the selection of covariates included in the model. Central tendency is often characterized as 1 minus the regression slope of reproduced distance r_t on stimulus distance s_t (Glasauer & Shi, 2022; Willemsen et al., 2024) or, equivalently, as the negative of the regression slope of reproduction error e_t (r_t - s_t) on stimulus distance s_t (see Figure 4.1A; Sun et al., 2020). Serial dependence has been defined as the regression slope of reproduction error e_t on the previous stimulus s_{t-1} (see Figure 4.1B; Glasauer & Shi, 2022; Willemsen et al., 2024). However, as illustrated in Figure 4.1C, central tendency and serial dependence are not independent if there is autocorrelation in the stimulus sequence (i.e., when s_{t-1} affects s_t; see Appendix for more details). Similarly, there could be other dependencies that affect the central tendency and serial dependence coefficients (for instance, a potential effect of s_{t-1} on e_t through e_{t-1}; see Figure 4.4).

Here, we use causal graphs and the *d*-separation criterion (Pearl, 2009), to disentangle central tendency and serial dependence in vestibular path integration under conditions with and without stimulus sequence autocorrelation. Specifically, we ask which part of the differences in central tendency and serial dependence between the autocorrelation conditions can be attributed to a statistical explanation and which part requires an explanation in terms of different stimulus processing in the brain.

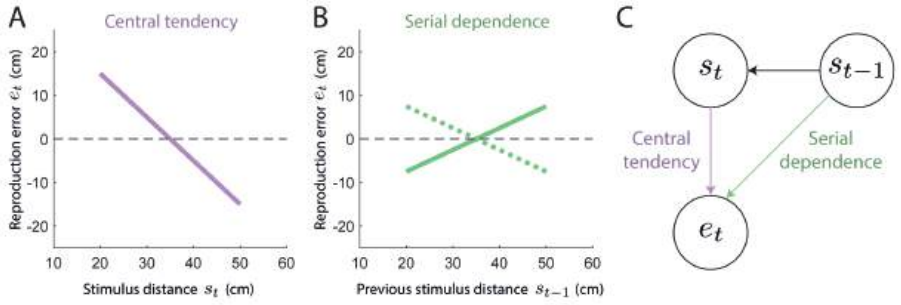

Figure 4.1. *A*: Reproduction error (reproduced distance - stimulus distance) as a function of stimulus distance. The shown line has a slope of -1, indicating a central tendency effect of 1. A regression line with a slope of 0 implies that there is no central tendency, and if also on top of the dashed line, that performance is veridical. *B*: Reproduction error against the stimulus distance on the previous trial. The solid line indicates an attractive serial dependence effect of 0.5, where the reproduction error on the current trial is generally more positive when there was a longer stimulus distance on the previous trial. The dotted line indicates a repulsive serial dependence effect of -0.5, where the reproduction error on the current trial is generally more negative when there was a longer stimulus distance on the previous trial. A regression line with a slope of 0 implies that there is no serial dependence. *C*: Central tendency (the effect of the stimulus distance on the current trial s_t on the reproduction error on the current trial e_t) and serial dependence (the effect of the stimulus distance on the previous trial s_{t-1} on the reproduction error on the current trial e_t) are not independent if there is autocorrelation in the stimulus sequence (i.e., when s_{t-1} affects s_t).

4.3 Methods

4.3.1 Participants

Twenty-five participants, naive to the purpose of the study, took part in the experiment. All participants had normal or corrected-to-normal vision, no hearing impairments, and no history of motion sickness. The study was approved by the ethics committee of the Faculty of Social Sciences at Radboud University Nijmegen and all participants gave written informed consent prior to the start of the experiment. Each participant completed a single experimental session of ~90 minutes and was compensated with course credits or €22.50. Although 24 participants were required for complete counterbalancing, one participant was excluded due to misunderstanding the task and producing reproduction movements in the wrong direction. This participant was therefore replaced by collecting data from an additional participant, resulting in a data set of 24 participants (19 women, 4 men, 1 non-binary person, aged 17–26 yr).

4.3.2 Setup

Participants were seated in a chair mounted on top of a linear motion platform, called a vestibular sled, that could be moved passively by the experimenter or actively by the participant using a steering wheel (see Figure 4.2). The sled was powered by a linear motor (TB15N; Tecnotion, Almelo, The Netherlands) and controlled by a servo drive (Kollmorgen S700; Danaher, Washington, DC), allowing it to move along the participant's interaural axis on a 93-cm-long track. The steering wheel (G27 Racing Wheel; Logitech, Lausanne, Switzerland) was attached to a table at chest level in front of the participant and had a rotation range of -450° to +450° with a resolution of 0.0549°. Throughout the experiment, the mapping between the steering wheel angle and the sled's linear velocity was set at 1 cm/s per degree. The task was performed in total darkness without any visual stimuli. Instruction messages prior to the task, as well as occasional messages throughout the experiment (e.g., to indicate breaks) were shown on an OLED screen (OLED77C3PUA; LG, Seoul, South Korea) placed in front of the sled. Participants wore in-ear headphones with active noise cancellation (QuietComfort 20; Bose, Framingham, MA) that played white noise to mask sound from the sled's motion, alternated by single-tone beeps to signal the different stages of each trial. In addition to the in-ear headphones, participants wore over-ear headphones with active noise cancellation (WH-1000XM5; Sony, Tokyo, Japan) to further block out the sound produced by the sled. The participant's head was fixated using cups placed against the top of the head. The participant also wore a five-point seat belt and could press one of the emergency buttons at the side of the chair to stop the sled at any time during the experiment. The experiment code was written in Python (v.3.10; Python Software Foundation).

4.3.3 Reproduction task

While seated on the vestibular sled, participants performed a distance reproduction task. During the stimulus movement, the sled passively moved the participant a predefined distance (see Figure 4.2A). This was succeeded by the reproduction movement, during which the participant actively tried to replicate the passively moved distance by steering the sled into the opposite direction (see Figure 4.2B). In other words, the participant aimed to return to the start position of the stimulus movement.

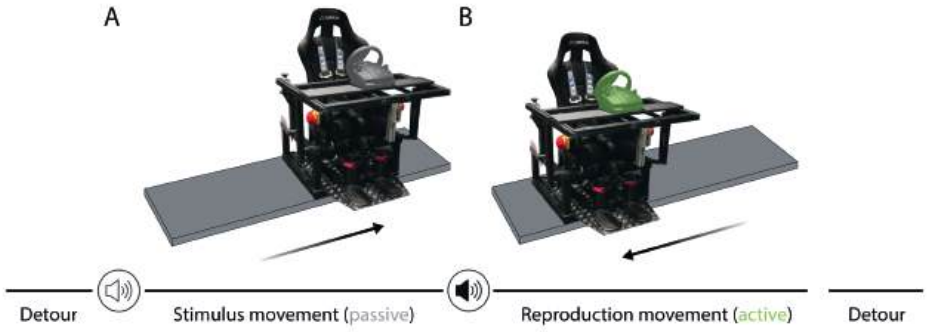

Figure 4.2. Vestibular distance reproduction task. *A*: The participant was seated on a vestibular sled, consisting of a chair placed on top of a linear motion platform. On every trial, a low-tone beep alerted the participant to the upcoming passive movement that would move them by an unknown stimulus distance. *B*: Afterwards, the second, high-tone beep prompted the participant to use the steering wheel and reproduce the stimulus distance by steering the sled back in the opposite direction. Trials were separated by two random detour movements that returned the sled to the start position.

In each trial, a low-tone beep (347 ms) indicated the upcoming stimulus movement. The duration of the stimulus movement varied randomly between 1.3 s and 1.6 s. We defined the lower bound such that all stimulus movements had a peak absolute acceleration below 980 cm/s^2 and a peak speed below 100 cm/s. The upper bound resulted in the shortest stimulus movement to have a peak absolute acceleration of ~38 cm/s^2 and a peak speed of ~20 cm/s, which well surpassed the vestibular thresholds (Kingma, 2005). For each participant, the stimulus movements were consistently in one direction, with the leftward and rightward directions counterbalanced across participants. Per participant, all stimulus movements started from the same start position, which was on the right side of the track for leftward stimulus movements and on the left side of the track for rightward stimulus movements, ensuring enough space on the track for all potential stimulus movements. The start position was determined for every participant individually depending on their largest stimulus distance. In the case of leftward stimulus movements, the start position was determined by adding the largest stimulus distance to the leftmost position on the sled track plus an additional small margin of 4 cm. For rightward stimulus movements, the start position was computed by subtracting the largest stimulus distance and the margin from the rightmost position on the track.

The stimulus movement was followed by a random waiting time between 0.5 s and 1 s, after which a high-tone beep (110 ms) cued the start of the reproduction movement. If the participant rotated the steering wheel before the beep, the trial

was aborted. Participants were instructed to make one smooth reproduction movement (without steering back or resuming steering after stopping) and were free to choose the duration of the movement. The sled could be steered up to a maximum speed of 100 cm/s and could be stopped by returning the steering wheel back to the upright position. The movement was terminated when the speed fell below 2 cm/s. The sled also stopped moving when the speed fell below 6 cm/s while the steering angle remained unchanged for 100 ms or the steering changed direction (mean ± SD across participants: 71 ± 59 trials out of a total of 260 trials). This second stopping criterion was added to prevent the case where the participant intended to stop the movement but did not fully return the steering wheel to the upright position. When one of these stopping criteria was met, the sled would not stop abruptly but would decelerate in 1 s to a speed of 0 cm/s. The sled also stopped moving when the end of the sled track was reached (mean ± SD: 2 ± 2 trials).

Participants received no feedback about their reproduction performance during the experiment (except during the training block, see below). To prevent the participant from obtaining implicit feedback about their reproduced distance, the sled was brought back to the start position for the next stimulus movement through two random detour movements. The first detour relocated the sled to a random position within ±30 cm from the middle of the track with a random duration between 1.8 s and 2.3 s. The second detour moved the sled to the start position in 1.3 s. All detour and stimulus movements followed a minimum-jerk profile.

4.3.4 Paradigm

To study how the amount of autocorrelation between the stimulus distances across trials affects central tendency and serial dependence biases in vestibular path integration, we created two experimental conditions per participant presenting the same stimulus distances with different stimulus orders. In the high-autocorrelation condition, stimulus distances followed a random walk while in the no-autocorrelation condition, the same distances were randomly shuffled (see Figure 4.3).

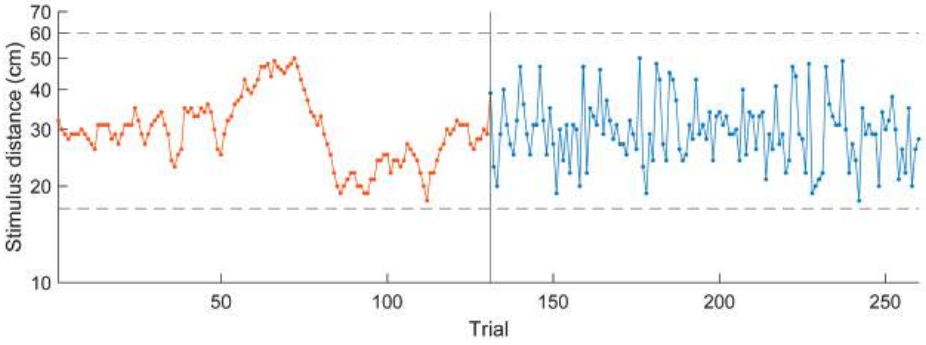

Figure 4.3. Example sequence of stimulus distances throughout the entire experimental session for a participant starting with the high-autocorrelation condition. During the first 130 test trials, the stimulus distances followed a random walk on logarithmic scale (orange). In the second half of the experiment, the same distances were presented in a randomly shuffled order (blue). The dashed lines indicate the minimum and maximum possible stimulus distance.

For each participant, we first generated 130 stimulus distances following a random walk. In line with our previous study (Willemsen et al., 2024), the random walk was generated on logarithmic scale such that the resulting stimulus distances were approximately normally distributed on this scale. For this transform, distances were made dimensionless by dividing by a reference distance (1 cm). On a linear scale, the distances varied between 17 cm and 60 cm, and the first distance of the random-walk sequence was set to the median of this distance range on logarithmic scale, which corresponds to 31.9 cm on linear scale. To create the remainder of the sequence, 129 random shifts were drawn from a normal distribution with a mean of 0 and SD of 0.08, and these were cumulatively summed to the first distance. Across participants, the stimulus distances on logarithmic scale varied between 2.83 and 4.05, the mean of the sequence between 3.37 and 3.50, the SD of the sequence between 0.20 and 0.27, and the lag-1 autocorrelation was larger than 0.9. We computed the lag-1 autocorrelation r_1 (Box et al., 2015) using

$$r_1 = \frac{\frac{1}{N}\sum_{t=1}^{N-1}(y_t - \overline{y})(y_{t+1} - \overline{y})}{c_0}. \tag{4.1}$$

Here, the numerator is the autocovariance of the sequence which is divided by the sample variance of the sequence c_0, resulting in an autocorrelation value between -1 and 1. Furthermore, N denotes the total number of samples in the sequence and $\overline{y}$ the sample mean of the sequence. To create the no-autocorrelation condition, the same 130 stimulus distances were shuffled until the autocorrelation of the sequences was between -0.001 and 0.001.

Participants experienced both conditions in a single experimental session of 260 test trials (see Figure 4.3 for an example sequence of stimulus distances) without being informed about the presence of the two conditions. The order of the conditions was counterbalanced across participants. There was a short break (~2 min) after every 52 trials (~10 min) with the room lights turned on to prevent dark adaptation.

Prior to the test trials, participants completed 20 training trials to get acquainted with the task. The stimulus distances on the training trials were drawn from a uniform distribution between 17 cm and 60 cm on linear scale. The training trials were performed in darkness and differed from the test trials in two respects. During the first 10 training trials, instruction texts were displayed on the screen alongside the beeps to indicate the various trial phases. Four instruction texts were shown for each trial, preceding the first detour, the second detour, the stimulus movement, and the reproduction movement, respectively. In the second half of the training trials, these instruction texts were not shown such that only the beeps indicated the different trial phases. The second difference with the test trials was that participants received feedback about their performance, displayed as the signed reproduction error in centimeters at the end of each training trial. We did not analyze the training trials.

4.3.5 Data analysis

Pre-processing

We analyzed data from the test trials offline in MATLAB (v.R2019a, MathWorks). The end position of the reproduction movement was defined as the sled position at the moment when the participant moved the steering wheel upright. We chose this position as opposed to the sled position after the slow-down period, as it more accurately reflects the participant's intended end position. Some of the recorded sled position profiles indicated that movement speed plateaued at a low but nonzero value before the slow-down period was initiated. The movement end was therefore corrected to the first time point where sled speed was < 8 cm/s (instead of the online threshold of 6 cm/s) while the steering angle remained constant for at least 100 ms or the steering direction changed. On average, the end position of 20 trials per participant were determined in this way (mean ± SD: 20 ± 15 trials). The reproduction error was computed as reproduced distance minus stimulus distance on logarithmic scale, with negative values indicating an undershoot and positive values an overshoot. We excluded trials if the participant initiated the reproduction movement too early, if reproduction movements were in the wrong direction, or if

the reproduced distance was less than 1 cm (mean ± SD: 5 ± 6 trials). There was no effect of movement direction on the mean unsigned reproduction error across trials (Wilcoxon rank-sum test, $p = 0.624$, rank-biserial correlation = 0.13), so participants were analyzed as a single group, disregarding this factor.

Central tendency and serial dependence computation

Figure 4.4A illustrates a causal diagram *G* (Pearl, 2009) of the high-autocorrelation condition. Variables are represented as nodes and possible causal relationships between the variables as directed edges. A path between two variables consists of a set of edges that connects the two variables (irrespective of the direction of the edges). In this diagram, the *s*-nodes represent the stimulus distances and the *e*-nodes the reproduction errors at different trials t. As the stimulus distances in this condition are presented in a random-walk sequence, we know that the current stimulus s_t depends on the previous stimulus s_{t-1} which in turn depends on s_{t-2} and so forth (the top row in Figure 4.4A). Furthermore, the current reproduction error may be affected by the current and previous stimulus distances (the vertical and diagonal edges in Figure 4.4A), and the previous reproduction error (the bottom row in Figure 4.4A).

The edge between the current stimulus s_t and the current reproduction error e_t represents the central tendency effect, whose coefficient CT we want to estimate. A negative coefficient suggests a central tendency effect, where the longer the stimulus distance is, the more it is underestimated (i.e., the more negative the reproduction error becomes). Finding a coefficient of 0 implies that there is no central tendency effect (i.e., the reproduction error is constant across stimulus distances) and a positive coefficient implies that there is anti-central tendency in the reproductions.

Similarly, the edge from the stimulus distance on the previous trial s_{t-1} to the reproduction error on the current trial e_t captures the serial dependence effect at lag 1. Here, we express serial dependence as the dependence of the current error on the previous stimulus distance ('absolute' serial dependence; e.g., Holland & Lockhead, 1968) instead of the dependence of the current error on the difference between the previous stimulus and the current stimulus ('relative' serial dependence; e.g., Fischer & Whitney, 2014). The latter metric can erroneously result in a serial dependence effect if stimuli are defined on an open scale (such as distances or durations) and the reproductions are constant across stimuli [see Appendix A in Glasauer & Shi (2022)]. A positive (attractive) serial dependence coefficient SD_1 indicates that if the participant experienced a longer stimulus

distance on the previous trial, they tend to show a larger overestimation (i.e., a more positive reproduction error) on the current trial. A coefficient of 0 implies that there is no serial dependence and a negative (repulsive) coefficient reflects that a longer stimulus distance on the previous trial tends to be followed by a larger underestimation (i.e., a more negative reproduction error) on the current trial.

As becomes apparent from the graph in Figure 4.4A, beside the direct path CT there are indirect paths through which s_t can affect e_t. For example, there exists an indirect path from s_t to e_t via common cause s_{t-1}. In order to accurately estimate the coefficient of the direct path CT, this indirect path should be 'blocked' by adding variable s_{t-1} to the adjustment set Z, i.e., by adding this variable as a regressor to the multiple linear regression model ($e_t = CT \cdot s_t + \beta \cdot s_{t-1} + \varepsilon$). More generally, all indirect paths that connect s_t and e_t should be blocked, in which case s_t is said to be *d*-separated from e_t. The coefficient CT is said to be identifiable when there exists an adjustment set Z that *d*-separates s_t from e_t and when Z contains no descendants of e_t [Theorem 5.3.1., the single-door criterion for direct effects, Pearl (2009)]. If these conditions are not satisfied, this may lead to a biased estimate of CT.

Beside the direct path CT, we can see that all indirect paths between s_t and e_t contain s_{t-1}, so by adding this variable to the adjustment set, all indirect paths between s_t and e_t are blocked (see Figure 4.4B). Similarly, to *d*-separate s_{t-1} and e_t (beside the direct path SD_1), s_t and e_{t-1} should be adjusted for, blocking all indirect paths between s_{t-1} and e_t (see Figure 4.4C). Thus, to estimate the direct CT effect, the regression of e_t on s_t also has to include the regressor s_{t-1}, and to estimate the direct SD_1 effect, the regression of e_t on s_{t-1} also has to include the regressors s_t and e_{t-1}. As the latter regression model contains the first (and adding the e_{t-1} regressor to the CT regression model does not open up paths between s_t and e_t), we combine the two multiple linear regression models. This results in one model that can be used to estimate both the central tendency effect CT and the serial dependence effect SD_1:

$$e_t = \beta_0 + CT \cdot s_t + SD_1 \cdot s_{t-1} + \beta_1 \cdot e_{t-1} + \varepsilon. \tag{4.2}$$

A similar causal graph can be drawn for the no-autocorrelation condition, but without edges between the stimulus distances. From this graph follows that to estimate CT, no variables have to be adjusted for, and to estimate SD_1, e_{t-1} should be adjusted for. The same regression model as above can also be used to estimate the central tendency and serial dependence effects in the no-

autocorrelation condition, because indirect paths between s_t and e_t remain blocked when also adjusting for s_{t-1} and e_{t-1}, and indirect paths between s_{t-1} and e_t remain blocked when also adjusting for s_t.

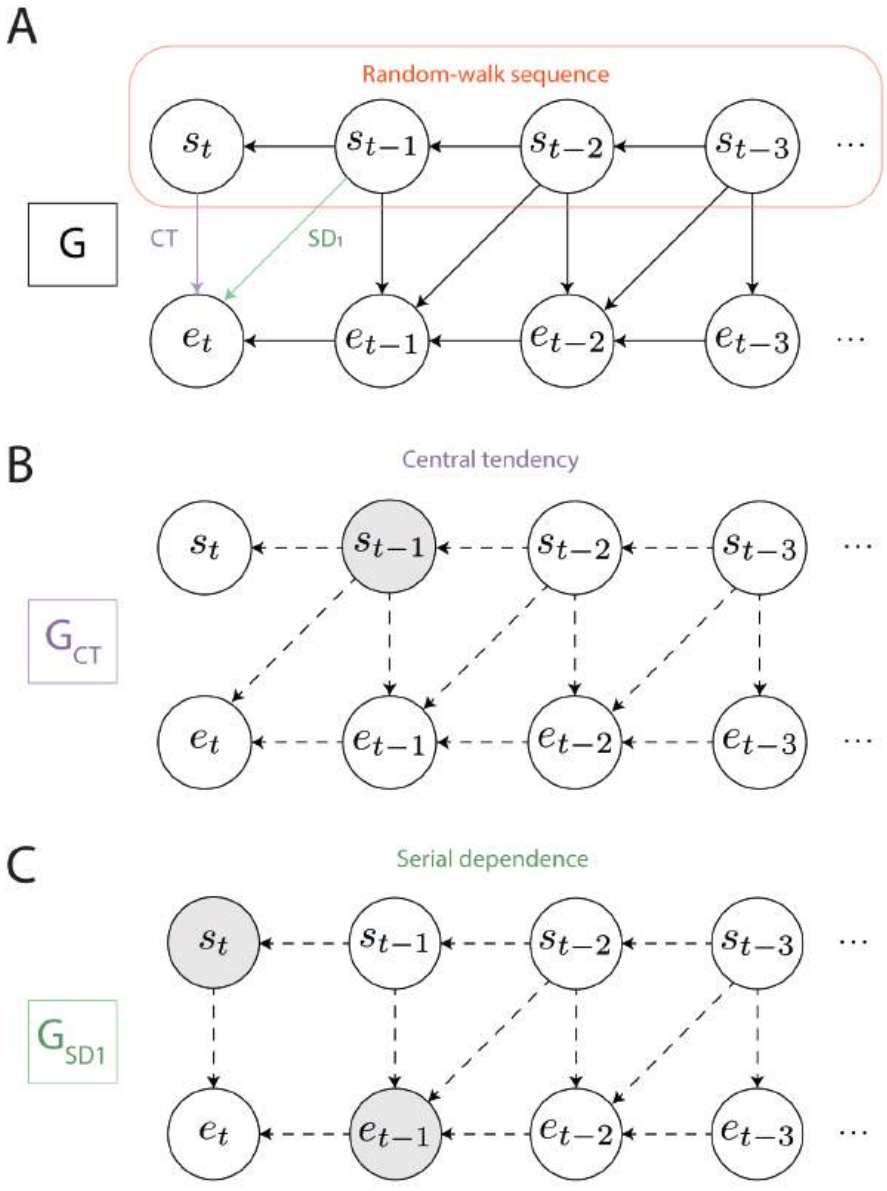

Figure 4.4. *A*: Causal diagram G representing the assumed causal relationships between the stimulus distances (s) and reproduction errors (e) across trials (t) in the high-autocorrelation condition. Variables are presented by nodes and possible causal relationships between the variables by directed edges. A path between two variables denotes a set of edges that connects the two variables (irrespective of the direction of the edges). The upper row of nodes represents the random-walk sequence, in which the previous stimulus affects the current stimulus. The edge CT between the current stimulus s_t and the current reproduction error e_t reflects the possible central tendency effect. Similarly, the edge SD_1 between the previous stimulus s_{t-1} and the current reproduction error e_t represents the possible serial dependence effect at lag 1. *B*: Application of the single-door criterion to determine which variables to include as regressors in a multiple linear regression model such that central tendency coefficient CT is identifiable. Graph G_{CT} is equal to graph G with edge CT removed. Dashed arrows indicate (parts of) blocked paths between s_t and e_t, and gray nodes represent the variables to add as regressors. By adding s_{t-1} as a regressor, all biasing paths between s_t and e_t are blocked, and CT can be estimated. *C*: Application of the single-door criterion to serial dependence coefficient SD_1. By adding s_t and e_{t-1} as regressors, all biasing paths between s_{t-1} and e_t are blocked, and SD_1 becomes identifiable.

To compare the central tendency and serial dependence across the autocorrelation conditions, we fitted this model to the data of each participant and each condition separately, on a logarithmic scale. Partial regression plots of the current reproduction error on the current stimulus distance, and of the current reproduction error on the previous stimulus distance are used to visualize the central tendency and serial dependence effects, respectively. These plots were created using the MATLAB function *plotAdded* and illustrate the effect of one regressor on the response variable while keeping the other regressors constant. The slope of the fitted line corresponds to the fitted partial regression coefficient (CT and SD_1, respectively).

To illustrate how accounting for the biasing paths affects the central tendency and serial dependence coefficients, we also computed the same coefficients by fitting two separate simple linear regressions to the data of each participant and condition. The models used to estimate the central tendency effect CT and the serial dependence effect SD_1 were $e_t = \beta_0 + CT \cdot s_t + \varepsilon$ and $e_t = \beta_0 + SD_1 \cdot s_{t-1} + \varepsilon$, respectively. The Appendix provides a comparison of the different central tendency and serial dependence metrics based on simulated data.

Statistical tests

To further analyze the central tendency and serial dependence coefficients, we used the following statistical tests. We first tested whether there was an effect of condition (no/high-autocorrelation) on the central tendency/serial dependence coefficients with paired-samples *t*-tests. One-sample *t*-tests were used to assess

whether the central tendency/serial dependence coefficients significantly differed from 0. Cohen's d (Cohen, 1988) and 95% confidence intervals are reported.

4.4 Results

Participants performed a vestibular distance reproduction task in the dark where they actively reproduced a stimulus movement that they had passively experienced. To manipulate the level of autocorrelation of the stimulus distances, we established a high-autocorrelation condition characterized by a random walk of stimuli, alongside a no-autocorrelation condition where the same stimuli were randomly shuffled. We examined the central tendency and serial dependence effects on the reproductions in these conditions.

4.4.1 Central tendency

Figure 4.5, A and B, present the simple linear regressions of reproduction error versus stimulus distance on the current trial, without adjusting for covariates, for a single participant in the no- and high-autocorrelation conditions, respectively. The slope of the fitted regression line corresponds to the central tendency coefficient CT. In both conditions, CT is negative indicating central tendency, with the high-autocorrelation condition showing less central tendency than the no-autocorrelation condition. For comparison, Figure 4.5, C and D, show the partial regression plots of the same participant based on the multiple linear regression model (see Equation 4.2), with adjustment for covariates. These adjusted values indicate that the effective variance in the stimulus distances is lower in the high-autocorrelation than the no-autocorrelation condition. In contrast to the analysis presented in Figure 4.5, A and B, the partial regression coefficients suggest that central tendency remains fairly consistent across conditions.

Figure 4.5, E and F, illustrate the regression lines for all participants, as estimated by the multiple linear regression model, which reveal no significant difference in central tendency between the conditions (paired-samples *t*-test: $p = 0.550$, Cohen's $d = 0.12$, $95\%\,\mathrm{CI} = [-0.07, 0.14]$). As visualized in Figure 4.6A, the CT values exhibit considerable variability between participants. Yet, they are on average negative across conditions ($\mathrm{M} = -0.38$, $\mathrm{SD} = 0.29$), indicating a substantial level of central tendency (one-sample *t*-test: $p < 0.001$, Cohen's $d = 1.35$, $95\%\,\mathrm{CI} = [-0.46, -0.31]$).

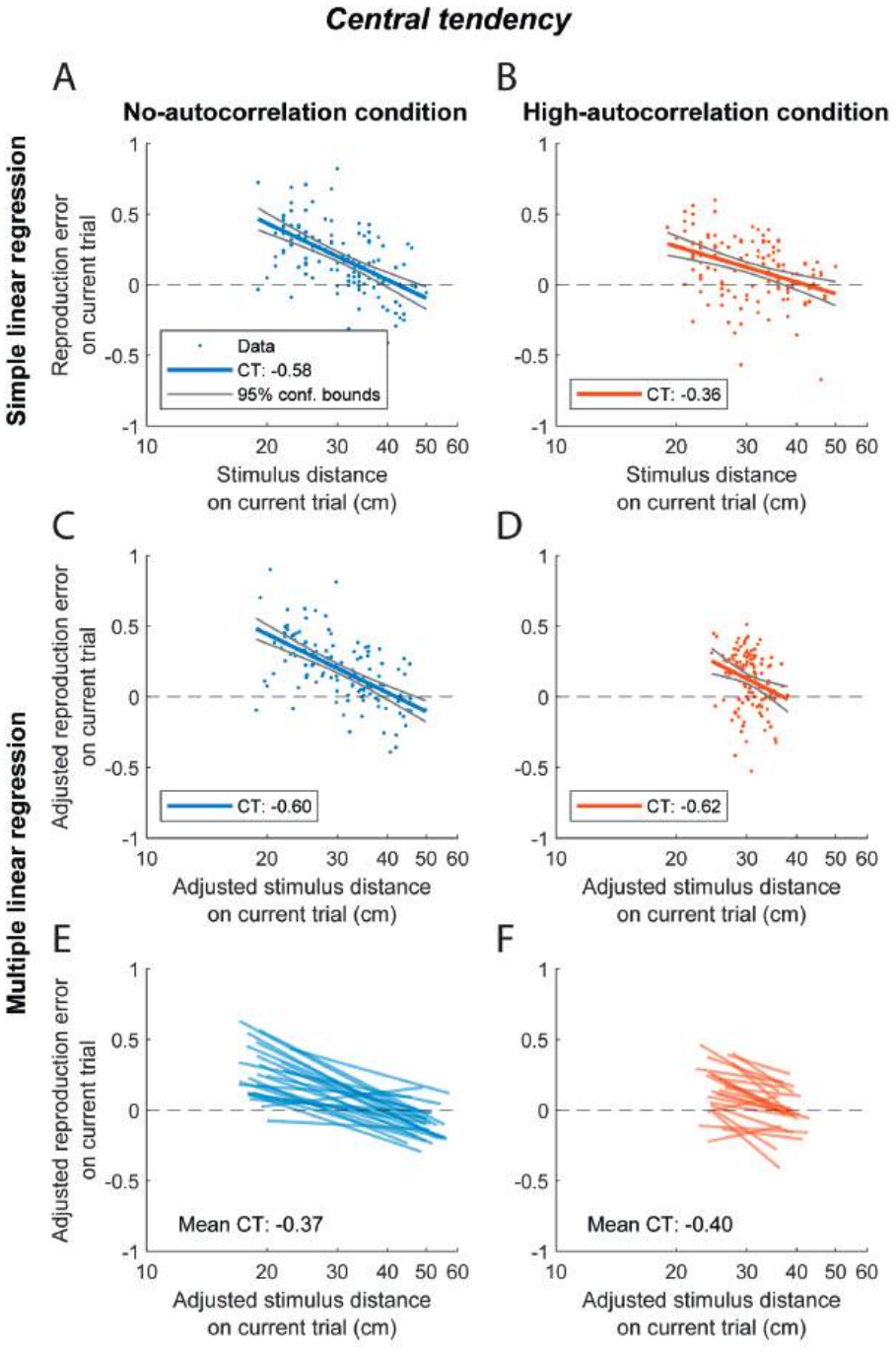
Central tendency
A
No-autocorrelation condition
B
High-autocorrelation condition
Simple linear regression
Reproduction error on current trial
Data
CT: -0.58
95% conf. bounds
CT: -0.36
Stimulus distance on current trial (cm)
C
D
Multiple linear regression
Adjusted reproduction error on current trial
CT: -0.60
CT: -0.62
Adjusted stimulus distance on current trial (cm)
E
F
Mean CT: -0.37
Mean CT: -0.40

Figure 4.5. Regression plots of the reproduction error on the current trial as a function of stimulus distance on the current trial in the no-autocorrelation (blue) and high-autocorrelation (orange) conditions on logarithmic scale for an individual participant (*A-D*) and all participants (*E-F*). Regression lines illustrate the central tendency, with the regression slope corresponding to the regression coefficient CT. *A-B*: Simple linear regression lines, with the CT value reported in the key. *C-D*: Partial regression lines based on the multiple linear regression model. *E-F*: Partial regression lines with the mean fitted CT coefficient across participants indicated.

For comparison, Figure 4.6B presents the CT values, as calculated with the simple linear regression. In both conditions, the mean CT coefficient across participants is significantly smaller than zero (no-autocorrelation: $\mathrm{M} = -0.36$, $\mathrm{SD} = 0.21$, $p < 0.001$, Cohen's $d = 1.70$, $95\%\,\mathrm{CI} = [-0.45, -0.28]$, high-autocorrelation: $\mathrm{M} = -0.26$, $\mathrm{SD} = 0.27$, $p < 0.001$, Cohen's $d = 0.98$, $95\%\,\mathrm{CI} = [-0.37, -0.16]$). More strikingly, the average CT values differed significantly between the two conditions (paired-samples *t*-test: $p = 0.016$, Cohen's $d = 0.53$, $95\%\,\mathrm{CI} = [-0.18, -0.03]$), demonstrating that not accounting for the autocorrelation in the stimulus sequence can result in different central tendency coefficients.

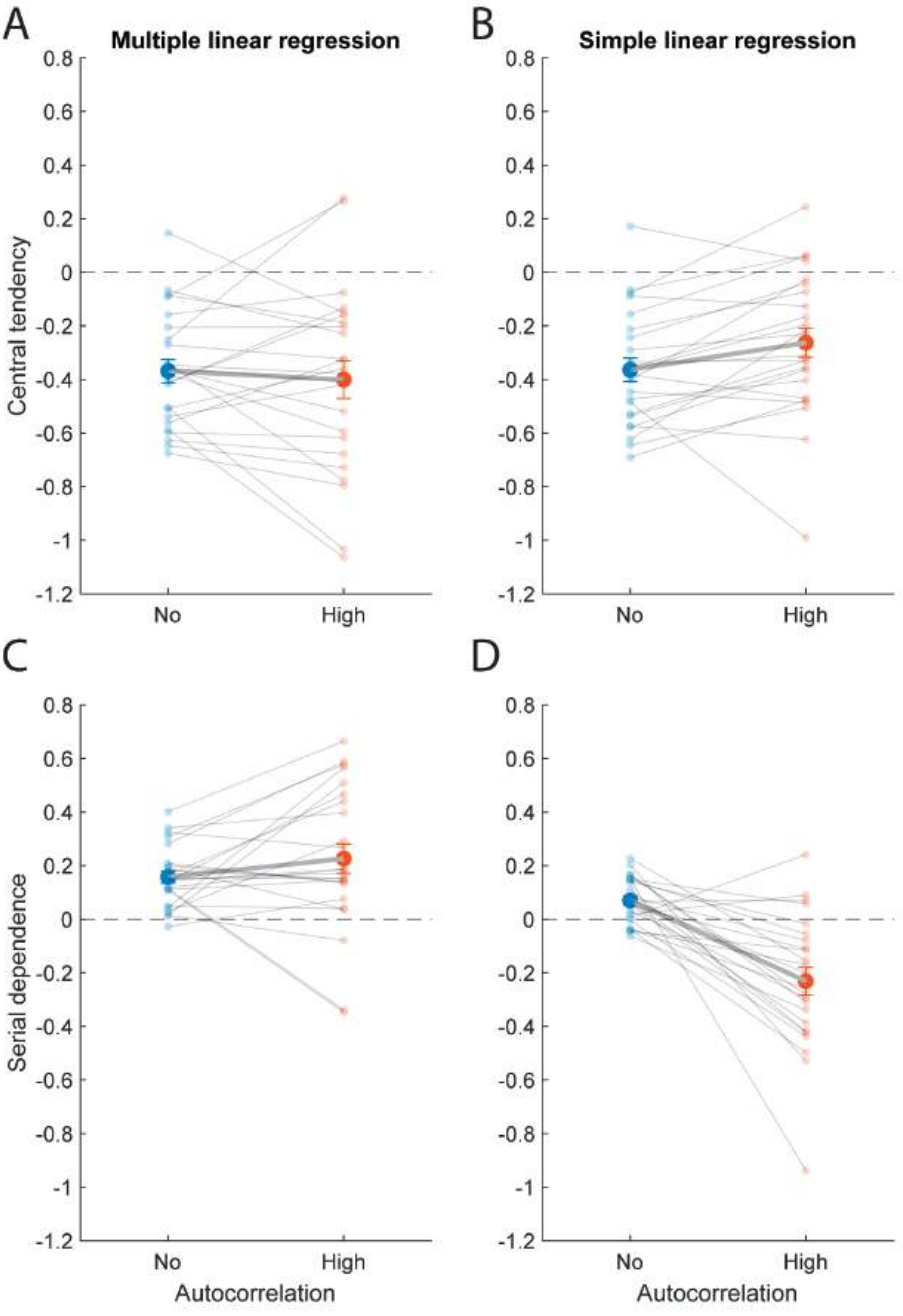
A
Multiple linear regression
B
Simple linear regression
C
D
Central tendency
Serial dependence
0.8
0.6
0.4
0.2
0
-0.2
-0.4
-0.6
-0.8
-1
-1.2
No
High
Autocorrelation

Figure 4.6. Central tendency (*A*, *B*) and serial dependence (*C*, *D*) regression coefficients in the no-autocorrelation (blue) and high-autocorrelation (orange) conditions. Panels *A* and *C* show the partial regression coefficients computed with the multiple linear regression model, and panels *B* and *D* show the regression coefficients computed with the two separate simple linear regression models. Bold data points and error bars represent the mean ± SE across participants. Transparent data points and their connecting lines show individual participants.

4.4.2 Serial dependence

Figure 4.7, A and B, show simple regression plots of the same exemplary participant as in Figure 4.5, but now with reproduction error on the current trial plotted against stimulus distance on the previous trial. The regression line illustrates the serial dependence, of which the slope corresponds to the fitted regression coefficient SD_1. In the no-autocorrelation condition, the positive SD_1 indicates that there is attractive serial dependence, whereas this coefficient is negative in the high-autocorrelation condition, representing repulsive serial dependence. Figure 4.7, C and D, display regression plots of the same data set adjusted for the other regressors in the multiple linear regression model (see Equation 4.2). Compared to the simple regression analysis, SD_1 remains positive in the no-autocorrelation, but shifts from negative to positive in the high-autocorrelation condition.

Figure 4.7, E and F, display the serial dependence lines for all participants, as determined by the multiple linear regression model. A paired-samples *t*-test indicated no significant difference between the average SD_1 coefficients of the no- and high-autocorrelation conditions ($p = 0.180$, Cohen's $d = 0.28$, $95\%\,\mathrm{CI} = [-0.17, 0.03]$). Despite substantial intersubject variability (see Figure 4.6C), SD_1 was on average positive across conditions ($\mathrm{M} = 0.19$, $\mathrm{SD} = 0.21$), suggesting attractive serial dependence (one-sample *t*-test: $p < 0.001$, Cohen's $d = 0.93$, $95\%\,\mathrm{CI} = [0.14, 0.25]$).

For comparison, Figure 4.6D shows these coefficients, as determined from fitting the simple linear regression. In this case, a paired-samples *t*-test revealed a significant difference between the two conditions ($p < 0.001$, Cohen's $d = 1.10$, $95\%\,\mathrm{CI} = [0.19, 0.41]$), with attractive serial dependence in the no-autocorrelation condition ($\mathrm{M} = 0.07$, $\mathrm{SD} = 0.08$, one-sample *t*-test: $p < 0.001$, Cohen's $d = 0.82$, $95\%\,\mathrm{CI} = [0.04, 0.10]$) and repulsive serial dependence in the high-autocorrelation condition ($\mathrm{M} = -0.23$, $\mathrm{SD} = 0.25$, one-sample *t*-test: $p < 0.001$, Cohen's $d = 0.92$, $95\%\,\mathrm{CI} = [-0.33, -0.13]$). Again, this highlights that the two analysis methods can lead to different results and therefore different interpretations of the data.

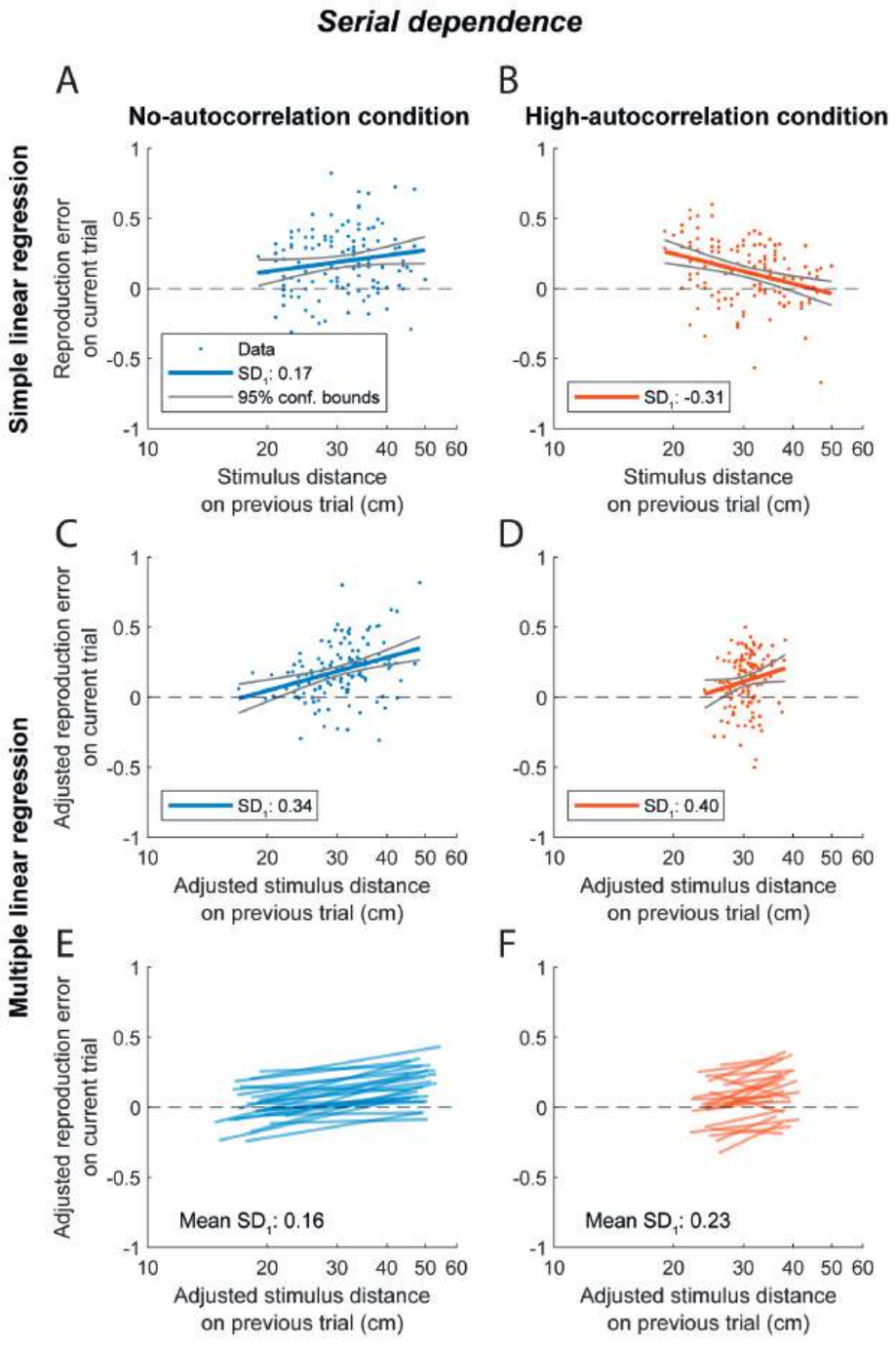
Serial dependence
A
No-autocorrelation condition
B
High-autocorrelation condition
Simple linear regression
Reproduction error on current trial
Data
SD1: 0.17
95% conf. bounds
SD1: -0.31
Stimulus distance on previous trial (cm)
C
D
Multiple linear regression
Adjusted reproduction error on current trial
SD1: 0.34
SD1: 0.40
Adjusted stimulus distance on previous trial (cm)
E
F
Mean SD1: 0.16
Mean SD1: 0.23

Figure 4.7. Regression plots of the reproduction error on the current trial as a function of stimulus distance on the previous trial in the no-autocorrelation (blue) and high-autocorrelation (orange) conditions on logarithmic scale. Regression lines illustrate the serial dependence, with the regression slope corresponding to the regression coefficient SD_1. The figure is in the same format as Figure 4.5, with the same individual participant.

4.5 Discussion

In this study, we investigated the effect of the autocorrelation in the stimulus sequence on central tendency and serial dependence in vestibular path integration. Participants performed a distance reproduction task using a vestibular sled in total darkness. On each trial, the participant was passively moved over a stimulus distance, which they actively reproduced by steering the sled back to the start position. Each participant completed two experimental conditions during which the same stimulus distances were presented but in different orders. In the high-autocorrelation condition, the stimuli followed a random walk, whereas in the no-autocorrelation condition, the stimulus distances were randomly shuffled. Central tendency and serial dependence were assessed either by conducting two separate simple linear regressions or by employing a single multiple linear regression model. The latter approach was derived from a causal diagram (see Figure 4.4; cf. Pearl, 2009), taking into account that the two perceptual biases may covary due to autocorrelated stimuli. We found that applying the two analytical methods to the vestibular path integration data set yielded different results regarding how autocorrelation influences both central tendency and serial dependence.

The simple linear regressions suggest that central tendency was weaker in the high-autocorrelation than in the no-autocorrelation condition. This approach also indicates that the level of stimulus autocorrelation can make the serial dependence coefficient flip sign: the high-autocorrelation condition demonstrated repulsive serial dependence, while the no-autocorrelation condition demonstrated attractive serial dependence. However, when we used multiple linear regression to jointly quantify both central tendency and serial dependence, thus accounting for their covariation as well as the effect of the previous reproduction error, we observed no significant differences in either perceptual bias between the two autocorrelation conditions. In both conditions, we found similar central tendency and attractive serial dependence effects, suggesting that these biases are independent of the specific stimulus sequence protocol that was used. Can we reconcile these different outcomes with findings from previous literature?

Our simple linear regression results align with the findings of Glasauer & Shi (2022), who reported that both central tendency and serial dependence in reproduced durations, estimated using separate simple linear regressions, depended on the sequence of the presented stimuli. The multiple linear regression coefficients of this study are consistent with the central tendency and serial dependence biases found in our previous study on vestibular path integration (Willemsen et al., 2024). In this earlier study, stimulus distances were randomly sampled from either a short- or long-distance distribution and presented in a mixed or blocked order, with stimulus autocorrelations (per distance and order type) that were on average close to 0 across participants (mean ± SD: -0.03 ± 0.13). The reproduced distances showed a similar amount of central tendency and attractive serial dependence as in the present study, for both distance types (short/long) and presentation contexts (mixed/blocked).

The novelty of the present study is that we found central tendency and serial dependence in vestibular path integration to be independent of stimulus autocorrelation, if these biases are estimated by a multiple linear regression model that accounts for their covariation. Thus, the differences in central tendency and serial dependence identified through the separate simple linear regressions are due to the different levels of autocorrelation that were not accounted for in the regressions, rather than due to differences in brain processing across the two conditions. As shown in the Appendix, separately estimating the biases in simulated reproductions that show central tendency but no serial dependence, can falsely result in a repulsive serial dependence coefficient when stimuli are autocorrelated. The autocorrelation in the stimuli makes that a short stimulus is likely to follow another short stimulus. If we tend to overestimate short stimuli irrespective of the previous stimulus (the central tendency effect), this will also show up as repulsive serial dependence, i.e., an overestimation that occurs if the previous stimulus was short.

Here, we show that central tendency and serial dependence in vestibular path integration persist regardless of stimulus autocorrelation, which suggests that they reflect robust neural processes that affect the estimation of self-motion, even when the stimulus changes predictably over time. Specifically, we found that reproductions showed central tendency: shorter stimulus distances were generally overestimated, while longer distances tended to be underestimated. This pattern aligns with previous findings in distance and heading perception, where central tendency has been consistently reported (Loomis et al., 1993; Warren & Saunders, 1995; Philbeck & Loomis, 1997; Israël et al., 1997; Grasso et al., 1999; Riecke et al., 2002; Bergmann et al., 2011; Petzschner & Glasauer, 2011; Petzschner et al., 2012;

Prsa et al., 2015; Sun et al., 2020). Furthermore, the reproduction errors showed attractive serial dependence, which indicates that self-motion perception of participants is also biased toward the stimulus distance of the immediately preceding trial. Attractive serial dependence effects have been widely reported in the perception literature (Fischer & Whitney, 2014; Liberman et al., 2014; Motala et al., 2020; Manassi & Whitney, 2022, 2024; Guan & Goettker, 2024). While attractive serial dependence in vestibular path integration may help to stabilize self-motion perception from trial to trial, it would reduce sensitivity to small changes between trials (Sun et al., 2020; Manassi & Whitney, 2024).

To computationally understand the underlying neurocognitive processes, numerous studies have adopted a Bayesian framework to explain central tendency and serial dependence. In this approach, the brain is thought to encode information about previous stimuli as a prior distribution, which is optimally combined with the sensory likelihood, using Bayes' rule (Jürgens & Becker, 2006; Petzschner & Glasauer, 2011; Petzschner et al., 2012; Prsa et al., 2015; Lakshminarasimhan et al., 2018). It can be shown that if the prior and likelihood are modeled as Gaussian distributions, their combination will result in a posterior distribution with a lower variance, reflecting more precise but potentially biased estimates. Research indicates that the posterior parietal cortex may play a role in these computations (Akrami et al., 2018).

Within the Bayesian framework, Glasauer & Shi (2022) proposed a Kalman filter model that iteratively combines the sensory measurement from the current trial with the stimulus estimate from the previous trial. It can be shown that the steady state of this model is similar to an ARX model on logarithmic scale (Shirzhiyan et al., 2023). By varying the Kalman filter's assumptions about the estimated stimulus distribution, the authors assessed how various beliefs about the generation of stimuli in the environment could explain the central tendency and serial dependence biases. Both central tendency and serial dependence effects, in duration perception as well as in visual path integration, were well explained by a model that assumes that the stimuli are drawn from a stimulus distribution of which the mean can fluctuate across trials (Glasauer & Shi, 2022). Additionally, this model demonstrated a reasonably good fit to the vestibular distance reproductions in our previous study, successfully capturing the central tendency effects in the data, although it was less effective in explaining the serial dependence effects (Willemsen et al., 2024). As the focus of the current study was on the computation of central tendency and serial dependence across different levels of stimulus autocorrelation, evaluating the fit of the Kalman filter model to the current data set was outside the scope of this study.

As a final consideration regarding the multiple linear regression analysis, it is important to note that the causal diagram from which it is derived represents an assumed causal structure underlying the high-autocorrelation condition. If relevant variables or connections are missing, there is a risk that direct effects may be misidentified. For example, earlier stimulus distances (see s_{t-2}, s_{t-3}, etc. in Figure 4.4A) might also influence the current reproduction error. The causal graph in Figure 4.4A implies that e_t and s_{t-2} are conditionally independent given s_{t-1} and e_{t-1}; an assumption that we tested using the high-autocorrelation data set. We fitted the multiple linear regression model $e_t = \beta_0 + \beta_1 \cdot s_{t-2} + \beta_2 \cdot s_{t-1} + \beta_3 \cdot e_{t-1} + \varepsilon$ and inspected the β_1 coefficient. Across participants, the mean ± SD of β_1 was 0.12 ± 0.26 but only significantly different from 0 for one participant. As a further check, we assumed that there was an effect of s_{t-2} (i.e., an edge between s_{t-2} and e_t in the causal graph), and added this variable as a regressor to the multiple linear regression model such that e_t and s_{t-1} were *d*-separated. We found similar mean coefficients for the central tendency and serial dependence effects. As adding this regressor would introduce more multicollinearity in the regression model, we decided to not include the regressor in the final model. The high amount of autocorrelation in the stimulus sequence comes with the disadvantage of a reduced effective variance in the stimulus distances (see Figure 4.5 and Figure 4.7), and therefore a reduced precision in the estimated regression coefficients. A possible solution could be to test an experimental condition with a medium amount of autocorrelation.

In conclusion, our findings indicate that the reproduced distances in the vestibular path integration task generally showed central tendency and attractive serial dependence. These perceptual biases were not affected by the level of stimulus autocorrelation, given that covariation of these biases through the stimulus autocorrelation as well as other covariates were taken into account in the model. This suggests that central tendency and serial dependence in vestibular path integration have a neurocognitive rather than a statistical origin.

4.6 Appendix

To compare different central tendency and serial dependence metrics, we simulated reproductions that show central tendency but no serial dependence, i.e., reproductions that tend towards the mean of the underlying stimulus distribution but that are independent of the stimulus distance presented on the previous trial. Such reproductions can be generated for a trial *t* using the following 'static' Bayesian model (Glasauer & Shi, 2022):

$$r_t = w \cdot s_t + (1 - w) \cdot \frac{\sum_{i=1}^{N} s_i}{N} + \varepsilon_t,$$

where r refers to the reproduced distance, s to the stimulus distance, N to the total number of trials, and ε to a small amount of normally distributed random noise centered on 0. Parameter w reflects the weighting between the stimulus on the current trial and the constant mean of all stimuli. The amount of central tendency in the reproductions is defined as $c = 1 - w$, and the serial dependence is always 0 as the current reproduction does not depend on the previous stimulus irrespective of the amount of central tendency. One simulation for a given w consisted of generating reproductions with the static model for a random-walk sequence of 130 stimulus distances (the high-autocorrelation condition), and then shuffling the resulting stimulus-reproduction pairs to create the no-autocorrelation condition. Next, the amount of central tendency and serial dependence in the simulated reproductions was computed using two different methods. First, we used two separate linear least-squares regressions. Central tendency was defined as the slope of the linear regression of the reproduction error (reproduced - stimulus distance) on the stimulus distance. Serial dependence was defined as the slope of the linear regression of the reproduction error of the current trial on the stimulus distance of the previous trial. Second, we computed central tendency and serial dependence as the partial regression coefficients CT and SD_1 in the multiple linear regression model described in the Methods. We performed 1000 simulations for $w = 0$, $w = 0.5$, and $w = 1$, and we report the mean of the central tendency and serial dependence values across simulations for both methods.

The results are presented in Table 4.A1. Both the simple and multiple linear regression methods compute the correct amount of central tendency (i.e., c) in both conditions. Note that the central tendency values are negative as central tendency is defined in terms of the effect of the stimulus distance on the reproduction error (see Figure 4.1A). Both methods also result in the correct amount of serial dependence (i.e., 0) in the no-autocorrelation condition (see

Figure 4.A1, A-C). However, in the high-autocorrelation condition, the central tendency in the reproductions manifests as repulsive serial dependence when computed using the simple linear regression method. This is illustrated in Figure 4.A1, D-F, for three example simulations with increasing amounts of central tendency. If we instead compute serial dependence using the multiple linear regression method in which we control for the current stimulus as well as other variables (see Methods), the resulting value is on average close to 0 across simulations (see Table 4.A1).

Table 4.A1. Central tendency and serial dependence in simulated reproductions of a no- or high-autocorrelation stimulus sequence, computed with two separate linear regressions (*SLR*) or one multiple linear regression model (*MLR*, see Methods). Cells show the mean bias across 1000 simulations with different amounts of introduced central tendency (c), controlled by model parameter w (where $c = 1 - w$).

		$w = 1$, $c = 0$		$w = 0.5$, $c = 0.5$		$w = 0$, $c = 1$	
Bias	**Autocorrelation**	***SLR***	***MLR***	***SLR***	***MLR***	***SLR***	***MLR***
Central tendency	None	0.00	0.00	-0.50	-0.50	-1.00	-1.00
	High	0.00	0.00	-0.50	-0.50	-1.00	-1.00
Serial dependence	None	0.00	0.00	0.00	0.00	0.00	-0.01
	High	0.00	0.00	-0.48	-0.01	-0.95	-0.02

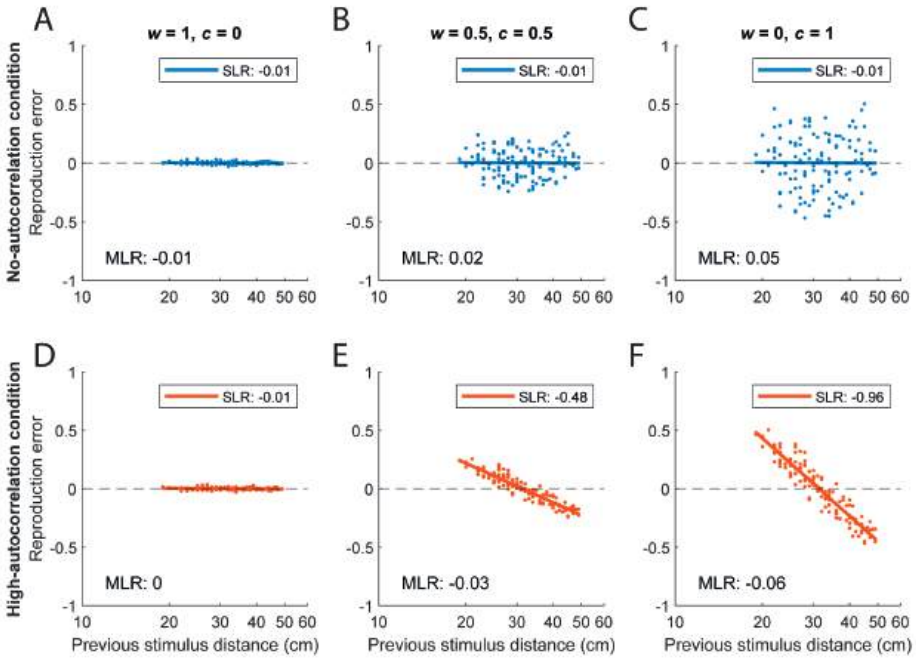

Figure 4.A1. The serial dependence in the no- (blue) and high-autocorrelation (orange) conditions of three example simulations with different amounts of introduced central tendency (c), controlled by model parameter w (where $c = 1 - w$). Serial dependence is plotted as reproduction error ($e_t = r_t - s_t$) against previous stimulus distance s_{t-1} on logarithmic scale. The slope of the simple linear regression (*SLR*) between these two variables is reported in the key. The corresponding serial dependence value as computed with the multiple linear regression (*MLR*) method (the partial regression coefficient SD_1, see Methods) is reported in each panel (but not plotted as this coefficient can only be correctly shown in a partial regression plot, see Methods).

Chapter 5

General discussion

How are we able to form coherent percepts from the vast amount of information available in the world around us? As we navigate our surroundings, our brain does not just receive information from our sensory organs, but importantly, also draws on memorized prior knowledge. In this thesis, I studied how prior experience influences spatial orientation and self-motion perception. In **Chapter 2**, I investigated to what extent the distribution of naturalistic head orientations could explain the Aubert effect in spatial orientation perception. In **Chapters 3** and **4**, I examined the effect of different stimulus distributions and presentation orders on central tendency and serial dependence biases in self-motion perception. In the first two sections of this chapter, I summarize and discuss the main findings of Chapter 2, and Chapters 3 and 4, respectively. In these sections I furthermore identify limitations and suggest ideas for future studies. Finally, I will explore the possible implementation and creation of Bayesian priors and end with a short conclusion.

5.1 Non-Gaussian natural head orientation statistics in spatial orientation perception

Spatial orientation perception has previously been studied in our lab by roll-tilting participants using a vestibular chair and subsequently quantifying the participant's perception of vertical (the subjective visual vertical task) and their body orientation in space (the subjective body tilt task). Findings show that when the head is tilted at large tilt angles, the perception of vertical is biased toward the tilt direction, called the Aubert effect (Aubert, 1861), whereas the perception of body orientation remains relatively accurate. Clemens et al. (2011) proposed a Bayesian inference model to explain the observations in these tasks. To model the Aubert effect, a Gaussian prior distribution of head roll centered on the upright orientation was included. This prior represented the idea that we usually keep our head upright and that extreme head tilts occur less frequently.

5.1.1 Natural statistics of head orientation

In **Chapter 2**, I asked whether head orientations measured outside the laboratory reflect the assumed Gaussian prior distribution. To answer this question, I evaluated which probability density function could best capture the distribution of head roll-tilt angles, measured across a set of naturalistic, unconstrained tasks. I found that the measured distributions were indeed centered on the upright head orientation and showed no systematic skewness. However, the participants' distributions consistently showed longer tails and higher peaks than predicted by a Gaussian distribution, best quantified by the more flexible *t*-location-scale distribution which includes a shape parameter to control the distribution's kurtosis. I conclude that head orientations measured outside the laboratory are symmetrically centered around the upright head orientation and follow a non-Gaussian distribution.

The data set of head roll tilts measured in everyday behaviors has been collected to supplement the growing literature on the natural statistics of head motion (Schwabe & Blanke, 2008; Carriot et al., 2014; Hausamann et al., 2019; Sinnott et al., 2023). The finding that the empirical head roll distributions were generally non-Gaussian extends earlier reports of the head's angular velocity and linear acceleration in naturalistic tasks, which showed comparable excess kurtosis (Carriot et al., 2014).

It could be considered a limitation of the out-of-laboratory experiment that it consisted of a set of relatively short tasks (walking, running, going up and down the stairs, sitting, and standing, resulting in approximately 30 min of recorded activities). To what extent do the head roll distributions from this experiment generalize to more natural, uninstructed behavior? Recently, Sinnott et al. (2023) recorded head orientations over a continuous 5-hour period, without any prescribed activities. The resulting head roll distribution across participants was centered on upright (0.58°) with a standard deviation of 6.21°, little skewness (0.12), and excess kurtosis (7.26, i.e., a kurtosis of 10.26). These values closely resemble the statistical moments that I found in Chapter 2, which suggests that the head roll measured in the relatively short tasks generalizes to more naturalistic, uninstructed behavior.

5.1.2 Bayesian inference models of spatial orientation perception

As priors in visual perception seem to reflect natural scene statistics (Adams et al., 2004; Girshick et al., 2011), I subsequently asked whether this is also the case for the perception of our head's orientation in space. More specifically, I studied whether the Clemens et al. (2011) model of spatial orientation perception could be improved by incorporating the empirical *t*-location-scale distribution, with its shape parameter estimated from head orientations measured outside the laboratory, as the head-in-space prior (model m2-TP, ν = 3.4 in Chapter 2). Surprisingly, I found that the *t*-location-scale prior performed substantially worse than the previously assumed Gaussian prior (model m1-GP) in explaining the spatial orientation data set from Clemens et al. (2011), and that this finding was consistent across various model variants. I conclude that incorporating the empirical, non-Gaussian distribution in the model by Clemens et al. (2011) does not provide a better explanation of spatial orientation perception than the original model with a Gaussian prior.

The new model (m2-TP, ν = 3.4) performed worse in capturing the Aubert effect, predicting smaller SVV biases at larger tilt angles than seen in the data. Replicating this finding, Sinnott et al. (2023) found that implementing their empirical head roll distribution as the prior in a static Bayesian inference model resulted in a worse fit to the SVV bias data of de Vrijer et al. (2009) than a Gaussian-prior model. In the same study, Sinnott et al. (2023) tested whether a non-linear relationship between otolith noise and absolute head tilt angle could redeem the empirical prior model. This model variant was again outperformed by the corresponding Gaussian-prior model, reflecting my finding that allowing the standard deviation of otolith noise to

be a free parameter for each absolute tilt angle did not improve the *t*-location-scale prior model (m3-TP).

The most striking difference between the Gaussian prior (m1-GP) and *t*-location-scale prior (m2-TP, $\nu = 3.4$) model variants is that the latter variant predicts a much higher perceptual uncertainty across the tilt range. Gradually increasing the shape parameter of the *t*-location-scale distribution such that the distribution became more Gaussian (m2-TP models), resulted in a consistent decrease in predicted perceptual variance and a corresponding increase in model performance. A theoretical reason for this finding is that the posterior variance is not necessarily lower than the variances of the prior and likelihood, if these two individual signals are not both represented as Gaussian distributions (Petty, 2018). If the prior is non-Gaussian, this could result in a high perceptual uncertainty at large tilt angles as predicted by the *t*-location-scale prior model – a situation the brain may want to prevent. If spatial orientation perception indeed follows Bayesian principles, the non-Gaussian distribution of everyday head tilts might be transformed into a Gaussian internal representation of probable head orientations, by means of additive Gaussian noise, introduced during transmission of head tilt information along vestibular afferents (Sadeghi et al., 2007; Mallery et al., 2010).

Alternatively, the natural statistics of head roll measured during active motion may be less informative for spatial orientation perception measured in stationary tasks (Carriot et al., 2014). Instead, there may exist context-dependent priors, encoding relevant information for different contexts or tasks. During active movements, such as walking, it is important to remain balanced to prevent falling. This process might be facilitated by a prior that reflects the natural statistics of head tilt during walking, informing the brain about probable head tilts that enable postural stability.

Within each data set in Chapter 2, participants were regarded as one group. However, the data and fitted parameter values illustrate that there is a degree of intersubject variability. An interesting future study would be to test whether individual differences in natural statistics of head roll can predict differences in spatial orientation perception. To do so, the same group of participants could be tested in the out-of-laboratory and laboratory-based experiments. For each participant, the natural statistics of head roll may be quantified by the best-fitting (Gaussian) distribution to the measured head roll tilts, and the subsequent fitted (mean and variance) parameter values may be used as the fixed parameters of the head-in-space prior in the Clemens et al. (2011) model.

Future studies may also explore sequential Bayesian inference models of spatial orientation perception, measured in continuous psychophysics paradigms (Bonnen et al., 2015; Huk et al., 2018; Straub & Rothkopf, 2022; Jörges et al., 2024). Continuous versions of the SBT and SVV tasks could involve participants rotating themselves or the visual line toward their estimate of the reference orientation or the vertical orientation, respectively (as in Tamura et al., 2017), resulting in a continuous instead of a binary response (CW/CCW). Future studies could also analyze possible short-term effects of previous stimuli on verticality and body orientation perception (i.e., serial dependence effects).

5.2 Effects of stimulus history on self-motion perception

Self-motion perception is essential for accurate path integration, a process that involves integration of successive self-motion signals to track travel distance and direction (Darwin, 1873; Mittelstaedt & Mittelstaedt, 1980; Etienne & Jeffery, 2004). To study how memorized information about previously encountered stimuli affects path integration, distance reproductions tasks are often used. Findings from virtual reproduction tasks, in which simulated optic flow provides visual self-motion signals, indicate that reproduced distances are biased by stimulus history (Glasauer & Shi, 2022): reproductions tend towards the mean of the experimental stimulus distribution – the central tendency effect (Hollingworth, 1910) – and are also affected on a shorter timescale by the immediately preceding stimulus – the serial dependence effect (Holland & Lockhead, 1968; Cross, 1973).

In **Chapters 3** and **4**, I studied to what extent central tendency and serial dependence affect vestibular self-motion perception, by testing participants in a physical distance reproduction task that mainly provided vestibular signals. In this task, a vestibular sled passively moved the participant over a stimulus distance, and subsequently, the participant actively reproduced this distance by steering the sled back to the starting point of the stimulus movement. I conclude that reproductions generally showed central tendency and attractive serial dependence, suggesting that vestibular self-motion perception is affected by stimulus history.

5.2.1 Sequential Bayesian inference models of self-motion perception

Magnitude perception has previously been studied with Bayesian models (Jürgens & Becker, 2006; Jazayeri & Shadlen, 2010; Petzschner & Glasauer, 2011; Ashourian

& Loewenstein, 2011; Petzschner et al., 2012; Prsa et al., 2015; Lakshminarasimhan et al., 2018; Glasauer & Shi, 2021, 2022). Some studies have modeled perception through the combination of incoming sensory signals with static prior knowledge about the statistics of previously experienced stimuli (e.g., Jazayeri & Shadlen, 2010). Other studies employed more iterative models, in which the estimate of the previous trial is used as prior knowledge for the current trial (e.g., Petzschner & Glasauer, 2011). Glasauer & Shi (2022) developed a sequential Bayesian inference (two-state) model that captures an intermediate assumption: stimuli are sampled from a probability distribution with a mean that may vary from trial to trial. This model contains the static and iterative assumptions as special cases which enables to compare how different assumptions explain magnitude perception.

In **Chapter 3**, I evaluated whether this model could provide further insights into how stimulus history influences reproduction behavior. I found that the predictions of both the static and two-state models matched the measured reproductions relatively well, suggesting that perception may have been influenced by the assumption that stimuli come from a relatively stable distribution. This corresponds to the finding of Glasauer & Shi (2022) that behavior of about half of their participants in a duration reproduction experiment was best explained by the two-state model and that for the remaining participants the static model was sufficient. Also consistent with Glasauer & Shi (2022), I observed that all model versions correctly predicted similar amounts of central tendency as measured in the reproduction data, and that the iterative model overestimated serial dependence whereas the static model underestimated serial dependence. Contrary to Glasauer & Shi (2022), also the two-state model underestimated the serial dependence in my data set, predicting similar serial dependence values as the static model. This was supported by the fitted q parameter values of the two-state model, which were on average close to 0, predicting a low level of serial dependence and essentially reducing the model to the static model for most participants.

It is unclear why the two-state model converged to the static model, resulting in an underestimation of the serial dependence of the measured reproduced distances. A potential explanation is that the reproduction data measured in the vestibular path integration task was too noisy from trial to trial, resulting in the two-state model not being able to capture the serial dependence at the level of the individual participant. Part of this noise may have been motor noise introduced during the active reproduction movement. A future study may test participants in a passive reproduction task, e.g., a task in which the passive stimulus movement is followed

by a passive reproduction movement, during which the participant presses a button when they perceive they have travelled the stimulus distance.

I further investigated whether reproduction behavior was affected by different experimental stimulus distributions and presentation orders. Stimulus distances were sampled from two probability distributions, centered on a relatively short and long distance, and tested in a blocked context, where the short and long distances were presented in two separate blocks, and a mixed context, where the same distances were randomly shuffled, resulting in one block. I extrapolated how the median stimulus distance would have been reproduced if it was part of the short- or long-distance distribution in the two contexts. I found that the estimated reproductions did not differ in the mixed context, whereas the estimated reproduction was generally longer in the long block than in the short block of the blocked context. Subsequently, I tested whether this finding could be captured by the two-state model, by extending the model such that it could take on different assumptions about the stimulus distribution across the mixed, short and long blocks. I also evaluated a variant of this model that allowed block-dependent vertical shifts, reflecting global under- or overestimations of the stimulus distances. I conclude that different levels of global underestimation across the blocks rather than different stimulus distribution assumptions captured the observed differences in the data.

A direction for future research could be to further investigate the origin of the different global underestimations. Interestingly, the average best-fitting Δx_{short}, Δx_{mixed}, and Δx_{long} parameter values seemed to decrease linearly with distance, on logarithmic scale. The shift term may therefore reflect increasing uncertainty in the position estimate as more distance is covered (Lakshminarasimhan et al., 2018).

5.2.2 Isolating central tendency and serial dependence in self-motion perception with causal models

In **Chapter 4**, I studied how stimulus autocorrelation affected central tendency and serial dependence in distance reproductions based on vestibular self-motion signals. A new set of participants performed the vestibular path integration experiment, in which stimulus distances were either presented in a randomized order (the no-autocorrelation condition) or in a random-walk order (the high-autocorrelation condition). By simulating reproductions that showed no serial dependence, and quantifying the central tendency and serial dependence as separate regression slopes, I observed that central tendency erroneously resulted in repulsive serial dependence if the stimuli were autocorrelated. To compare the

central tendency and serial dependence values across the no- and high-autocorrelation conditions, the different autocorrelation levels should therefore be controlled for in the regression model. I aimed to isolate the central tendency and serial dependence effects by representing the causal relations between the stimuli and reproduction errors in the measured data set in a causal graph (Pearl, 2009). By applying the graphical *d*-separation criterion[2], variables were identified that should be adjusted for in the regression, resulting in a multiple linear regression model that was used to jointly quantify the central tendency and serial dependence effects.

The central tendency and serial dependence values as estimated with the separate regressions indicated that the reproductions in the high-autocorrelation condition showed less central tendency, and more negative serial dependence than in the no-autocorrelation condition, in line with earlier findings (Glasauer & Shi, 2021, 2022). However, when quantifying the effects with the multiple linear regression model, the estimated values were similar across autocorrelation conditions, reflecting the same level of central tendency and attractive serial dependence, comparable to the effects I found in Chapter 3. I conclude that central tendency and serial dependence in distance reproductions based on vestibular self-motion signals were not affected by stimulus autocorrelation, which suggests that these biases are not caused by the experimental stimulus randomization protocol but arise from neurocognitive processes.

In the final causal graph, edges from the stimulus distance on the current trial (reflecting the central tendency effect) and the previous trial (reflecting the serial dependence effect), and the previous reproduction error, to the current reproduction error were included. Earlier stimulus distances (at trial $t-2$, $t-3$, etc.) could potentially have also affected the current reproduction error (creating biasing paths that would affect the serial dependence estimate), but the data did not reflect such effects. Earlier studies have also pointed out the importance of isolating central tendency and serial dependence effects (Jesteadt et al., 1977; Tong & Dubé, 2022; Saarela et al., 2023). To my knowledge, causal modeling has not yet been applied to disentangle these two effects on magnitude perception but may guide future development of appropriate regression models for perception experiments and possibly also other experiments with autocorrelated stimuli.

2. During causal modeling, I analyzed *d*-separation in the causal graphs using *DAGitty* (Textor et al., 2016), a useful browser-based environment (and R package) for the creation and analysis of causal diagrams.

Incorporating both the stimulus on the current trial and the stimulus on the previous trial as regressors in the model resulted in multicollinearity in the high-autocorrelation condition. Multicollinearity reduces the effective variance in the stimulus distances and therefore also reduces the precision of the estimated regression coefficients. Reducing the amount of autocorrelation in a replication study may still allow a comparison to a no-autocorrelation condition, while also improving the precision of the coefficients.

5.2.3 Serial dependencies in perception

The reproductions measured in the vestibular path integration tasks of **Chapters 3** and **4** showed attractive serial dependence, where the reproduction on the current trial was on average attracted toward the stimulus on the previous trial. Many studies within the perception literature have found attractive serial dependence (Fischer & Whitney, 2014; Liberman et al., 2014; Motala et al., 2020; Manassi & Whitney, 2022, 2024; Guan & Goettker, 2024), but there are also reports of repulsive serial dependence, where the current reproduction is biased away from the previous stimulus (Fritsche et al., 2017; Sun et al., 2020). The attractive serial dependence effects that I found in this thesis were not well explained by sequential Bayesian inference models with stable or iterative priors (**Chapter 3**), and were not introduced through the experimental stimulus randomization protocol (**Chapter 4**).

Instead, self-motion perception may be attracted toward the previous stimulus as a way to make perceptual representations more stable over time. Fischer & Whitney (2014) proposed perceptual continuity fields as a possible mechanism: spatiotemporal regions in which visual stimuli are being perceived as more similar than they actually are. Within these regions, serial dependence is thought to become higher as subsequent stimuli occur closer in time or space, when features of the current and past stimuli are more similar, or when more attention is devoted to the previous stimulus (Manassi & Whitney, 2024). The specific tuning of these properties may depend on a variety of factors, such as the task the brain tries to solve, or the degree to which the brain tries to match the serial dependence in perception to the autocorrelations in the natural stimulus statistics (van Bergen & Jehee, 2019; Ortega et al., 2023; Manassi & Whitney, 2024). In line with the idea that attractive serial dependence promotes stable representations, repulsive serial dependence may be a process through which sensitivity to changes between subsequent stimuli is increased (Sun et al., 2020).

Fritsche et al. (2017) tested the same group of participants in two visual orientation perception tasks and found different serial dependence patterns. When participants

reproduced the orientation of a Gabor stimulus by adjusting a response bar, responses showed an attractive serial dependence on the previous stimulus orientation. However, when participants judged which of two stimuli was oriented more clockwise, the responses showed repulsive serial dependence on the previous stimulus orientation. The authors reasoned that responses in the first experiment include both perceptual and post-perceptual decision processes, whereas the second experiment more directly targets perception of the stimulus orientation. The distance reproduction task in **Chapters 3** and **4** is in essence similar to the first task in Fritsche et al. (2017), with both tasks resulting in attractive serial dependence effects. As I only performed an adjustment task, I cannot distinguish between perceptual and post-perceptual processes. An interesting future study would be to also test participants in a distance comparison task, in which the participant judges which of two stimulus distances is shorter (or longer), to evaluate how this affects serial dependence of reproduced distances.

5.3 Bayesian priors in the brain

Many of the findings presented in this thesis are derived and formulated within the Bayesian inference framework. The Bayesian models used in this thesis provide insights into the possible computations involved in spatial perception, but make no predictions about how these computations are represented and implemented in the brain (Marr, 1982; Chater et al., 2006). How and where could the brain implement these computations? One of the proposed mechanisms is probabilistic population coding (Ma et al., 2006; Funamizu et al., 2016; Spratling, 2016). This mechanism suggests that neuronal populations encode probability distributions as a result of neuronal variability (Ma et al., 2006) and may in theory be capable of implementing a 2-D Kalman filter (Beck et al., 2011). Funamizu et al. (2016) provided additional evidence, suggesting that the mouse posterior parietal cortex performs sequential Bayesian inference during distance estimation, using probabilistic population codes.

The combined results of this thesis suggest that vestibular perception is influenced by prior knowledge about task-relevant stimulus history, built up across multiple timescales. Prolonged exposure to stable features of natural stimuli over our lifetime (i.e., through the usual upright head orientation) seems to shape spatial orientation perception (i.e., through the upright head-in-space prior; **Chapter 2**). What we have experienced on a shorter timescale also affects vestibular perception (**Chapters 3** and **4**). Here, a distinction can be made between central tendency effects, reflecting a representation of stimulus statistics built up across multiple

trials, and serial dependence effects of immediately preceding stimuli. This apparent distinction is currently under active investigation, with recent findings suggesting that the central tendency effect is not the result of an explicit representation of the stimulus distribution in the posterior parietal cortex, but that central tendency emerges from serial dependence effects in working memory (Boboeva et al., 2024). The effects of consolidated long-term (**Chapter 2**) and more flexible short-term information about stimulus history (**Chapters 3** and **4**) were separately studied in this thesis, but likely simultaneously affect vestibular perception (Sun et al., 2024).

The environmental context in which someone finds themselves determines the distribution of sensory signals that they perceive. Examples of such contexts that have been discussed in this thesis are active versus passive movement contexts (**Chapter 2**), as well as mixed versus blocked (**Chapter 3**), and no- versus high-autocorrelation stimulus presentation contexts (**Chapter 4**). Throughout our lives, we encounter a variety of different contexts, and our brain likely has different memories that are relevant for these contexts. How does the brain know the context we are in, and how does it create and update new memories? Heald et al. (2021) proposed the idea of contextual inference, which suggests that the brain continuously computes a posterior distribution, reflecting the probability of each known context and a novel context being currently active. This posterior distribution may in turn guide both apparent learning, the change in how existing memories are expressed, and proper learning, the updating and creation of memories.

While behavior in many perceptual and cognitive experiments seems well explained within the Bayesian framework, it remains relatively unexplored how such models perform in explaining more complex real-world behavior. The spatial orientation and self-motion perception experiments presented in this thesis constrained vestibular perception to a relatively narrow set of stimuli while also restricting motion. It is therefore difficult to generalize these findings to more complex everyday perception of orientation and self-motion. Future work may approach this problem from two directions: by adding more degrees of freedom to constrained laboratory-based experiments, or by restricting degrees of freedom in out-of-laboratory behavior. Experiments following the first line of reasoning could try to mimic more naturalistic contexts in the laboratory, e.g., by studying self-motion perception while displacing the vestibular sled as if the participant is driving on a slippery road (similar to the task in Liu et al., 2024). Alternatively (or ideally in parallel), future studies may investigate out-of-laboratory perception in everyday tasks (similar to the first experiment in **Chapter 2**). Such experiments could involve

measuring the orientation of the head and body using inertial measurement units (IMUs), while the participant engages in an everyday activity and continuously indicates their perceived direction of verticality, e.g. by aligning a rod to which an IMU is attached, with their perceived direction of verticality. This continuous data set could then be used to verify whether sequential Bayesian inference models generalize to unconstrained everyday behavior.

5.4 Conclusion

In this thesis, I investigated different types of prior knowledge that may influence spatial orientation and self-motion perception. Prior knowledge obtained through prolonged experience, i.e., the natural statistics of head orientation, differs from the Gaussian head-in-space prior that can successfully explain biases in verticality perception (Clemens et al., 2011). Besides such prior knowledge acquired over a long time span, short-term prior knowledge of the experimental stimulus distribution also affects perception. Self-motion perception during vestibular path integration experiments generally tends toward the mean of the experimental stimulus distribution and toward the stimulus presented on the immediately preceding trial. These findings give insight into how previous experiences shape our perception and which computations may underlie such perceptual processes. Future work could further investigate how the interplay between relatively stable natural statistics and short-term sensory statistics shapes spatial orientation and self-motion perception.

References

Adams, W. J., Graf, E. W., & Ernst, M. O. (2004). Experience can change the "light-from-above" prior. *Nature Neuroscience*, *7*(10), 1057–1058. https://doi.org/10.1038/nn1312

Akaike, H. (1974). A new look at the statistical model identification. *IEEE Transactions on Automatic Control*, *19*(6), 716–723. https://doi.org/10.1109/TAC.1974.1100705

Akrami, A., Kopec, C. D., Diamond, M. E., & Brody, C. D. (2018). Posterior parietal cortex represents sensory history and mediates its effects on behaviour. *Nature*, *554*(7692), 368–372. https://doi.org/10.1038/nature25510

Alberts, B. B. G. T., de Brouwer, A. J., Selen, L. P. J., & Medendorp, W. P. (2016). A Bayesian account of visual-vestibular interactions in the rod-and-frame task. *eNeuro*, *3*(5), ENEURO.0093-16.2016. https://doi.org/10.1523/ENEURO.0093-16.2016

Alberts, B. B. G. T., Selen, L. P. J., & Medendorp, W. P. (2019). Age-related reweighting of visual and vestibular cues for vertical perception. *Journal of Neurophysiology*, *121*(4), 1279–1288. https://doi.org/10.1152/jn.00481.2018

Alberts, B. B. G. T., Selen, L. P. J., Verhagen, W. I. M., & Medendorp, W. P. (2015). Sensory substitution in bilateral vestibular a-reflexic patients. *Physiological Reports*, *3*(5), e12385. https://doi.org/10.14814/phy2.12385

Angelaki, D. E., & Cullen, K. E. (2008). Vestibular system: The many facets of a multimodal sense. *Annual Review of Neuroscience*, *31*(1), 125–150. https://doi.org/10.1146/annurev.neuro.31.060407.125555

Angelaki, D. E., & Laurens, J. (2020). Time course of sensory substitution for gravity sensing in visual vertical orientation perception following complete vestibular loss. *eNeuro*, *7*(4), ENEURO.0021-20.2020. https://doi.org/10.1523/ENEURO.0021-20.2020

Ashourian, P., & Loewenstein, Y. (2011). Bayesian inference underlies the contraction bias in delayed comparison tasks. *PLOS ONE*, *6*(5), e19551. https://doi.org/10.1371/journal.pone.0019551

Attias, H., & Schreiner, C. (1996). Temporal low-order statistics of natural sounds. *Advances in Neural Information Processing Systems, 9*. https://proceedings.neurips.cc/paper/1996/hash/dc4c44f624d600aa568390f1f1104aa0-Abstract.html

Attneave, F. (1954). Some informational aspects of visual perception. *Psychological Review*, *61*(3), 183–193. https://doi.org/10.1037/h0054663

Aubert, H. (1861). Eine scheinbare bedeutende Drehung von Objecten bei Neigung des Kopfes nach rechts oder links. *Archiv Für Pathologische Anatomie Und Physiologie Und Für Klinische Medicin*, *20*(3–4), 381–393. https://doi.org/10.1007/BF02355256

Bayes, T. (1763). LII. An essay towards solving a problem in the doctrine of chances. By the late Rev. Mr. Bayes, F. R. S. communicated by Mr. Price, in a letter to John Canton, A. M. F. R. S. *Philosophical Transactions of the Royal Society of London*, *53*, 370–418.

Bays, P. M., & Wolpert, D. M. (2007). Computational principles of sensorimotor control that minimize uncertainty and variability. *Journal of Physiology*, *578*(2), 387–396. https://doi.org/10.1113/jphysiol.2006.120121

Beck, J. M., Latham, P. E., & Pouget, A. (2011). Marginalization in neural circuits with divisive normalization. *Journal of Neuroscience*, *31*(43), 15310–15319. https://doi.org/10.1523/JNEUROSCI.1706-11.2011

Becker, W., Nasios, G., Raab, S., & Jürgens, R. (2002). Fusion of vestibular and podokinesthetic information during self-turning towards instructed targets. *Experimental Brain Research*, *144*(4), 458–474. https://doi.org/10.1007/s00221-002-1053-5

Bergmann, J., Krauß, E., Münch, A., Jungmann, R., Oberfeld, D., & Hecht, H. (2011). Locomotor and verbal distance judgments in action and vista space. *Experimental Brain Research*, *210*(1), 13–23. https://doi.org/10.1007/s00221-011-2597-z

Bishop, C. M. (2006). *Pattern recognition and machine learning* (1st ed.; M. I. Jordan, J. Kleinberg, & B. Schölkopf, Eds.). New York, NY, USA: Springer.

Blanks, R. H. I., Curthoys, I. S., & Markham, C. H. (1975). Planar relationships of the semicircular canals in man. *Acta Oto-Laryngologica*, *80*(1–6), 185–196. https://doi.org/10.3109/00016487509121318

Boboeva, V., Pezzotta, A., Clopath, C., & Akrami, A. (2024). Unifying network model links recency and central tendency biases in working memory. *eLife*, *12*, RP86725. https://doi.org/10.7554/eLife.86725.3

Bonnen, K., Burge, J., Yates, J., Pillow, J., & Cormack, L. K. (2015). Continuous psychophysics: Target-tracking to measure visual sensitivity. *Journal of Vision*, *15*(3), 14. https://doi.org/10.1167/15.3.14

Box, G. E. P., Jenkins, G. M., Reinsel, G. C., & Ljung, G. M. (2015). *Time series analysis: Forecasting and control* (5th ed.). Hoboken, NJ, USA: John Wiley & Sons.

Brenner, E., & Smeets, J. B. J. (2018). Depth perception. In *Stevens' handbook of experimental psychology and cognitive neuroscience* (4th ed., Vol. 2, pp. 385–414). Wiley. https://doi.org/10.1002/9781119170174

Brooks, J. X., Carriot, J., & Cullen, K. E. (2015). Learning to expect the unexpected: Rapid updating in primate cerebellum during voluntary self-motion. *Nature Neuroscience*, *18*(9), 1310–1317. https://doi.org/10.1038/nn.4077

Brooks, J. X., & Cullen, K. E. (2009). Multimodal integration in rostral fastigial nucleus provides an estimate of body movement. *Journal of Neuroscience*, *29*(34), 10499–10511. https://doi.org/10.1523/JNEUROSCI.1937-09.2009

Brooks, J. X., & Cullen, K. E. (2019). Predictive sensing: The role of motor signals in sensory processing. *Biological Psychiatry: Cognitive Neuroscience and Neuroimaging*, *4*(9), 842–850. https://doi.org/10.1016/j.bpsc.2019.06.003

Carriot, J., Brooks, J. X., & Cullen, K. E. (2013). Multimodal integration of self-motion cues in the vestibular system: Active versus passive translations. *Journal of Neuroscience*, *33*(50), 19555–19566. https://doi.org/10.1523/JNEUROSCI.3051-13.2013

Carriot, J., Jamali, M., Chacron, M. J., & Cullen, K. E. (2014). Statistics of the vestibular input experienced during natural self-motion: Implications for neural processing. *Journal of Neuroscience*, *34*(24), 8347–8357. https://doi.org/10.1523/JNEUROSCI.0692-14.2014

Chater, N., Tenenbaum, J. B., & Yuille, A. (2006). Probabilistic models of cognition: Conceptual foundations. *Trends in Cognitive Sciences*, *10*(7), 287–291. https://doi.org/10.1016/j.tics.2006.05.007

Cicchini, G. M., Arrighi, R., Cecchetti, L., Giusti, M., & Burr, D. C. (2012). Optimal encoding of interval timing in expert percussionists. *Journal of Neuroscience*, *32*(3), 1056–1060. https://doi.org/10.1523/JNEUROSCI.3411-11.2012

Clemens, I. A. H. (2015). *Multisensory integration in spatial orientation and self-motion perception* (Doctoral dissertation). Radboud University Nijmegen. https://hdl.handle.net/2066/143186

Clemens, I. A. H., de Vrijer, M., Selen, L. P. J., van Gisbergen, J. A. M., & Medendorp, W. P. (2011). Multisensory processing in spatial orientation: An inverse probabilistic approach. *Journal of Neuroscience*, *31*(14), 5365–5377. https://doi.org/10.1523/JNEUROSCI.6472-10.2011

Cohen, J. (1973). Eta-squared and partial eta-squared in fixed factor anova designs. *Educational and Psychological Measurement*, *33*(1), 107–112. https://doi.org/10.1177/001316447303300111

Cohen, J. (1988). *Statistical power analysis for the behavioral sciences*. New York, NY, USA: Routledge.

Cooke, J. R. H. (2019). *Statistical models of object tracking* (Doctoral dissertation). Radboud University Nijmegen. https://hdl.handle.net/2066/208569

Cross, D. V. (1973). Sequential dependencies and regression in psychophysical judgments. *Perception & Psychophysics*, *14*(3), 547–552. https://doi.org/10.3758/BF03211196

Cullen, K. E. (2019). Vestibular processing during natural self-motion: Implications for perception and action. *Nature Reviews Neuroscience*, *20*(6), 346–363. https://doi.org/10.1038/s41583-019-0153-1

Cullen, K. E. (2023). Internal models of self-motion: Neural computations by the vestibular cerebellum. *Trends in Neurosciences*, *46*(11), 986–1002. https://doi.org/10.1016/j.tins.2023.08.009

Cuturi, L. F., & MacNeilage, P. R. (2013). Systematic biases in human heading estimation. *PLOS ONE*, *8*(2), e56862. https://doi.org/10.1371/journal.pone.0056862

Darwin, C. (1873). Origin of certain instincts. *Nature*, *7*(179), 417–418.

de Vrijer, M., Medendorp, W. P., & van Gisbergen, J. A. M. (2008). Shared computational mechanism for tilt compensation accounts for biased verticality percepts in motion and pattern vision. *Journal of Neurophysiology*, *99*(2), 915–930. https://doi.org/10.1152/jn.00921.2007

de Vrijer, M., Medendorp, W. P., & van Gisbergen, J. A. M. (2009). Accuracy-precision trade-off in visual orientation constancy. *Journal of Vision*, *9*(2), 9. https://doi.org/10.1167/9.2.9

Dehaene, S. (2003). The neural basis of the Weber–Fechner law: A logarithmic mental number line. *Trends in Cognitive Sciences*, *7*(4), 145–147. https://doi.org/10.1016/S1364-6613(03)00055-X

Delhaye, B. P., Long, K. H., & Bensmaia, S. J. (2018). Neural basis of touch and proprioception in primate cortex. *Comprehensive Physiology*, *8*(4), 1575–1602. https://doi.org/10.1002/cphy.c170033

Doucet, A., Freitas, N., & Gordon, N. (2001). *Sequential Monte Carlo methods in practice* (A. Doucet, N. Freitas, & N. Gordon, Eds.). New York, NY, USA: Springer New York. https://doi.org/10.1007/978-1-4757-3437-9

Duffy, S., Huttenlocher, J., Hedges, L. V., & Crawford, L. E. (2010). Category effects on stimulus estimation: Shifting and skewed frequency distributions. *Psychonomic Bulletin & Review*, *17*(2), 224–230. https://doi.org/10.3758/PBR.17.2.224

Durgin, F. H., Akagi, M., Gallistel, C. R., & Haiken, W. (2009). The precision of locomotor odometry in humans. *Experimental Brain Research*, *193*(3), 429–436. https://doi.org/10.1007/s00221-008-1640-1

Eggert, T. (1998). *Der Einfluss orientierter Texturen auf die subjektive visuelle Vertikale und seine systemtheoretische Analyse* (Doctoral dissertation). Munich Technical University.

Ellis, A. W., & Mast, F. W. (2017). Toward a dynamic probabilistic model for vestibular cognition. *Frontiers in Psychology*, *8*, 138. https://doi.org/10.3389/fpsyg.2017.00138

Ernst, M. O., & Banks, M. S. (2002). Humans integrate visual and haptic information in a statistically optimal fashion. *Nature*, *415*(6870), 429–433. https://doi.org/10.1038/415429a

Etienne, A. S., & Jeffery, K. J. (2004). Path integration in mammals. *Hippocampus*, *14*(2), 180–192. https://doi.org/10.1002/hipo.10173

Fischer, J., & Whitney, D. (2014). Serial dependence in visual perception. *Nature Neuroscience*, *17*(5), 738–743. https://doi.org/10.1038/nn.3689

Frenz, H., & Lappe, M. (2005). Absolute travel distance from optic flow. *Vision Research*, *45*(13), 1679–1692. https://doi.org/10.1016/j.visres.2004.12.019

Fritsche, M., Mostert, P., & de Lange, F. P. (2017). Opposite effects of recent history on perception and decision. *Current Biology*, *27*(4), 590–595. https://doi.org/10.1016/j.cub.2017.01.006

Funamizu, A., Kuhn, B., & Doya, K. (2016). Neural substrate of dynamic Bayesian inference in the cerebral cortex. *Nature Neuroscience*, *19*(12), 1682–1689. https://doi.org/10.1038/nn.4390

Geisler, W. S. (2008). Visual perception and the statistical properties of natural scenes. *Annual Review of Psychology*, *59*(1), 167–192. https://doi.org/10.1146/annurev.psych.58.110405.085632

Ghahramani, Z., Wolpert, D. M., & Jordan, M. I. (1997). Computational models of sensorimotor integration. *Advances in Psychology*, *119*, 117–147. https://doi.org/10.1016/S0166-4115(97)80006-4

Gibson, J. J. (1950). *The perception of the visual world*. Boston, MA, USA: Houghton Mifflin.

Girshick, A. R., Landy, M. S., & Simoncelli, E. P. (2011). Cardinal rules: Visual orientation perception reflects knowledge of environmental statistics. *Nature Neuroscience*, *14*(7), 926–932. https://doi.org/10.1038/nn.2831

Glasauer, S., & Shi, Z. (2021). The origin of Vierordt's law: The experimental protocol matters. *PsyCh Journal*, *10*(5), 732–741. https://doi.org/10.1002/pchj.464

Glasauer, S., & Shi, Z. (2022). Individual beliefs about temporal continuity explain variation of perceptual biases. *Scientific Reports*, *12*, 10746. https://doi.org/10.1038/s41598-022-14939-8

Grasso, R., Glasauer, S., Georges-François, P., & Israël, I. (1999). Replication of passive whole-body linear displacements from inertial cues: Facts and mechanisms. *Annals of the New York Academy of Sciences*, *871*(1), 345–366. https://doi.org/10.1111/j.1749-6632.1999.tb09197.x

Griffiths, T. L., & Kalish, M. L. (2005). A Bayesian view of language evolution by iterated learning. *Proceedings of the Annual Meeting of the Cognitive Science Society, 27(27)*. https://escholarship.org/uc/item/0vb7c896

Guan, S., & Goettker, A. (2024). Individual differences reveal similarities in serial dependence effects across perceptual tasks, but not to oculomotor tasks. *Journal of Vision*, *24*(12), 2. https://doi.org/10.1167/jov.24.12.2

Gumbel, E. J. (1985). *Statistics of extremes*. New York, NY, USA: Colombia University Press.

Harris, L. R., Jenkin, M. R., Zikovitz, D., Redlick, F. P., Jaekl, P., Jasiobedzka, U. T., … Allison, R. S. (2002). Simulating self-motion I: Cues for the perception of motion. *Virtual Reality*, *6*(2), 75–85. https://doi.org/10.1007/s100550200008

Hausamann, P. A., Daumer, M., MacNeilage, P. R., & Glasauer, S. (2019). Ecological momentary assessment of head motion: Toward normative data of head stabilization. *Frontiers in Human Neuroscience*, *13*, 179. https://doi.org/10.3389/fnhum.2019.00179

Heald, J. B., Lengyel, M., & Wolpert, D. M. (2021). Contextual inference underlies the learning of sensorimotor repertoires. *Nature*, *600*(7889), 489–493. https://doi.org/10.1038/s41586-021-04129-3

Hitier, M., Besnard, S., & Smith, P. F. (2014). Vestibular pathways involved in cognition. *Frontiers in Integrative Neuroscience*, *8*, 59. https://doi.org/10.3389/fnint.2014.00059

Ho, Y. C., & Lee, R. C. K. (1964). A Bayesian approach to problems in stochastic estimation and control. *IEEE Transactions on Automatic Control*, *9*(4), 333–339. https://doi.org/10.1109/TAC.1964.1105763

Holland, M. K., & Lockhead, G. R. (1968). Sequential effects in absolute judgments of loudness. *Perception & Psychophysics*, *3*(6), 409–414. https://doi.org/10.3758/BF03205747

Hollingworth, H. L. (1910). The central tendency of judgment. *Journal of Philosophy, Psychology and Scientific Methods*, *7*(17), 461–469. https://doi.org/10.2307/2012819

Huk, A., Bonnen, K., & He, B. J. (2018). Beyond trial-based paradigms: Continuous behavior, ongoing neural activity, and natural stimuli. *Journal of Neuroscience*, *38*(35), 7551–7558. https://doi.org/10.1523/JNEUROSCI.1920-17.2018

Israël, I., Grasso, R., Georges-François, P., Tsuzuku, T., & Berthoz, A. (1997). Spatial memory and path integration studied by self-driven passive linear displacement. I. Basic properties. *Journal of Neurophysiology*, *77*(6), 3180–3192. https://doi.org/10.1152/jn.1997.77.6.3180

Jacobs, R. A. (1999). Optimal integration of texture and motion cues to depth. *Vision Research*, *39*(21), 3621–3629. https://doi.org/10.1016/S0042-6989(99)00088-7

Jamali, M., Carriot, J., Chacron, M. J., & Cullen, K. E. (2019). Coding strategies in the otolith system differ for translational head motion vs. static orientation relative to gravity. *eLife*, *8*, e45573. https://doi.org/10.7554/eLife.45573

Jazayeri, M., & Shadlen, M. N. (2010). Temporal context calibrates interval timing. *Nature Neuroscience*, *13*(8), 1020–1026. https://doi.org/10.1038/nn.2590

Jenkinson, A. F. (1955). The frequency distribution of the annual maximum (or minimum) values of meteorological elements. *Quarterly Journal of the Royal Meteorological Society*, *81*(348), 158–171. https://doi.org/10.1002/qj.49708134804

Jesteadt, W., Luce, R. D., & Green, D. M. (1977). Sequential effects in judgments of loudness. *Journal of Experimental Psychology: Human Perception and Performance*, *3*(1), 92–104. https://doi.org/10.1037/0096-1523.3.1.92

Jörges, B., Bansal, A., & Harris, L. R. (2024). Precision and temporal dynamics in heading perception assessed by continuous psychophysics. *PLOS ONE*, *19*(10), e0311992. https://doi.org/10.1371/JOURNAL.PONE.0311992

Jürgens, R., & Becker, W. (2006). Perception of angular displacement without landmarks: Evidence for Bayesian fusion of vestibular, optokinetic, podokinesthetic, and cognitive information. *Experimental Brain Research*, *174*(3), 528–543. https://doi.org/10.1007/s00221-006-0486-7

Kalman, R. E. (1960). A new approach to linear filtering and prediction problems. *Journal of Basic Engineering*, *82*(1), 35–45. https://doi.org/10.1115/1.3662552

Kass, R. E., & Raftery, A. E. (1995). Bayes factors. *Journal of the American Statistical Association*, *90*(430), 773–795. https://doi.org/10.1080/01621459.1995.10476572

Khan, S., & Chang, R. (2013). Anatomy of the vestibular system: A review. *NeuroRehabilitation*, *32*(3), 437–443. https://doi.org/10.3233/NRE-130866

Kingma, H. (2005). Thresholds for perception of direction of linear acceleration as a possible evaluation of the otolith function. *BMC Ear, Nose and Throat Disorders*, *5*, 5. https://doi.org/10.1186/1472-6815-5-5

Kirby, E. D., Glenn, M. J., Sandstrom, N. J., & Williams, C. L. (2024). 7.4 Balance: A sense of where you are. In *Introduction to Behavioral Neuroscience*. Houston, TX, USA: OpenStax. https://openstax.org/books/introduction-behavioral-neuroscience/pages/7-4-balance-a-sense-of-where-you-are

Kolb, B., & Whishaw, I. Q. (2014). *An introduction to brain and behavior* (4th ed.). New York, NY, USA: Worth Publishers.

Körding, K. P., & Wolpert, D. M. (2004). Bayesian integration in sensorimotor learning. *Nature*, *427*(6971), 244–247. https://doi.org/10.1038/nature02169

Lakshminarasimhan, K. J., Petsalis, M., Park, H., DeAngelis, G. C., Pitkow, X., & Angelaki, D. E. (2018). A dynamic Bayesian observer model reveals origins of bias in visual path integration. *Neuron*, *99*(1), 194–206. https://doi.org/10.1016/j.neuron.2018.05.040

Landy, M. S., Maloney, L. T., Johnston, E. B., & Young, M. (1995). Measurement and modeling of depth cue combination: In defense of weak fusion. *Vision Research*, *35*(3), 389–412. https://doi.org/10.1016/0042-6989(94)00176-M

Lappe, M., & Frenz, H. (2009). Visual estimation of travel distance during walking. *Experimental Brain Research*, *199*(3–4), 369–375. https://doi.org/10.1007/s00221-009-1890-6

Lappe, M., Jenkin, M. R., & Harris, L. R. (2007). Travel distance estimation from visual motion by leaky path integration. *Experimental Brain Research*, *180*(1), 35–48. https://doi.org/10.1007/s00221-006-0835-6

Lappe, M., Stiels, M., Frenz, H., & Loomis, J. M. (2011). Keeping track of the distance from home by leaky integration along veering paths. *Experimental Brain Research*, *212*(1), 81–89. https://doi.org/10.1007/s00221-011-2696-x

Laurens, J., & Angelaki, D. E. (2011). The functional significance of velocity storage and its dependence on gravity. *Experimental Brain Research*, *210*(3–4), 407–422. https://doi.org/10.1007/s00221-011-2568-4

Laurens, J., & Angelaki, D. E. (2017). A unified internal model theory to resolve the paradox of active versus passive self-motion sensation. *eLife*, *6*, e28074. https://doi.org/10.7554/eLife.28074

Laurens, J., & Droulez, J. (2007). Bayesian processing of vestibular information. *Biological Cybernetics*, *96*(4), 389–404. https://doi.org/10.1007/s00422-006-0133-1

Laurens, J., Meng, H., & Angelaki, D. E. (2013). Neural representation of orientation relative to gravity in the macaque cerebellum. *Neuron*, *80*(6), 1508–1518. https://doi.org/10.1016/j.neuron.2013.09.029

Li, W., & Matin, L. (2005). Visually perceived vertical (VPV): Induced changes in orientation by 1-line and 2-line roll-tilted and pitched visual fields. *Vision Research*, *45*(15), 2037–2057. https://doi.org/10.1016/j.visres.2005.01.014

Liberman, A., Fischer, J., & Whitney, D. (2014). Serial dependence in the perception of faces. *Current Biology*, *24*(21), 2569–2574. https://doi.org/10.1016/j.cub.2014.09.025

Liu, J.-Y., Cooke, J. R. H., Selen, L. P. J., & Medendorp, W. P. (2024). Visuoinertial and visual feedback in online steering control. *bioRxiv*. https://doi.org/10.1101/2024.11.20.624619

Loomis, J. M., Klatzky, R. L., Golledge, R. G., Cicinelli, J. G., Pellegrino, J. W., & Fry, P. A. (1993). Nonvisual navigation by blind and sighted: Assessment of path integration ability. *Journal of Experimental Psychology: General*, *122*(1), 73–91. https://doi.org/10.1037/0096-3445.122.1.73

Lopez, C., & Blanke, O. (2011). The thalamocortical vestibular system in animals and humans. *Brain Research Reviews*, *67*(1–2), 119–146. https://doi.org/10.1016/j.brainresrev.2010.12.002

Ma, W. J., Beck, J. M., Latham, P. E., & Pouget, A. (2006). Bayesian inference with probabilistic population codes. *Nature Neuroscience*, *9*(11), 1432–1438. https://doi.org/10.1038/nn1790

MacNeilage, P. R. (2020). Characterization of natural head movements in animals and humans. In B. Fritzsch & H. Straka (Eds.), *The Senses: A Comprehensive Reference* (2nd ed., Vol. 6, pp. 69–87). Elsevier.

Mallery, R. M., Olomu, O. U., Uchanski, R. M., Militchin, V. A., & Hullar, T. E. (2010). Human discrimination of rotational velocities. *Experimental Brain Research*, *204*(1), 11–20. https://doi.org/10.1007/s00221-010-2288-1

Mamassian, P., & Goutcher, R. (2001). Prior knowledge on the illumination position. *Cognition*, *81*(1), B1–B9. https://doi.org/10.1016/S0010-0277(01)00116-0

Manassi, M., & Whitney, D. (2022). Illusion of visual stability through active perceptual serial dependence. *Science Advances*, *8*(2), eabk2480. https://doi.org/10.1126/sciadv.abk2480

Manassi, M., & Whitney, D. (2024). Continuity fields enhance visual perception through positive serial dependence. *Nature Reviews Psychology*, *3*(5), 352–366. https://doi.org/10.1038/s44159-024-00297-x

Marr, D. (1982). *Vision*. San Franciso, CA, USA: W. H. Freeman.

McDonald, J. B., & Newey, W. K. (1988). Partially adaptive estimation of regression models via the generalized t distribution. *Econometric Theory*, *4*(3), 428–457. https://doi.org/10.1017/S0266466600013384

Medendorp, W. P. (2011). Spatial constancy mechanisms in motor control. *Philosophical Transactions of the Royal Society B: Biological Sciences*, *366*(1564), 476–491. https://doi.org/10.1098/rstb.2010.0089

Mitchell, D. E., Kwan, A., Carriot, J., Chacron, M. J., & Cullen, K. E. (2018). Neuronal variability and tuning are balanced to optimize naturalistic self-motion coding in primate vestibular pathways. *eLife*, *7*, e43019. https://doi.org/10.7554/eLife.43019

Mittelstaedt, H. (1983). A new solution to the problem of the subjective vertical. *Naturwissenschaften*, *70*(6), 272–281. https://doi.org/10.1007/BF00404833

Mittelstaedt, H. (1997). Interaction of eye-, head-, and trunk-bound information in spatial perception and control. *Journal of Vestibular Research*, *7*(4), 283–302. https://doi.org/10.3233/VES-1997-740

Mittelstaedt, H. (1998). Origin and processing of postural information. *Neuroscience & Biobehavioral Reviews*, *22*(4), 473–478. https://doi.org/10.1016/S0149-7634(97)00032-8

Mittelstaedt, M.-L., & Glasauer, S. (1991). Idiothetic navigation in gerbils and humans. *Zoologische Jahrbücher - Abteilung Für Allgemeine Zoologie Und Physiologie Der Tiere*, *95*, 427–435.

Mittelstaedt, M.-L., & Mittelstaedt, H. (1980). Homing by path integration in a mammal. *Naturwissenschaften*, *67*(11), 566–567. https://doi.org/10.1007/BF00450672

Motala, A., Zhang, H., & Alais, D. (2020). Auditory rate perception displays a positive serial dependence. *I-Perception*, *11*(6), 1–17. https://doi.org/10.1177/2041669520982311

Murai, Y., & Yotsumoto, Y. (2016). Timescale- and sensory modality-dependency of the central tendency of time perception. *PLOS ONE*, *11*(7), e0158921. https://doi.org/10.1371/journal.pone.0158921

NEUROtiker. (2007). *Lateral view of a human brain, main gyri labeled* [Image]. Wikimedia Commons. https://commons.wikimedia.org/wiki/File:Gehirn,_lateral_-_Hauptgyri_beschriftet.svg

Niehof, N. (2020). *Visuovestibular cue combination in vertical perception* (Doctoral dissertation). Radboud University Nijmegen. https://hdl.handle.net/2066/221916

Obrist, D. (2011). *Fluid mechanics of the inner ear* (Habilitation thesis). ETH Zürich. https://doi.org/10.3929/ethz-a-007318979

Olkkonen, M., & Allred, S. R. (2014). Short-term memory affects color perception in context. *PLOS ONE*, *9*(1), e86488. https://doi.org/10.1371/journal.pone.0086488

Olkkonen, M., McCarthy, P. F., & Allred, S. R. (2014). The central tendency bias in color perception: Effects of internal and external noise. *Journal of Vision*, *14*(11), 5. https://doi.org/10.1167/14.11.5

Orban, G. A., Sepe, A., & Bonini, L. (2021). Parietal maps of visual signals for bodily action planning. *Brain Structure and Function*, *226*(9), 2967–2988. https://doi.org/10.1007/s00429-021-02378-6

Ortega, J., Chen, Z., & Whitney, D. (2023). Serial dependence in emotion perception mirrors the autocorrelations in natural emotion statistics. *Journal of Vision*, *23*(3), 12. https://doi.org/10.1167/jov.23.3.12

Parise, C. V., Knorre, K., & Ernst, M. O. (2014). Natural auditory scene statistics shapes human spatial hearing. *Proceedings of the National Academy of Sciences*, *111*(16), 6104–6108. https://doi.org/10.1073/pnas.1322705111

Paulin, M. G., & Hoffman, L. F. (2019). Models of vestibular semicircular canal afferent neuron firing activity. *Journal of Neurophysiology*, *122*(6), 2548–2567. https://doi.org/10.1152/jn.00087.2019

Pavão, R., Sussman, E. S., Fischer, B. J., & Peña, J. L. (2020). Natural ITD statistics predict human auditory spatial perception. *eLife*, *9*, e51927. https://doi.org/10.7554/eLife.51927

Pearl, J. (2009). *Causality* (2nd ed.). Cambridge, UK: Cambridge University Press.

Petty, G. W. (2018). On some shortcomings of Shannon entropy as a measure of information content in indirect measurements of continuous variables. *Journal of Atmospheric and Oceanic Technology*, *35*(5), 1011–1021. https://doi.org/10.1175/JTECH-D-17-0056.1

Petzschner, F. H., & Glasauer, S. (2011). Iterative Bayesian estimation as an explanation for range and regression effects: A study on human path integration. *Journal of Neuroscience*, *31*(47), 17220–17229. https://doi.org/10.1523/JNEUROSCI.2028-11.2011

Petzschner, F. H., Glasauer, S., & Stephan, K. E. (2015). A Bayesian perspective on magnitude estimation. *Trends in Cognitive Sciences*, *19*(5), 285–293. https://doi.org/10.1016/J.TICS.2015.03.002

Petzschner, F. H., Maier, P., & Glasauer, S. (2012). Combining symbolic cues with sensory input and prior experience in an iterative Bayesian framework. *Frontiers in Integrative Neuroscience*, *6*, 58. https://doi.org/10.3389/fnint.2012.00058

Philbeck, J. W., & Loomis, J. M. (1997). Comparison of two indicators of perceived egocentric distance under full-cue and reduced-cue conditions. *Journal of Experimental Psychology: Human Perception and Performance*, *23*(1), 72–85. https://doi.org/10.1037/0096-1523.23.1.72

Pomante, A. (2019). *Models and mechanisms of spatial orientation* (Doctoral dissertation). Radboud University Nijmegen. https://hdl.handle.net/2066/213537

Prsa, M., Jimenez-Rezende, D., & Blanke, O. (2015). Inference of perceptual priors from path dynamics of passive self-motion. *Journal of Neurophysiology*, *113*(5), 1400–1413. https://doi.org/10.1152/jn.00755.2014

Purves, D., Augustine, G. J., & Fitzpatrick, D. (2001). *Neuroscience* (2nd ed.). Sunderland, MA, USA: Sinauer Associates.

Redlick, F. P., Jenkin, M. R., & Harris, L. R. (2001). Humans can use optic flow to estimate distance of travel. *Vision Research*, *41*(2), 213–219. https://doi.org/10.1016/S0042-6989(00)00243-1

Riecke, B. E., van Veen, H. A. H. C., & Bülthoff, H. H. (2002). Visual homing is possible without landmarks: A path integration study in virtual reality. *Presence: Teleoperators and Virtual Environments*, *11*(5), 443–473. https://doi.org/10.1162/105474602320935810

Roach, N. W., McGraw, P. V., Whitaker, D. J., & Heron, J. (2017). Generalization of prior information for rapid Bayesian time estimation. *Proceedings of the National Academy of Sciences*, *114*(2), 412–417. https://doi.org/10.1073/pnas.1610706114

Rosenthal, R., Cooper, H., & Hedges, L. V. (1994). Parametric measures of effect size. In *The handbook of research synthesis* (2nd ed., Vol. 621, pp. 231–244). New York, NY, USA.

Ruderman, D. L., & Bialek, W. (1994). Statistics of natural images: Scaling in the woods. *Physical Review Letters*, *73*(6), 814–817. https://doi.org/10.1103/physrevlett.73.814

Saarela, T. P., Niemi, S. M., & Olkkonen, M. (2023). Independent short- and long-term dependencies in perception. *Journal of Vision*, *23*(5), 12. https://doi.org/10.1167/jov.23.5.12

Sadeghi, S. G., Chacron, M. J., Taylor, M. C., & Cullen, K. E. (2007). Neural variability, detection thresholds, and information transmission in the vestibular system. *Journal of Neuroscience*, *27*(4), 771–781. https://doi.org/10.1523/JNEUROSCI.4690-06.2007

Schwabe, L., & Blanke, O. (2008). The vestibular component in out-of-body experiences: A computational approach. *Frontiers in Human Neuroscience*, *2*, 17. https://doi.org/10.3389/neuro.09.017.2008

Schwarz, G. (1978). Estimating the dimension of a model. *Annals of Statistics*, *6*(2), 461–464. https://doi.org/10.1214/aos/1176344136

Servier. (2016). *Stages of life* [Image]. Servier Medical Art. https://smart.servier.com/smart_image/shape-human-ov/

Shirzhiyan, Z., Martínez-Montes, E., Pérez Hidalgo-Gato, J., von Werder, D., Shi, Z., & Glasauer, S. (2023). Modeling trial-to-trial dependence in magnitude perception: Bayes or ARX? *Bernstein Conference*. https://doi.org/10.12751/nncn.bc2023.133

Simoncelli, E. P., & Olshausen, B. A. (2001). Natural image statistics and neural representation. *Annual Review of Neuroscience*, *24*(1), 1193–1216. https://doi.org/10.1146/annurev.neuro.24.1.1193

Sinnott, C. B., Hausamann, P. A., & MacNeilage, P. R. (2023). Natural statistics of human head orientation constrain models of vestibular processing. *Scientific Reports*, *13*(1), 5882. https://doi.org/10.1038/s41598-023-32794-z

Spratling, M. W. (2016). A neural implementation of Bayesian inference based on predictive coding. *Connection Science*, *28*(4), 346–383. https://doi.org/10.1080/09540091.2016.1243655

Stocker, A. A., & Simoncelli, E. P. (2006). Noise characteristics and prior expectations in human visual speed perception. *Nature Neuroscience*, *9*(4), 578–585. https://doi.org/10.1038/nn1669

Straub, D., & Rothkopf, C. A. (2022). Putting perception into action with inverse optimal control for continuous psychophysics. *eLife*, *11*, e76635. https://doi.org/10.7554/eLife.76635

Sun, Q., Wang, J.-Y., & Gong, X.-M. (2024). Conflicts between short- and long-term experiences affect visual perception through modulating sensory or motor response systems: Evidence from Bayesian inference models. *Cognition*, *246*, 105768. https://doi.org/10.1016/j.cognition.2024.105768

Sun, Q., Zhang, H., Alais, D., & Li, L. (2020). Serial dependence and center bias in heading perception from optic flow. *Journal of Vision*, *20*(10), 1. https://doi.org/10.1167/jov.20.10.1

Sutter, K. (2023). *Motor planning, control and learning in health and disease* (Doctoral dissertation). Radboud University Nijmegen. https://hdl.handle.net/2066/292969

Taboga, M. (2021). Maximum likelihood—Numerical optimization algorithm. In *Lectures on probability theory and mathematical statistics*. Online appendix: Kindle Direct Publishing. https://www.statlect.com/fundamentals-of-statistics/maximum-likelihood-algorithm

Tamura, A., Wada, Y., Kurita, A., Matsunobu, T., Inui, T., & Shiotani, A. (2017). Visual effects on the subjective visual vertical and subjective postural head vertical during static roll-tilt. *Laryngoscope Investigative Otolaryngology*, *2*(3), 125–130. https://doi.org/10.1002/lio2.72

ter Horst, A. C., Koppen, M., Selen, L. P. J., & Medendorp, W. P. (2015). Reliability-based weighting of visual and vestibular cues in displacement estimation. *PLOS ONE*, *10*(12), e0145015. https://doi.org/10.1371/journal.pone.0145015

Textor, J., van der Zander, B., Gilthorpe, M. S., Liskiewicz, M., & Ellison, G. T. H. (2016). Robust causal inference using directed acyclic graphs: The R package "dagitty." *International Journal of Epidemiology*, *45*(6), 1887–1894. https://doi.org/10.1093/ije/dyw341

Tong, K., & Dubé, C. (2022). A tale of two literatures: A fidelity-based integration account of central tendency bias and serial dependency. *Computational Brain & Behavior*, *5*(1), 103–123. https://doi.org/10.1007/s42113-021-00123-0

Tuthill, J. C., & Azim, E. (2018). Proprioception. *Current Biology*, *28*(5), R194–R203. https://doi.org/10.1016/j.cub.2018.01.064

Udo De Haes, H. A. (1970). Stability of apparent vertical and ocular countertorsion as a function of lateral tilt. *Perception & Psychophysics*, *8*(3), 137–142. https://doi.org/10.3758/BF03210192

Ugray, Z., Lasdon, L., Plummer, J., Glover, F., Kelly, J., & Martí, R. (2007). Scatter search and local NLP solvers: A multistart framework for global optimization. *INFORMS Journal on Computing*, *19*(3), 328–340. https://doi.org/10.1287/ijoc.1060.0175

Vaitl, D., Mittelstaedt, H., & Baisch, F. (1997). Shifts in blood volume alter the perception of posture. *International Journal of Psychophysiology*, *27*(2), 99–105. https://doi.org/10.1016/S0167-8760(97)00053-6

Vaitl, D., Mittelstaedt, H., Saborowski, R., Stark, R., & Baisch, F. (2002). Shifts in blood volume alter the perception of posture: Further evidence for somatic graviception. *International Journal of Psychophysiology*, *44*(1), 1–11. https://doi.org/10.1016/S0167-8760(01)00184-2

van Bergen, R. S., & Jehee, J. F. M. (2019). Probabilistic representation in human visual cortex reflects uncertainty in serial decisions. *Journal of Neuroscience*, *39*(41), 8164–8176. https://doi.org/10.1523/JNEUROSCI.3212-18.2019

van Beuzekom, A. D., & van Gisbergen, J. A. M. (2000). Properties of the internal representation of gravity inferred from spatial-direction and body-tilt estimates. *Journal of Neurophysiology*, *84*(1), 11–27. https://doi.org/10.1152/jn.2000.84.1.11

van Helvert, M. J. L. (2025). *Neural control of reaching and steering* (Doctoral dissertation). Radboud University Nijmegen. https://doi.org/10.54195/9789465150307

van Helvert, M. J. L., Selen, L. P. J., van Beers, R. J., & Medendorp, W. P. (2022). Predictive steering: Integration of artificial motor signals in self-motion estimation. *Journal of Neurophysiology*, *128*(6), 1395–1408. https://doi.org/10.1152/jn.00248.2022

Ventre-Dominey, J. (2014). Vestibular function in the temporal and parietal cortex: Distinct velocity and inertial processing pathways. *Frontiers in Integrative Neuroscience*, *8*, 53. https://doi.org/10.3389/fnint.2014.00053

Verstynen, T., & Sabes, P. N. (2011). How each movement changes the next: An experimental and theoretical study of fast adaptive priors in reaching. *Journal of Neuroscience*, *31*(27), 10050–10059. https://doi.org/10.1523/JNEUROSCI.6525-10.2011

Vinje, W. E., & Gallant, J. L. (2002). Natural stimulation of the nonclassical receptive field increases information transmission efficiency in V1. *Journal of Neuroscience*, *22*(7), 2904–2915. https://doi.org/10.1523/JNEUROSCI.22-07-02904.2002

von Holst, E., & Mittelstaedt, H. (1950). Das Reafferenzprinzip: Wechselwirkungen zwischen Zentralnervensystem und Peripherie. *Naturwissenschaften*, *37*(20), 464–476. https://doi.org/10.1007/BF00622503

Walsh, E. G. (1961). Role of the vestibular apparatus in the perception of motion on a parallel swing. *Journal of Physiology*, *155*(3), 506–513. https://doi.org/10.1113/jphysiol.1961.sp006643

Warren, W. H., & Saunders, J. A. (1995). Perceiving heading in the presence of moving objects. *Perception*, *24*(3), 315–331. https://doi.org/10.1068/p240315

Willemsen, S. C. M. J., Oostwoud Wijdenes, L., van Beers, R. J., Koppen, M., & Medendorp, W. P. (2024). Central tendency and serial dependence in vestibular path integration. *Journal of Neurophysiology*, *132*(5), 1481–1493. https://doi.org/10.1152/jn.00271.2024

Xsens. (2018). *MTw Awinda user manual*. https://www.movella.com/support/software-documentation

Zhou, B., Hofmann, D., Pinkoviezky, I., Sober, S. J., & Nemenman, I. (2018). Chance, long tails, and inference in a non-Gaussian, Bayesian theory of vocal learning in songbirds. *Proceedings of the National Academy of Sciences*, *115*(36), E8538–E8546. https://doi.org/10.1073/pnas.1713020115

Nederlandse samenvatting

Veel aspecten van onze waarneming en ons gedrag worden beïnvloed door voorkennis. We zijn ons meestal niet bewust van deze invloed, maar zo nu en dan merk je de effecten van voorkennis, bijvoorbeeld wanneer je een mok optilt waarvan je dacht dat er nog koffie in zat maar de mok bijna leeg blijkt te zijn. Voorkennis heeft ook invloed op onze ruimtelijke waarneming. Wanneer je bijvoorbeeld naar een nieuwe bestemming wandelt, ervaar je de terugweg vaak anders dan de heenweg, onder andere doordat we op de terugweg voorkennis hebben over de af te leggen afstand. In dit proefschrift heb ik onderzoek gedaan naar hoe voorkennis onze vestibulaire waarneming van ruimtelijke oriëntatie (**Hoofdstuk 2**) en zelfbeweging (**Hoofdstukken 3** en **4**) beïnvloedt.

Dit onderzoek bestond uit het meten van proefpersonen in gedragsexperimenten en het modelleren van de verzamelde data middels wiskundige modellen. De modellen in dit proefschrift vallen onder het Bayesiaanse raamwerk, waarin sensorische informatie (de *likelihood*) en voorkennis (de *prior*) over dezelfde stimulus (bijvoorbeeld een afstand) worden gecombineerd tot een statistisch optimale schatting (de *posterior*). Hoe zekerder het brein is over een signaal, hoe meer dit signaal wordt meegewogen in de uiteindelijke schatting, om zo tot een preciezere schatting te komen dan wanneer het alleen de individuele signalen had gebruikt. Eerdere studies hebben laten zien dat systematische afwijkingen in het gedrag van proefpersonen verklaard kunnen worden door het sturende effect van voorkennis op waarneming.

In **Hoofdstuk 2** deed ik onderzoek naar de eerder veronderstelde aanname dat voorkennis over de meest waarschijnlijke hoofdoriëntatie in alledaags gedrag, de waarneming van ruimtelijke oriëntatie beïnvloedt. Eerder psychofysisch onderzoek heeft aangetoond dat wanneer een proefpersoon zijwaarts is gekanteld in de ruimte, de waarneming van verticaliteit verschuift in de richting van de kanteling, alsof hoofdoriëntatie wordt onderschat. Deze onderschatting kon goed worden verklaard door een Bayesiaans model dat uitgaat van een Gaussische prior, gecentreerd op de rechtopstaande hoofdpositie (Clemens et al., 2011). Deze voorkennis weerspiegelt waarschijnlijk de verdeling van natuurlijke hoofdoriëntaties in het dagelijks leven. Ik liet zien dat hoofdoriëntaties tijdens alledaags gedrag inderdaad gecentreerd zijn op de rechtopstaande hoofdpositie, maar dat de verdeling langere staarten heeft dan verwacht volgens de Gaussische aanname. Het opnemen van de gemeten hoofdoriëntatie-verdeling als prior in het Bayesiaanse model gaf modelvoorspellingen die niet de eerder gemeten

psychofysische data konden verklaren. Dit suggereert dat deze prior intern niet wordt gerepresenteerd als de empirisch gemeten verdeling van hoofdoriëntaties.

In **Hoofdstuk 3** onderzocht ik hoe de waarneming van zelfbeweging wordt beïnvloed door de verdeling en presentatievolgorde van stimulusafstanden tijdens een experiment. Proefpersonen voerden een afstandsreproductietaak uit in een bewegende stoelopstelling. Gedurende iedere trial werd de proefpersoon eerst passief bewogen over een stimulusafstand waarna de proefpersoon de waargenomen afstand actief reproduceerde door de stoel terug te sturen naar de startlocatie. Ik toonde aan dat er effecten zijn van de eerder ervaren stimulusafstanden op het reproductiegedrag: de gereproduceerde afstanden neigden naar het gemiddelde van de experimentele stimulusverdeling (een centrale tendens) en naar de stimulus in de direct voorafgaande trial (een seriële afhankelijkheid). Zowel een (*static*) Bayesiaans model dat aanneemt dat stimulusafstanden worden getrokken uit een vaste stimulusverdeling, als een (*two-state*) Bayesiaans model dat aanneemt dat het gemiddelde van deze verdeling over trials kan variëren, konden de centrale-tendenseffecten in de gereproduceerde afstanden goed verklaren, maar in mindere mate de seriële-afhankelijkheidseffecten. Ik liet ook zien dat reproductiegedrag wordt beïnvloed door stimuluscontext en dat dit effect kan worden gemodelleerd door het two-state model met verschillende blok-afhankelijke globale onderschattingen.

In **Hoofdstuk 4** deed ik onderzoek naar hoe de waarneming van zelfbeweging wordt beïnvloed door stimulusautocorrelatie. Een nieuwe groep proefpersonen voerde de afstandsreproductietaak uit, ditmaal in twee autocorrelatiecondities: stimulusafstanden werden willekeurig gepresenteerd in de geen-autocorrelatieconditie, en in een *random-walk*- (“dronkemanswandeling”) volgorde in de hoge-autocorrelatieconditie. Middels simulaties liet ik zien dat wanneer de stimulusautocorrelatie hoog is, centrale-tendenseffecten en seriële-afhankelijkheidseffecten covariëren. Om deze effecten in beide condities correct te kunnen schatten, representeerde ik de veronderstelde causale effecten tussen de stimulusafstanden en reproductiefouten in een causaal diagram en paste ik het *d*-separatieprincipe toe om te bepalen welke variabelen als covariaten moeten worden meegenomen in een meervoudig lineair regressiemodel. Op basis van dit model concludeerde ik dat de centrale tendens en seriële afhankelijkheid niet verschilden tussen de twee autocorrelatiecondities en dat de gevonden effecten overeenkwamen met die uit Hoofdstuk 3. Dit suggereert dat centrale tendens en seriële afhankelijkheid niet ontstaan door het experimentele randomisatieprotocol maar het gevolg zijn van neurocognitieve processen.

Ik concludeer dat vestibulaire waarneming wordt beïnvloed door voorkennis over taakrelevante stimulusgeschiedenis, opgebouwd over meerdere tijdschalen. Toekomstige studies zouden verder kunnen onderzoeken hoe het samenspel tussen relatief stabiele voorkennis over natuurlijke stimuli en kortetermijninformatie over recent ervaren stimuli de waarneming van ruimtelijke oriëntatie en zelfbeweging beïnvloedt.

Research data management

This research followed the applicable laws and ethical guidelines. Research data management was conducted according to the FAIR principles. The paragraphs below specify in detail how this was achieved.

Ethics

This thesis is based on the results of human studies, which were conducted in accordance with the principles of the Declaration of Helsinki. The Ethical Committee of the faculty of Social Sciences (ECSS) has given a positive advice to conduct these studies to the Dean of the faculty, who formally approved the conduct of these studies (ECSW2017-0805-504, ECSW-2022-082). Data collection was performed at the Donders Centre for Cognition. Informed consent was obtained on paper following the Centre procedure. The forms are archived in the central archive of the Centre for 10 years after the termination of the studies. This research was funded by an internal grant from the Donders Centre for Cognition.

Findable and accessible

The table below details where the data and research documentation for each chapter can be found on the Radboud Data Repository. All data archived as a Data Sharing Collection (DSC) remain available for at least 10 years after termination of the studies.

Chapter	DAC	RDC	DSC	DSC License
2	DAC_2020.00113_740	RDC_2020.00113_885	DSC_2020.00113_493	RU-DI-NH-1.0
3	DAC_2022.00151_785	RDC_2022.00151_271	DSC_2022.00151_092	RU-HD-1.1
			DSC_2022.00151_318	GPL-3.0
4	DAC_2024.00135_783	RDC_2024.00135_696	DSC_2024.00135_205	
			DSC_2024.00135_842	

DAC = Data Acquisition Collection, RDC = Research Documentation Collection, DSC = Data Sharing Collection

The manuscript of **Chapter 4** is in revision. The data and scripts have been shared with the reviewers in the DSCs and will be made publicly available once the article has been published. DSC_2024.00135_205 and DSC_2024.00135_842 will then be shared under the RU-HD-2.0 and GPL-3.0 licenses, respectively.

Interoperable and reusable

The raw data are stored in the Data Acquisition Collection (DAC) in their original form. For the Research Documentation Collection (RDC) and DSC, long-lived file formats have been used, ensuring that data remains usable in the future. We provide a description of the experimental setup, raw data (DAC and DSC), and the analysis scripts (RDC and DSC) to make sure that the results are reproducible.

Privacy

The privacy of the participants in this thesis has been warranted using random individual subject codes. A pseudonymization key linked this random code with the personal data. This pseudonymization key was stored on a network drive that was only accessible to members of the project who needed access to it because of their role within the project. The pseudonymization key was stored separately from the research data. The pseudonymization keys were destroyed within one month after finalization of these projects.

About the author

Sophie Willemsen was born in Tiel, the Netherlands, on May 23, 1997. In 2015, she started the bachelor's program in Artificial Intelligence at Radboud University Nijmegen. She wrote her bachelor's thesis on the effect of auditory distractors on the perception of tinnitus-like stimuli in a dichotic listening paradigm, which she researched during an internship in the Brain-Computer Interfacing lab of the Donders Institute for Brain, Cognition and Behaviour. After obtaining her bachelor's degree in 2018, Sophie started the master's program in Artificial Intelligence at Radboud University Nijmegen. She wrote her master's thesis on target foraging behavior in sequential reaching tasks, which she investigated during an internship at the Sensorimotor lab of the Donders Institute for Brain, Cognition and Behaviour. After obtaining her master's degree in 2020, Sophie continued her career as a PhD candidate in the Sensorimotor lab. During her PhD, she studied the influence of prior experience on spatial orientation and self-motion perception, of which the results are presented in this thesis. Sophie is currently working as a methodologist at Statistics Netherlands (Centraal Bureau voor de Statistiek).

Portfolio

Courses & workshops

Course	*Organizer*
Learning Theory (2020-2021)	Johns Hopkins University
Psychophysics 1 (2021)	Radboud University
Project Management for PhD Candidates (2021)	Radboud University
Art of Presenting Science (2022)	Radboud University
Scientific Integrity (2022)	Donders Graduate School

Conferences & summer schools

Event	*Location*
NCM (2021)	Online
Neuromatch Academy: Computational Neuroscience (2021)	Online
NVP (2021)	Egmond aan Zee, the Netherlands
IJCNN (2023)	Gold Coast, Australia
Donders Discussions (2023)	Nijmegen, the Netherlands
SfN (2023)	Washington DC, USA

Teaching activities

Internship supervision of	*Study program*	*Duration*
Giorgia Corrado (2021)	Bachelor Artificial Intelligence	6 months
Tim Hiemstra (2021)	Bachelor Artificial Intelligence	6 months
Michiel Koenis (2021)	Bachelor Artificial Intelligence	6 months
Mart van ‘t Spijker (2021)	Bachelor Artificial Intelligence	6 months
Neele Ulken (2023-2024)	Master Cognitive Neuroscience	10 months

Teaching assistant for	*Study program*
Advanced Academic and Professional Skills (2020-2021, 2021-2022)	Master Artificial Intelligence
Signal Analysis and MATLAB (2021-2022, 2022-2023)	Bachelor Artificial Intelligence, Bachelor Psychology

Outreach & societal impact

Activity	*Location*
Demo at Donders Citylab (2022)	Nijmegen, the Netherlands
Demo at Science Festival Radboud Kids (2023)	Nijmegen, the Netherlands

Acknowledgements

Throughout my PhD, I was very fortunate to be surrounded by many wonderful people. I would like to thank all of you (whether or not you are mentioned by name in the remainder of this text) for your advice, support, and encouragement. Without you, writing this thesis would not have been possible!

Leonie, **Rob**, **Mathieu**, and **Pieter**, thank you very much for your supervision throughout these years. I have learned so much from you, both on a professional and on a personal level, and I feel very lucky to have had not just two, or three, but four experts guiding me along the way! I enjoyed our many interesting and fun discussions, which often took longer than scheduled (to my delight). **Leonie**, thank you not only for your scientific insights and help in the lab but also for your invaluable practical advice. I always felt very much supported by you and appreciate how you kept an eye out for my time and progress. **Rob**, thank you for sharing your extensive knowledge and keen eye for detail with me. Your supervision already began during my master's internship; I have fond memories of our first coding sessions, which are what really sparked my interest in computational modeling. **Mathieu**, thank you for all your help; you even kept coming back to the office for our weekly meetings during your retirement. I always found it reassuring to know that I could turn to you with all my (statistics) questions. **Pieter**, thank you for your guidance, your enthusiasm and for always believing in me. Your lectures inspired me to do my master's internship in the Sensorimotor lab and I am thankful that you gave me the opportunity to stay for some more years to do my PhD in that amazing environment!

I would also like to thank the other (former and current) members of the Sensorimotor lab for their help and feedback, as well as for the memories we made during our hallway chats, lunch breaks and trips: **Antonella**, **Anushree**, **Arun**, **Asia**, **Aslan**, **Bart**, **Brandon**, **Erik**, **Floris**, **Gaia**, **Garima**, **Hüseyin**, **Ilse**, **Ivar**, **James**, **Janny**, **Judith**, **Katrin K.**, **Katrin S.**, **Kevin**, **Laura**, **Lonneke**, **Luc**, **Lucas**, **Luke**, **Maaike**, **Manon**, **Maria**, **Mathilde**, **Milou**, **Neele**, **Nika**, **Noël**, **Palak**, **Purva**, **Rob P.**, **Siebe**, **Tobias**, **Valeria**, and **Yvonne**. **Milou** and **Yvonne**, thank you for being my paranymphs, office mates and amazing friends! I am happy we got to spend a lot of time together working in the office, coding in the lab, taking courses and attending conferences. I admire your scientific minds and I am sure you will keep on achieving great things in the future. **Janny**, **Judith** and **Katrin K.**, thank you for the fun times in Egmond aan Zee during the NVP 2021 conference! **Mathilde**, thank you for being a great colleague and friend! I very much enjoyed getting to know you

during our many conversations, often with an iced coffee in hand. **Brandon**, **Kevin** and **Luc**, thank you for all your help in the Sled lab; you made spending hours in the basement without sunlight a lot of fun! **Antonella**, **Ivar**, **Lucas** and **Maaike**, I am grateful that I was able to build upon your data collection and modelling work, which formed the foundation for Chapter 2; thank you! **James** and **Aslan**, I learned a lot from our chats about modeling; thank you for your insights and time! **Neele**, thank you for trusting me to be one of your thesis supervisors and for your feedback throughout your internship. I am happy that you are now continuing your career as a PhD candidate; I wish you all the best!

The research presented in this thesis would not have been possible without the support of the great people 'behind the scenes'. **Jolanda**, **Karin** and **Vanessa**, thank you for answering all my questions and for the fun chats. **Annemiek**, thank you for everything you do for the Donders Graduate School. I very much enjoyed the events organized by the DGS, especially the session on how to finish your PhD, which came at the perfect time for me and was very helpful and encouraging. **Miriam**, **Pauline**, **Jiska** and **Ronny**, thank you for the amazing research support! I would also like to thank the Technical Support Group, in particular **Wilbert** and **Gerard** for all their help in the Sled lab and enabling us to do such cool experiments. Thank you to all the **participants** for taking part in these experiments; I could not have done it without you!

Abdullahi, **Baran**, **Bas**, **Bente**, **Julia**, **Lars**, **Manon**, **Niels**, **Thomas**, **Tim**, **Tommie** en **Yana**; ik ben heel blij dat ik jullie heb leren kennen tijdens de introductieweek van onze bachelor en dat ik mocht aanhaken bij 'Groepje 1'. Bedankt voor alle leuke programmeersessies, feestjes en herinneringen! **Floris** en **Jelmer**, bedankt voor jullie steun tijdens het schrijven van dit proefschrift en het regelmatig checken hoe het met me ging. **Dominique**, **Janneke**, **Jet**, **Jonne**, **Kenya**, **Lisanne** en **Sanne**, bedankt dat jullie al bijna 15 jaar mijn lieve vriendinnen zijn. Ik vind het heel bijzonder hoe we alles met elkaar kunnen delen; hopelijk heb ik jullie niet al te veel verveeld met verhalen over mijn onderzoek!

Lieve **familie** en **schoonfamilie**, dank jullie wel voor jullie interesse, steun en liefde! Lieve **papa** en **mama**, dank jullie wel dat jullie mijn grootste fans zijn. Ik ben waar ik ben door jullie en daar ben ik jullie heel dankbaar voor. Van appeltaart bij de haard na het fietsen door de regen, naar helpen met wiskundehuiswerk en 'Kareltje' programmeren; jullie waren en zijn er altijd voor mij. Bedankt voor jullie nieuwsgierigheid, vertrouwen, geduld en hulp! Lieve **Elise**, ik ben trots dat ik me jouw grote zus mag noemen. Bedankt voor al je steun de afgelopen jaren en dat je er altijd voor me bent! Dank jullie wel, lieve schoonouders **Sorin** en **Maria**, voor al jullie liefde, interesse en advies. Ik voel me bevoorrecht dat ik zulke geweldige

mensen er als extra ouders bij heb mogen krijgen. Lieve **Sorin**, bedankt voor al je hulp en onze urenlange discussies over de wetenschap! Lieve **Maria**, ik mis je. Wat een fantastisch persoon was je en wat was je een inspiratie voor velen. Bedankt voor je liefde en vertrouwen. Het is gelukt, maar ik weet dat je daar niet aan twijfelde!

Lieve **Stefan**, ik eindig mijn proefschrift graag met jou. Wat bijzonder dat jij in mijn leven bent gekomen en dat we samen het leven mogen delen. Het is moeilijk in het kort samen te vatten wat jij voor mij betekent dus bij deze een incomplete poging. Bedankt dat je mijn beste vriend bent en bedankt voor al je steun en liefde de afgelopen jaren tijdens mijn PhD en daarbuiten. Dank je wel voor al die uren samen kletsen over mijn onderzoek, je slimme inzichten, je grapjes en je geruststelling. Zonder jou was het niet gelukt!

Donders Graduate School

For a successful research Institute, it is vital to train the next generation of scientists. To achieve this goal, the Donders Institute for Brain, Cognition and Behaviour established the Donders Graduate School in 2009. The mission of the Donders Graduate School is to guide our graduates to become skilled academics who are equipped for a wide range of professions. To achieve this, we do our utmost to ensure that our PhD candidates receive support and supervision of the highest quality.

Since 2009, the Donders Graduate School has grown into a vibrant community of highly talented national and international PhD candidates, with over 500 PhD candidates enrolled. Their backgrounds cover a wide range of disciplines, from physics to psychology, medicine to psycholinguistics, and biology to artificial intelligence. Similarly, their interdisciplinary research covers genetic, molecular, and cellular processes at one end and computational, system-level neuroscience with cognitive and behavioral analysis at the other end. We ask all PhD candidates within the Donders Graduate School to publish their PhD thesis in the Donders Thesis Series. This series currently includes over 600 PhD theses from our PhD graduates and thereby provides a comprehensive overview of the diverse types of research performed at the Donders Institute. A complete overview of the Donders Thesis Series can be found on our website: https://www.ru.nl/donders/donders-series.

The Donders Graduate School tracks the careers of our PhD graduates carefully. In general, the PhD graduates end up at high-quality positions in different sectors, for a complete overview see https://www.ru.nl/donders/destination-our-former-phd. A large proportion of our PhD alumni continue in academia (>50%). Most of them first work as a postdoc before growing into more senior research positions. They work at top institutes worldwide, such as University of Oxford, University of Cambridge, Stanford University, Princeton University, UCL London, MPI Leipzig, Karolinska Institute, UC Berkeley, EPFL Lausanne, and many others. In addition, a large group of PhD graduates continue in clinical positions, sometimes combining it with academic research. Clinical positions can be divided into medical doctors, for instance, in genetics, geriatrics, psychiatry, or neurology, and in psychologists, for instance as healthcare psychologist, clinical neuropsychologist, or clinical psychologist. Furthermore, there are PhD graduates who continue to work as researchers outside academia, for instance at non-profit or government organizations, or in pharmaceutical companies. There are also PhD graduates who

work in education, such as teachers in high school, or as lecturers in higher education. Others continue in a wide range of positions, such as policy advisors, project managers, consultants, data scientists, web- or software developers, business owners, regulatory affairs specialists, engineers, managers, or IT architects. As such, the career paths of Donders PhD graduates span a broad range of sectors and professions, but the common factor is that they almost all have become successful professionals.

For more information on the Donders Graduate School, as well as past and upcoming defenses please visit: http://www.ru.nl/donders/graduate-school/phd/.

DONDERS INSTITUTE

Radboud University

Radboudumc